
Photonic Integration and Acousto-Optics in Aluminum Nitride

Siddhartha Ghosh

**Microscale Acoustic and Photonic Systems Laboratory
Department of Electrical and Computer Engineering
Northeastern University
Boston, MA 02115
s.ghosh@northeastern.edu**

**NNCI Etch Symposium
University of Pennsylvania, Philadelphia, PA
April 22, 2022**





Outline

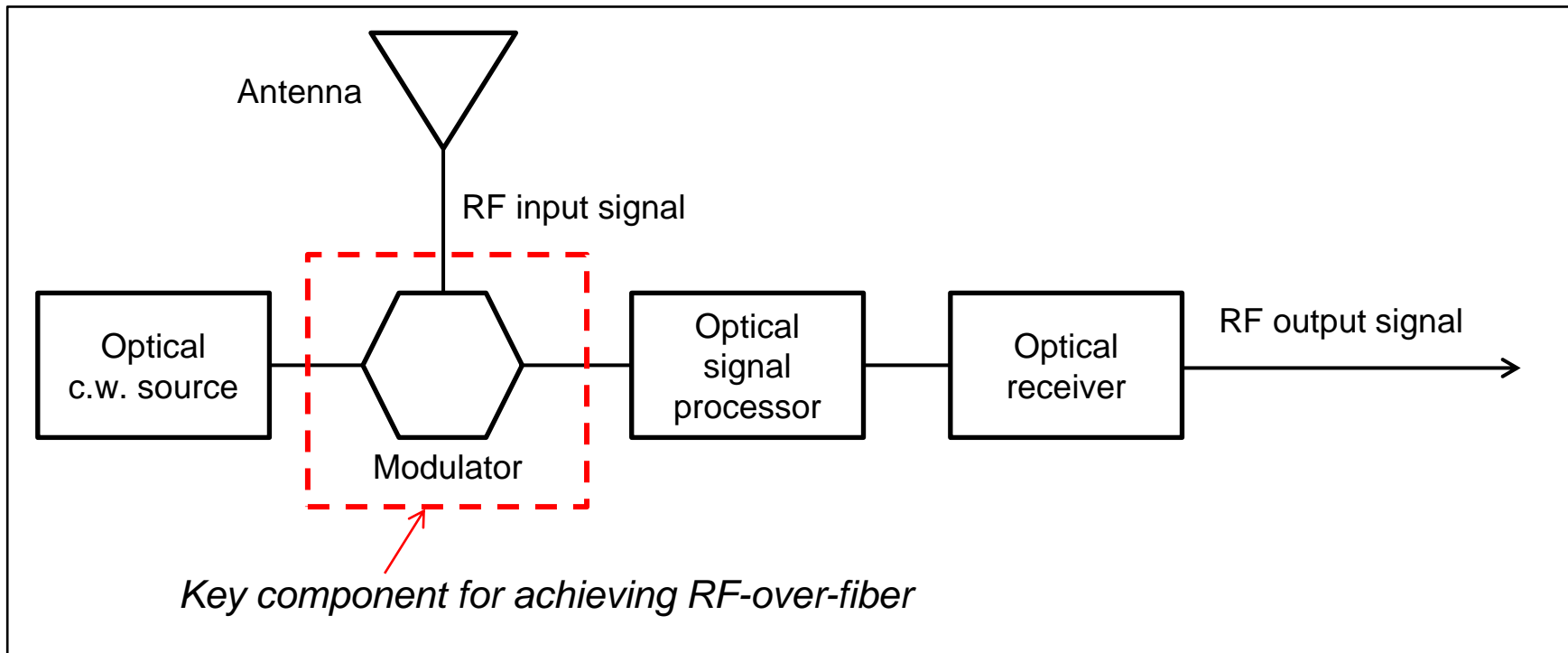
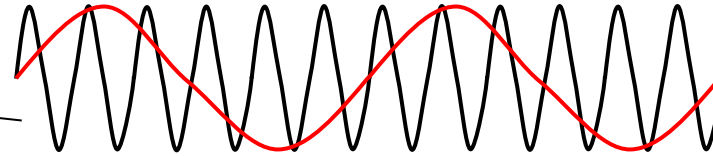
- **Motivation and background**
- **Material selection**
- **Light coupling in AlN**
- **Acousto-optic modulator**
- **200-mm process development**

Classical Applications in RF-Photonics

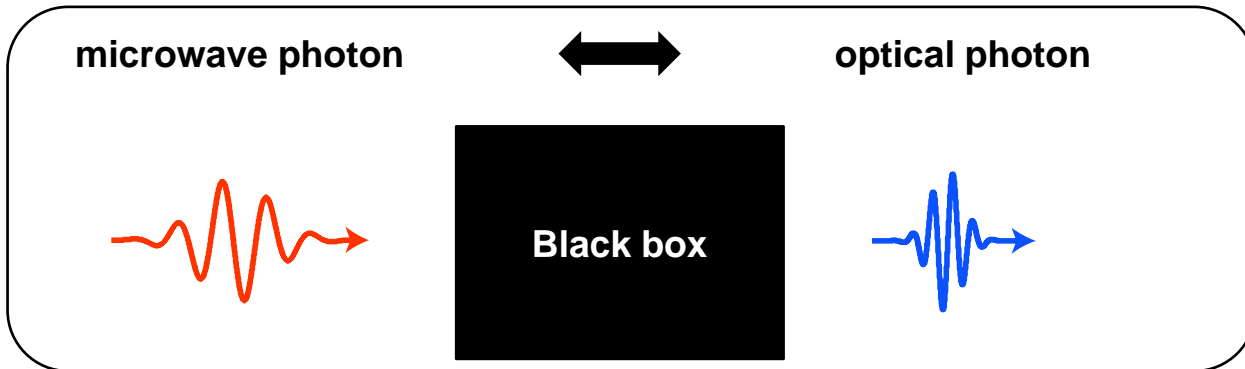
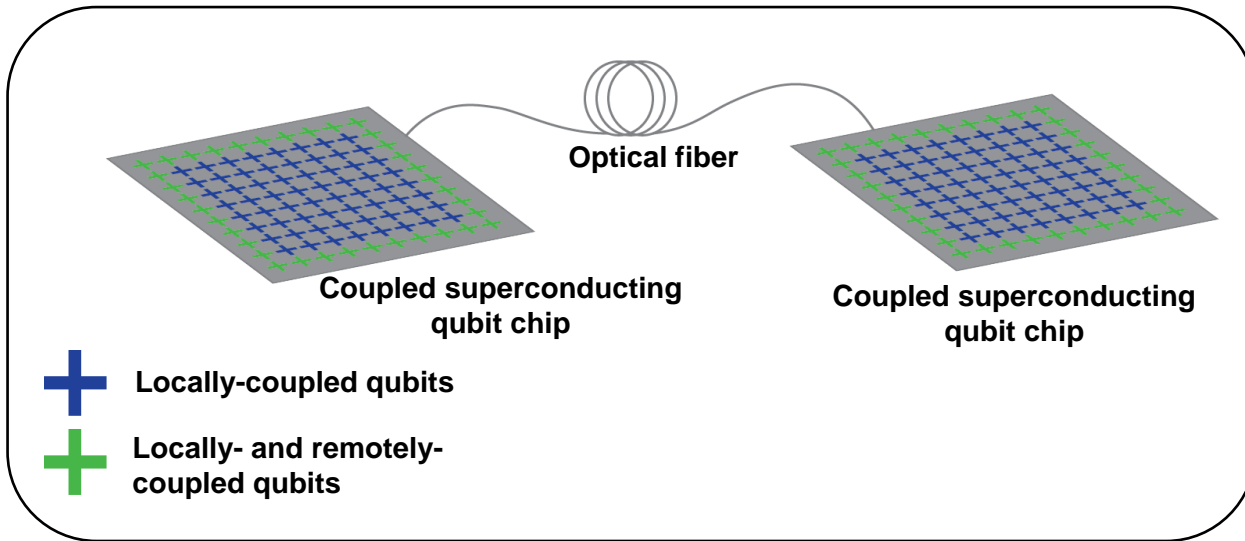
- **Optical links provide several advantages for controlling radio frequency (RF) signals in various communications applications**

Use of light as a carrier:

- ✓ Increased channel capacity
- ✓ Frequency-independent low-loss delay lines



Coherent Microwave-to-Optical Conversion: A Quantum Interface

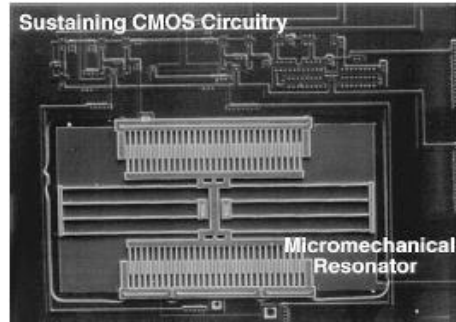


- Optical fibers can be used to transmit photons over long distances with very low loss
- Reversible coherent conversion between microwave and optical regimes can facilitate coupling of qubits in different cryostats
- Other applications include
 - Interface for components of a hybrid quantum system, e.g. a quantum network
 - High-bandwidth routing of control and readout signals from/into a cryostat
 - Optical detection of microwaves for radar, medical imaging, classical communication, navigation, etc.

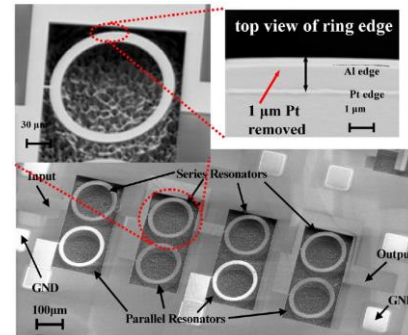
A quantum interface is an enabling technology for robust quantum computers and networks

MEMS for Integrated RF-Photonics

- MEMS technology has been widely demonstrated for its compact filtering capabilities, CMOS compatibility and use in RF reference oscillators



Nguyen & Howe, *JSSC* **34**, 1999



Piazza et al., *JMEMS* **16**, 2007

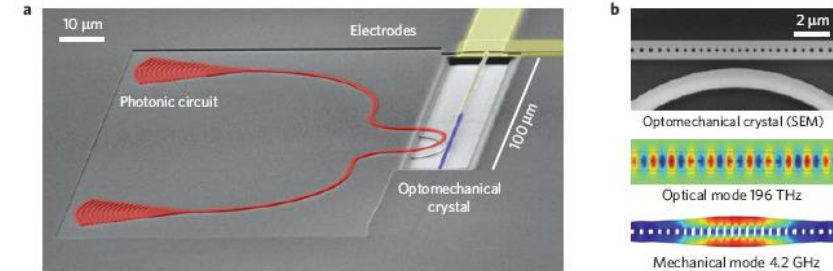


- Piezoelectric actuation offers:**

- ✓ Scaling to higher/ multiple frequencies with lithographically-defined features
- ✓ Strong electromechanical coupling
- ✓ Low motional impedances/Matching to 50Ω electronics

- Advances in cavity optomechanics have produced highly sensitive detection techniques with useful applications in communications and fundamental science

We seek to capitalize on these capabilities by creating devices that function in both the acoustic and optical domains



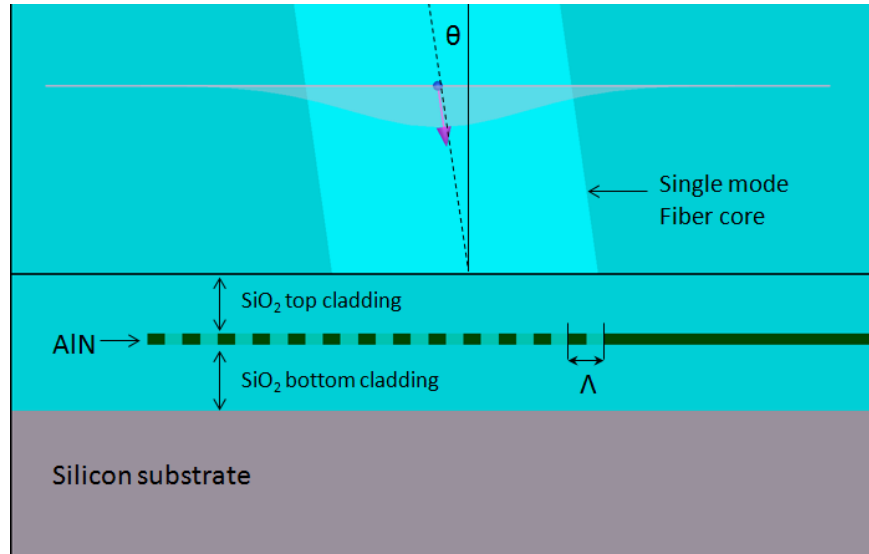
Bochmann et al., *Nat. Physics* **9**, 2013



Integrated Photonic Material Options

Function / Property	III-V Compound Semiconductors (InP, GaAs, GaN)	Silicon (Si) + Germanium (Ge)	Silicon Dioxide (SiO ₂) & Silicon Nitride (Si ₃ N ₄)	Lithium Niobate (LiNbO ₃)	Aluminum Nitride (AlN)	Polymers	Hexagonal Silicon Carbide (4H-SiC)
Efficient Light Emission	Direct Bandgap						
Efficient Light Detection							
Electro-Optic Modulation							
Electro-Absorption Mod							
Free-Carrier Modulation							
Thermo-Optic Modulation							
Piezoelectric							
Acousto-Optic Modulation							
Low-Loss Passives							
Efficient Nonlinearities	2 nd & 3 rd order	3 rd order	3 rd order	2 nd & 3 rd	2 nd & 3 rd	2 nd & 3 rd	2 nd & 3 rd
High-Power Handling							
Monolithic Electronics							
Foundry Compatible							

Grating Coupler Design

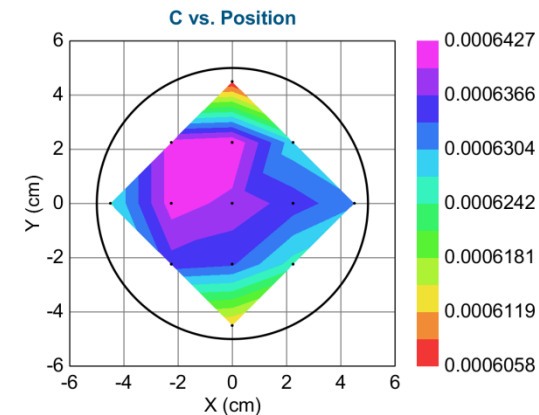
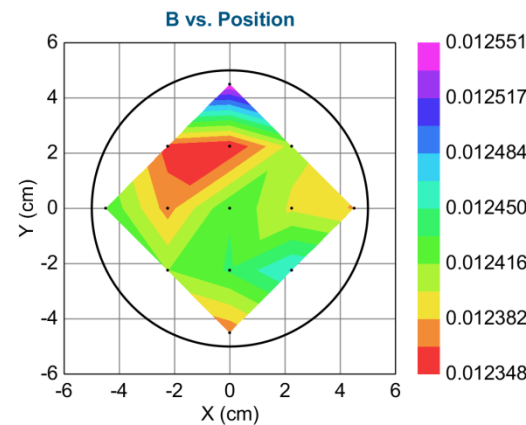
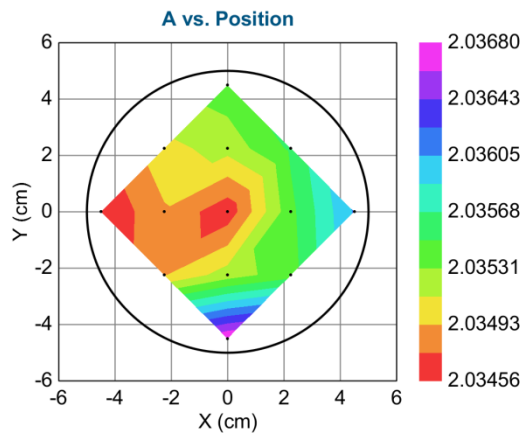


Approximate grating pitch from Bragg condition:

$$\frac{1}{\Lambda} = \frac{n_{eff}}{\lambda} - \frac{n_o}{\lambda} \sin \theta$$

Fix: $\theta = 8^\circ$, $t_{AIN} = 400\text{nm}$, SiO_2 cladding, $\lambda = 1550 \text{ nm}$

Polycrystalline AlN: 400nm thick

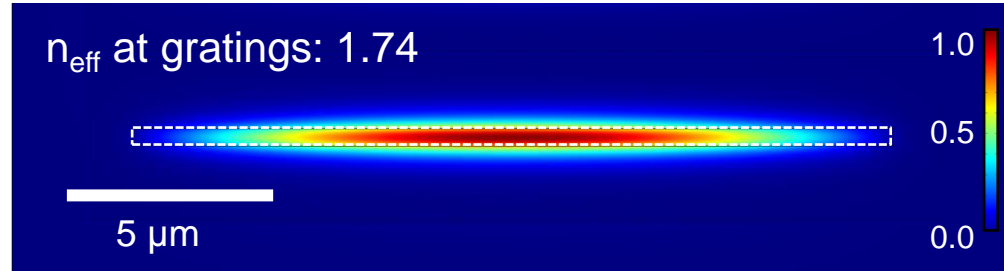


$$A = 2.0353 \pm 8.03 \times 10^{-4}$$

$$B = 0.0124 \pm 2.39 \times 10^{-4}$$

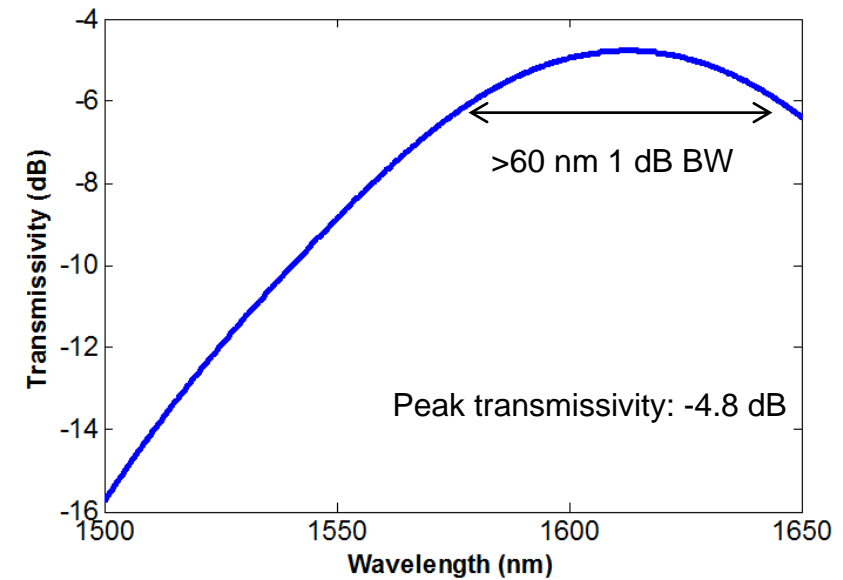
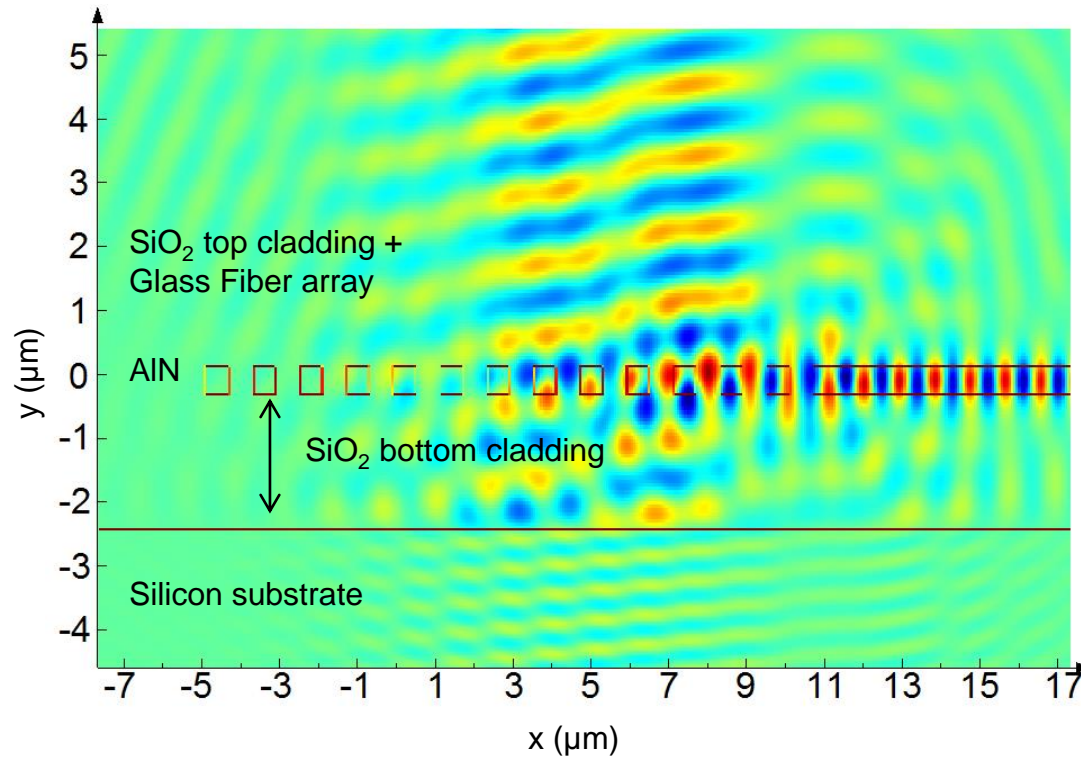
$$C = 0.0006 \pm 3.28 \times 10^{-5}$$

Grating Coupler Simulation

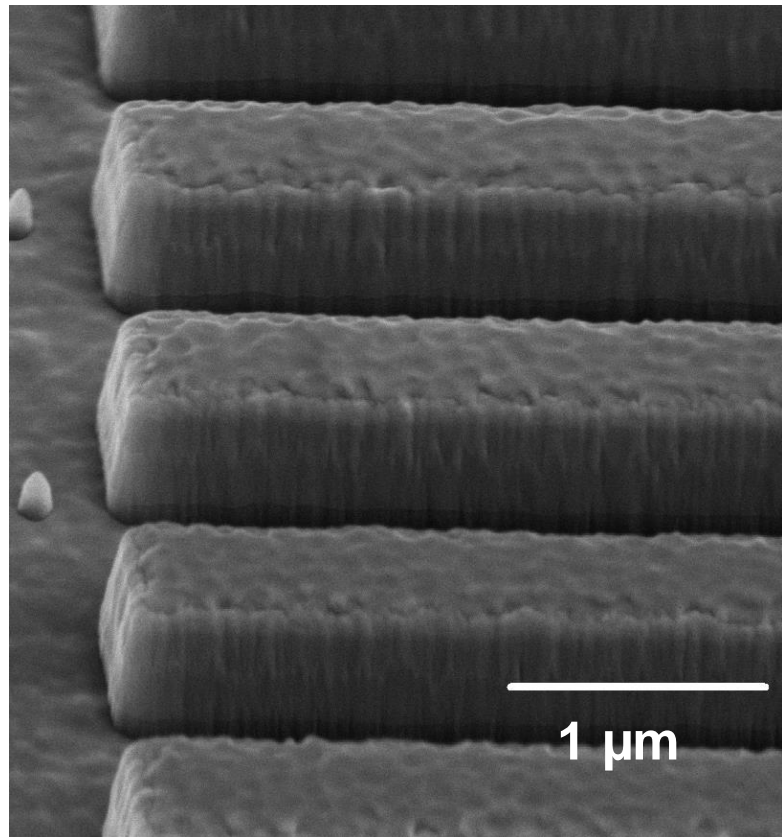
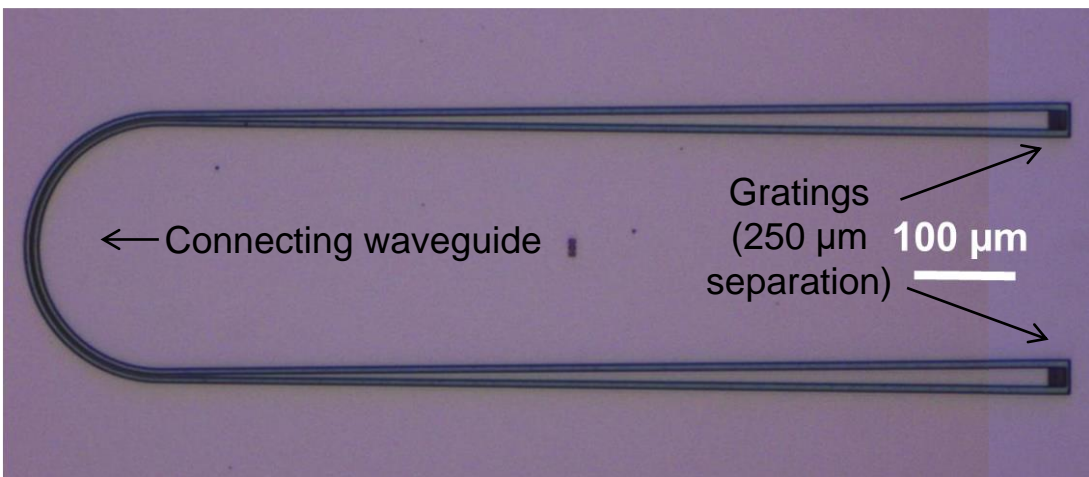
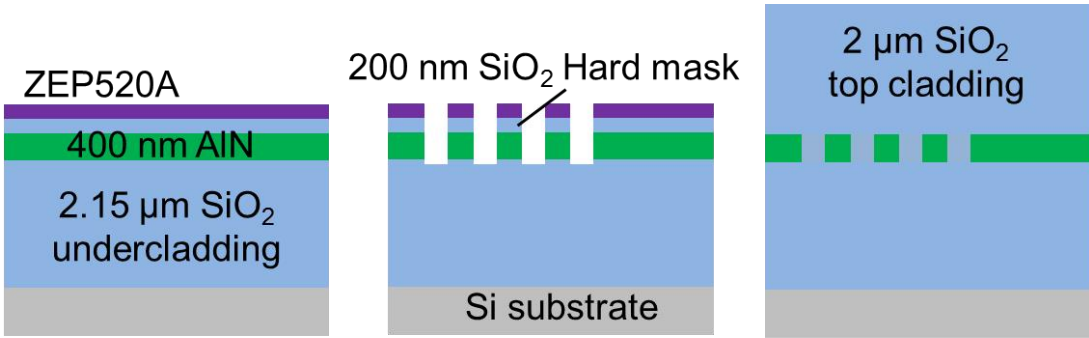


n_{eff} (average) = 1.6, $\Lambda = 1.2 \mu\text{m}$

Cladding layers: 2.15 μm & 2.0 μm

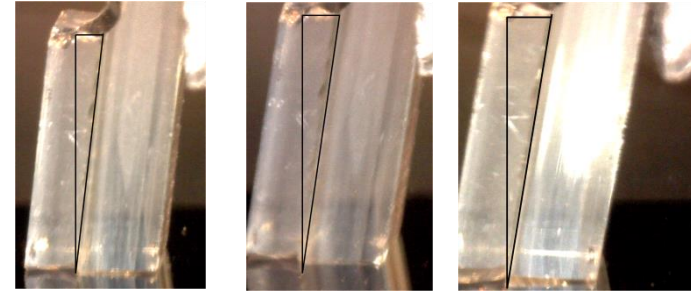
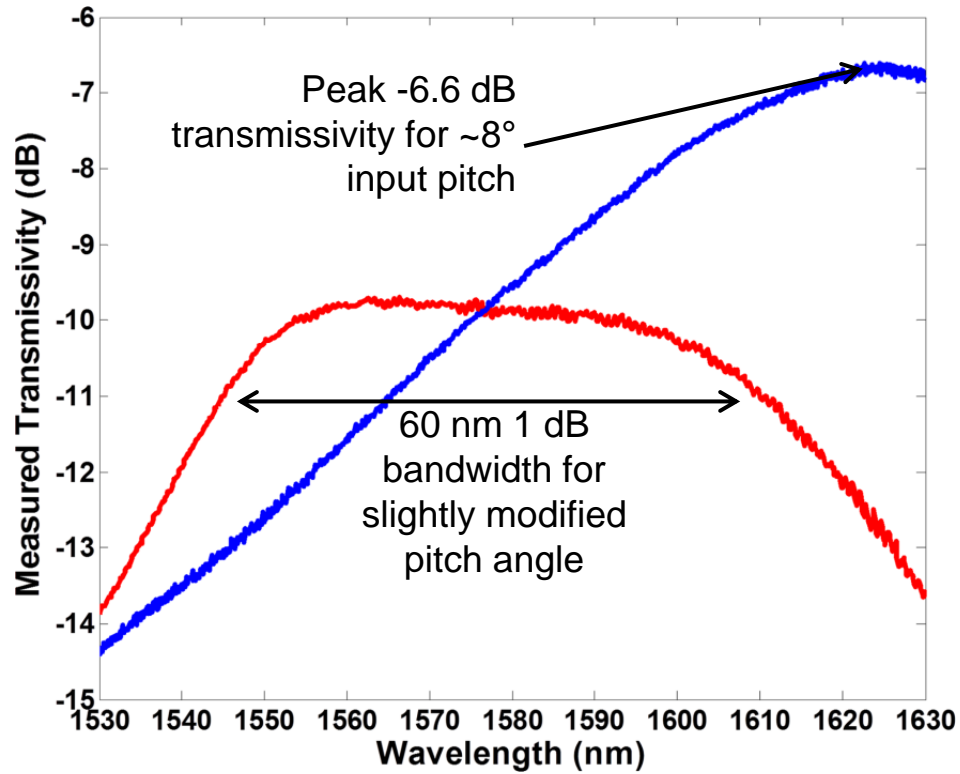


Fabrication

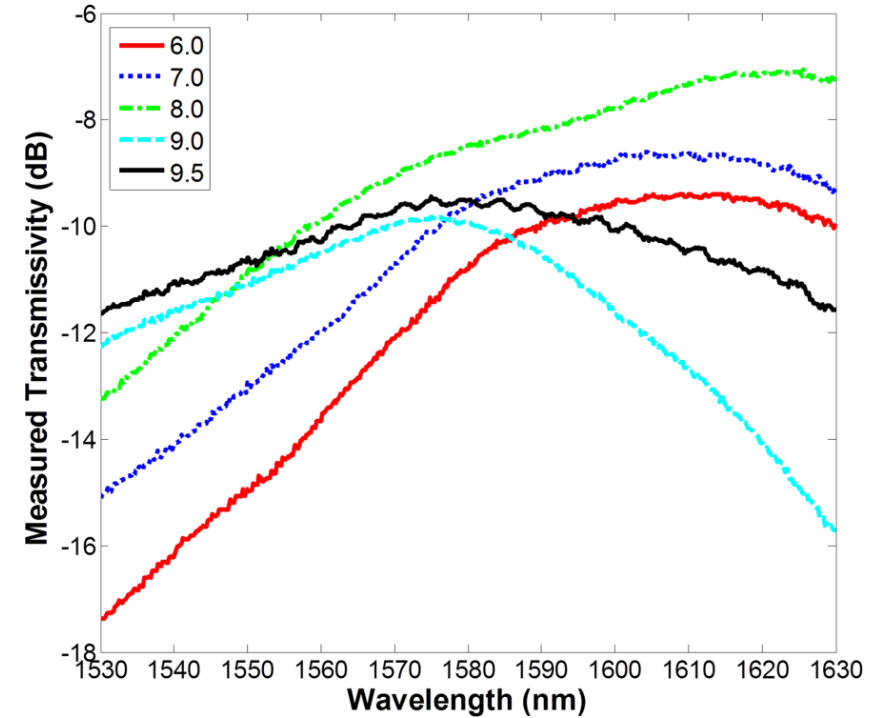


AlN etch – Plasmatherm Versaline	
RF Power	125 W
ICP Power	400 W
Pressure:	5 mT
Cl2 flow:	25 sccm
BCl3 flow:	5 sccm
Ar flow:	70 sccm
Temperature:	25C electrode 120C lid 70C liner 120C spool

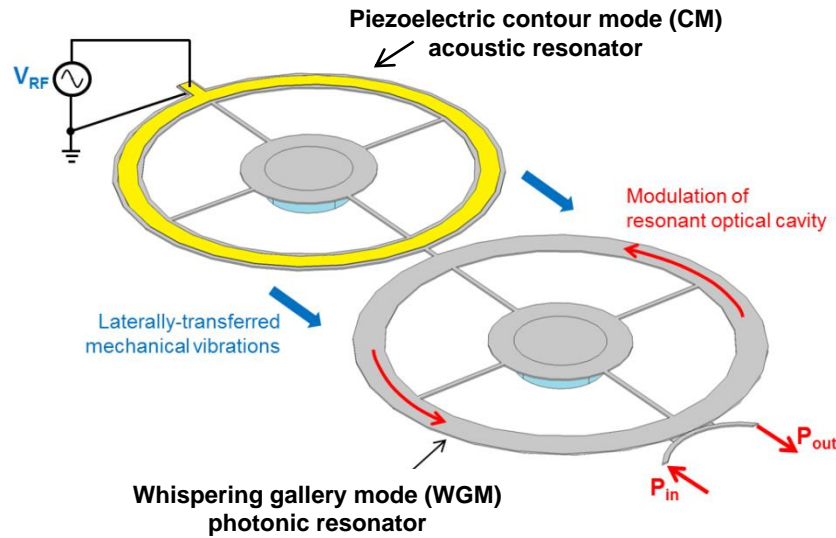
Grating Measurements



Varying pitch angle (8° initial):



Acousto-Optic Modulator – Concept

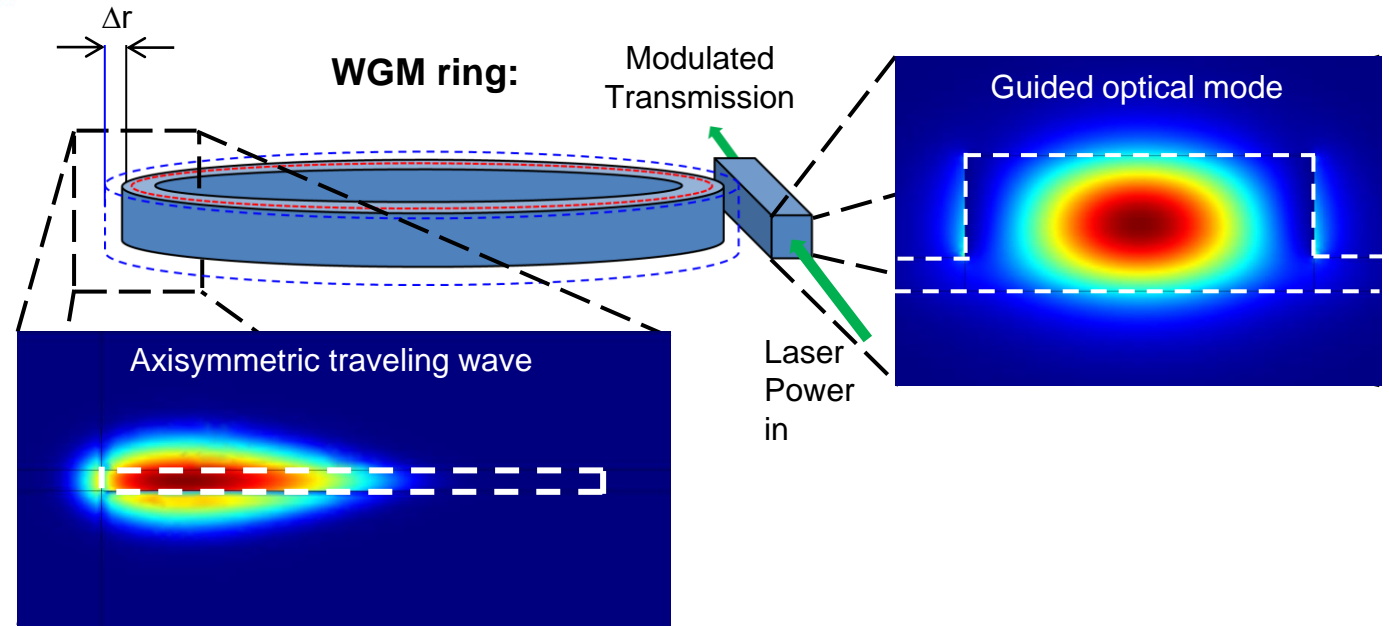
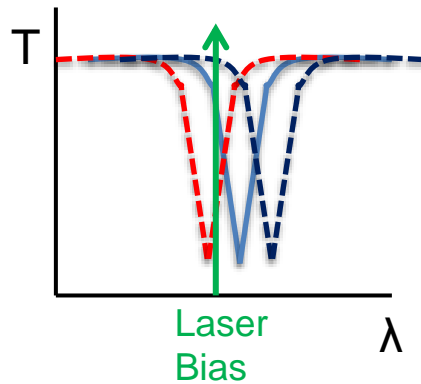


- Piezoelectric actuation generates perturbations to the optical resonance condition:

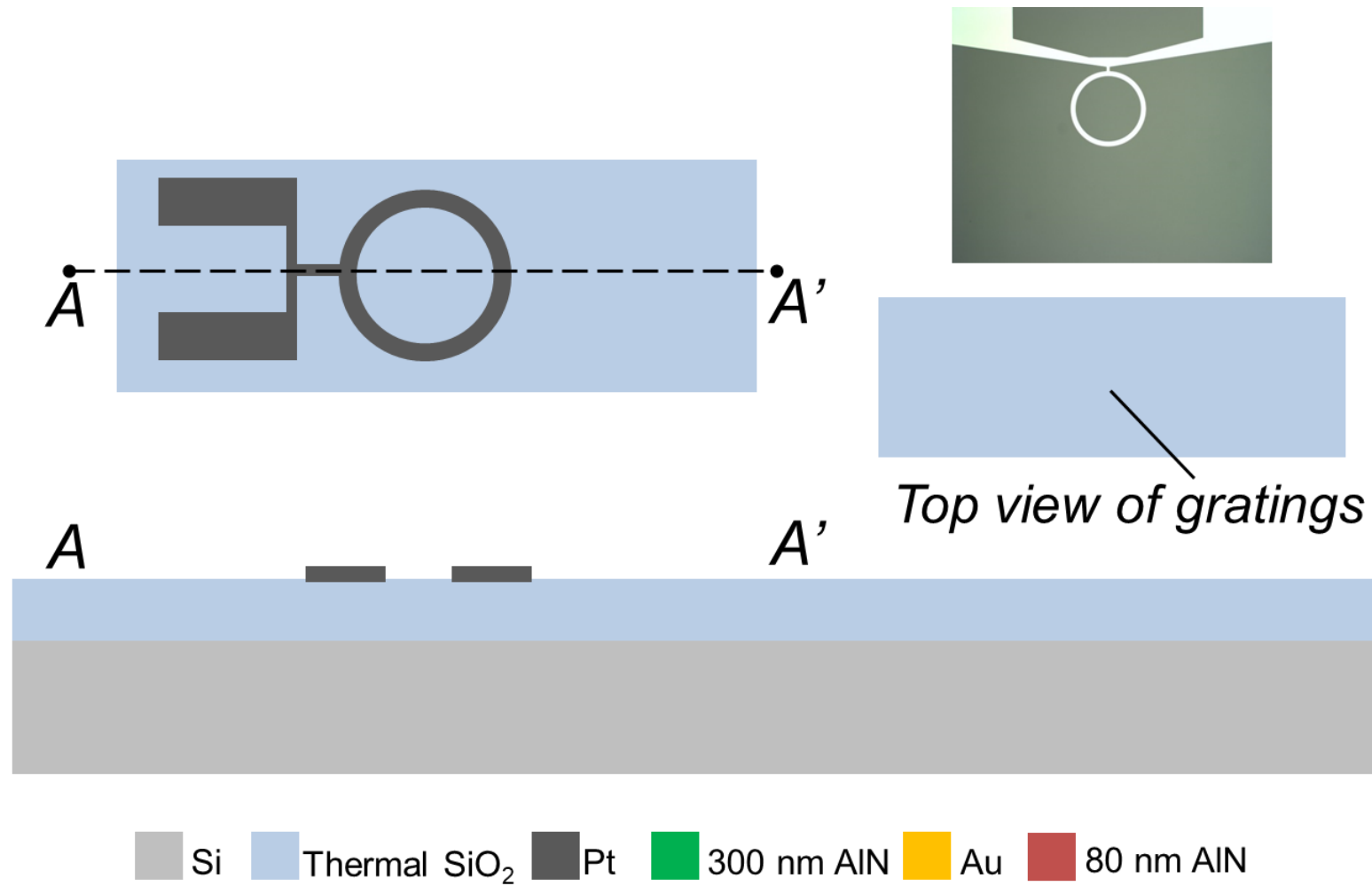
$$m\lambda_o = n_{eff} \cdot 2\pi R$$

- Optical intensity modulation of the output given by:

$$P_{mod} = \frac{dT}{d\lambda} \cdot \frac{d\lambda}{dr} \cdot \Delta r \leftarrow \Delta r = \eta_{om} V_{rms}$$

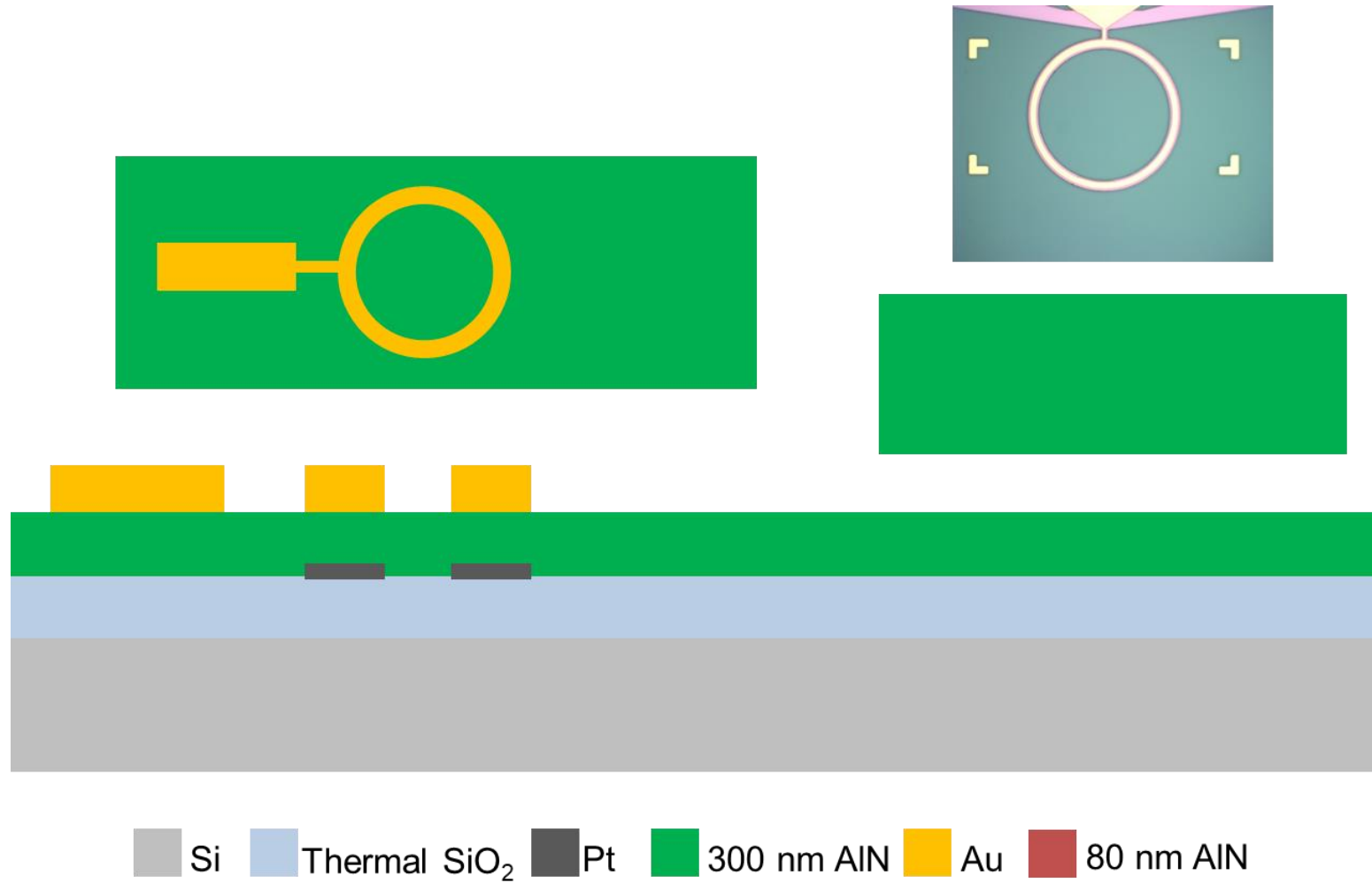


Lift-off for Pt Bottom Electrodes on Thermally Oxidized HR Wafer

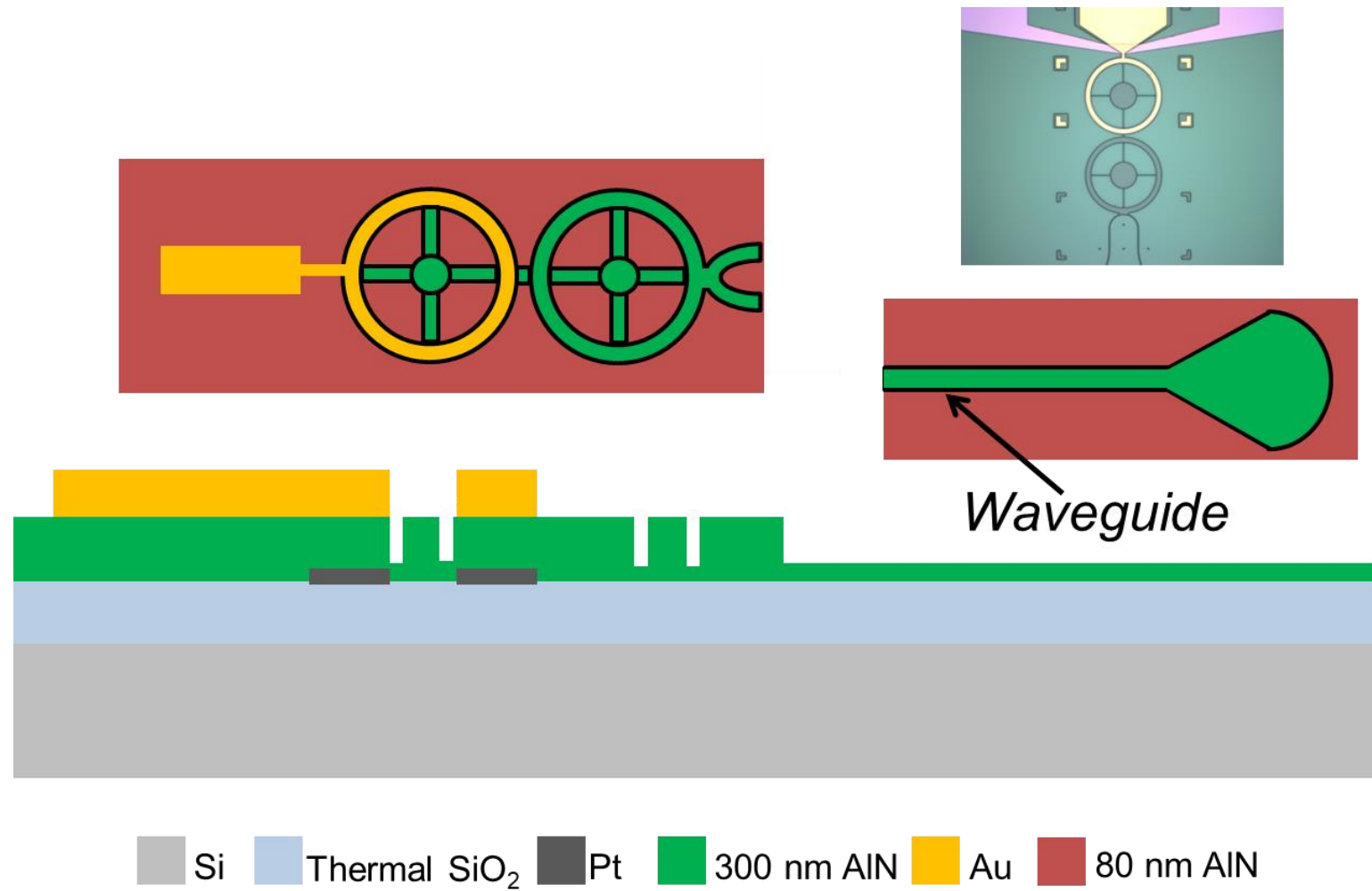




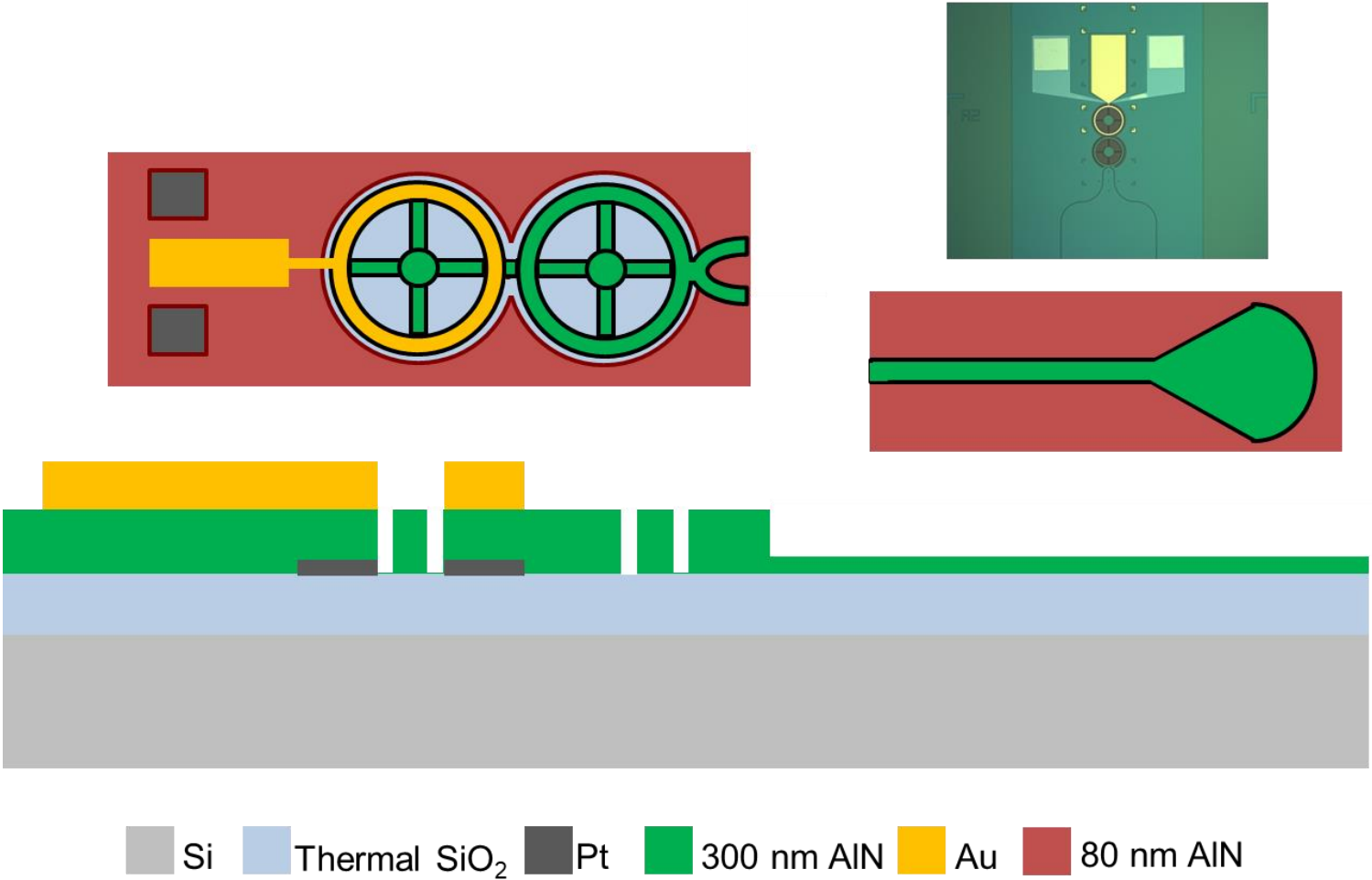
300 nm AlN Deposition & Lift-off for Au Top Electrodes



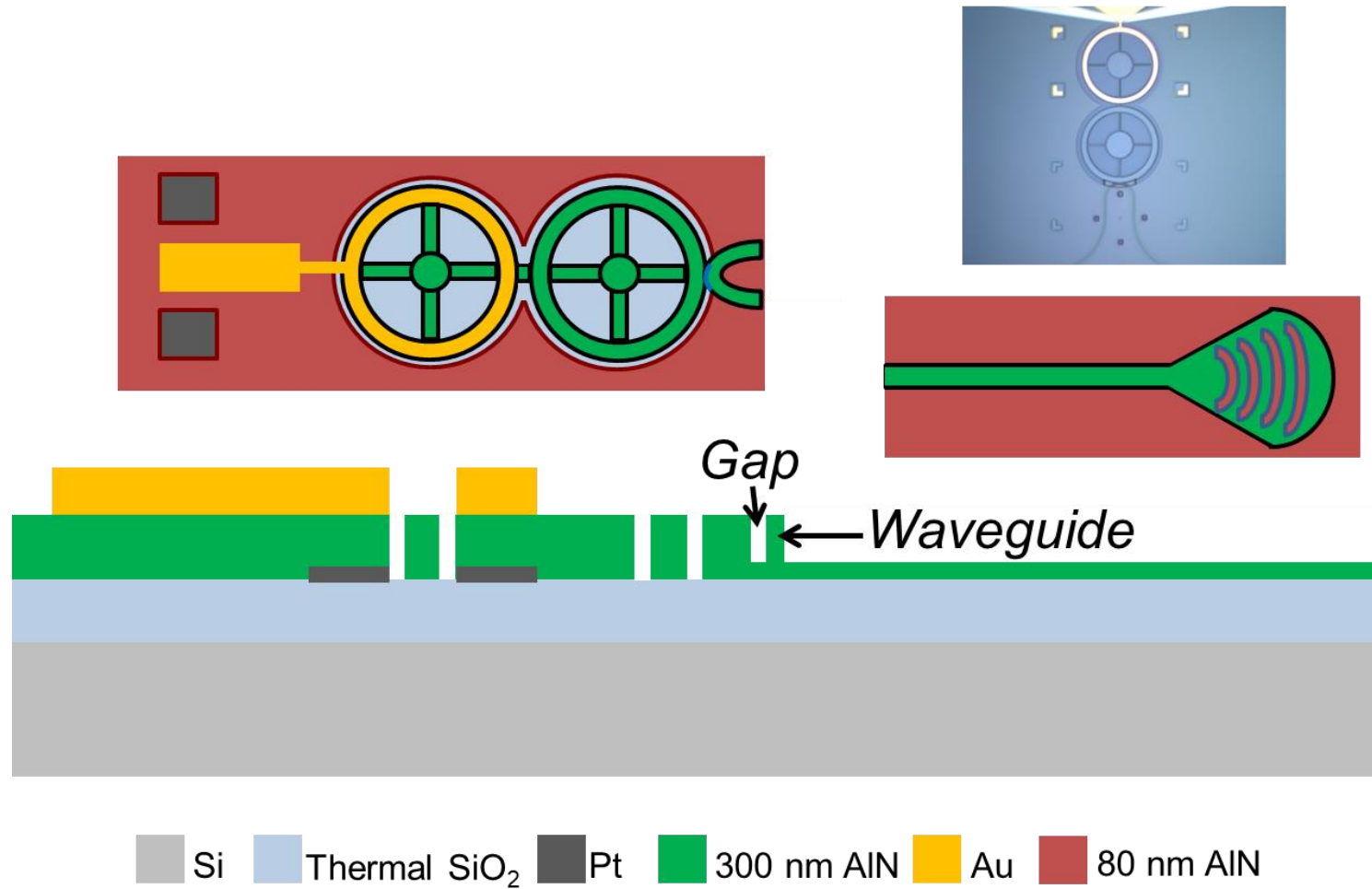
1st AlN Partial Etch: Define Large Features (Resonators, Waveguides)



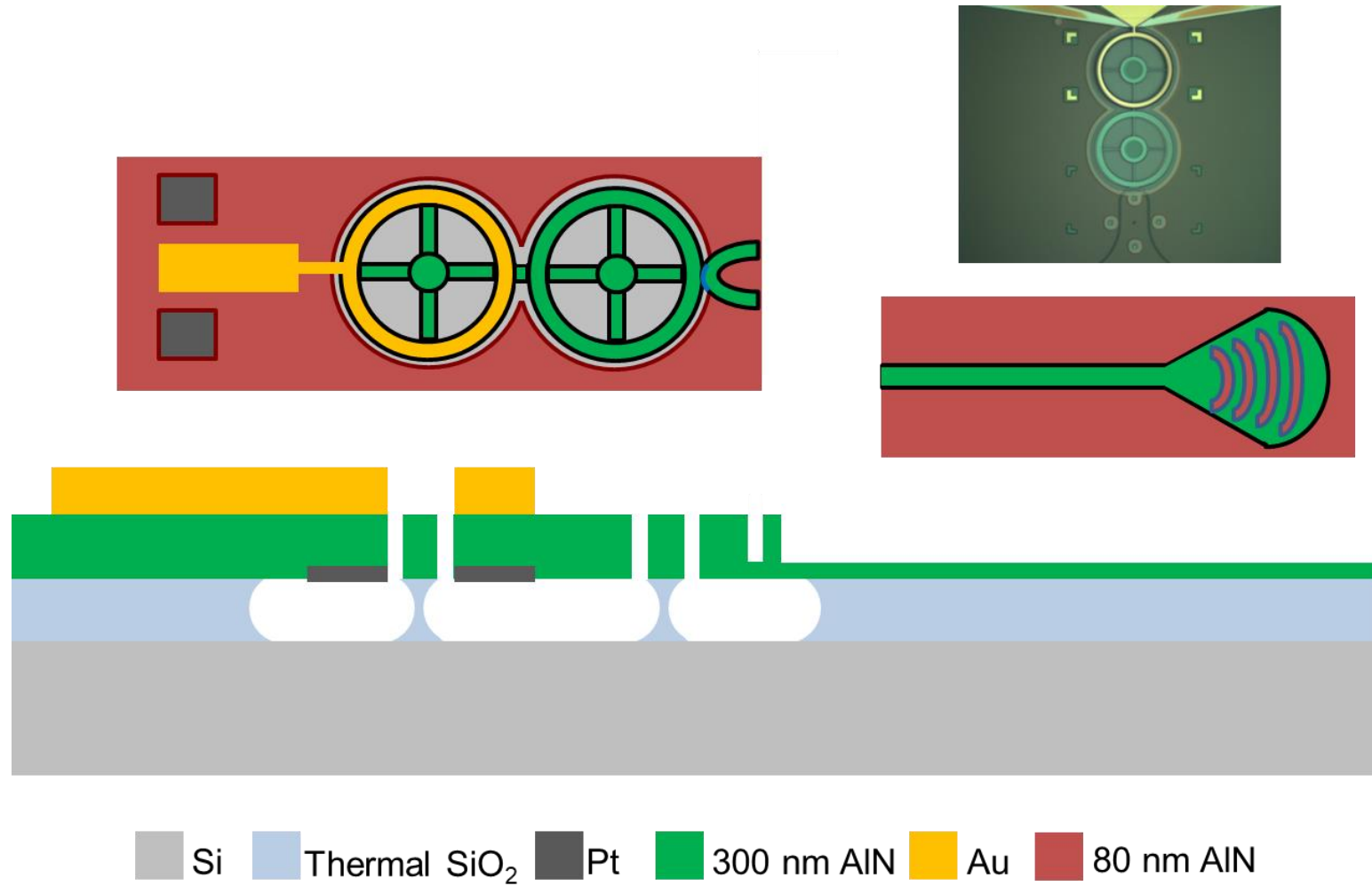
Define Vias (to bottom Pt) and Release Windows – Etch through AlN



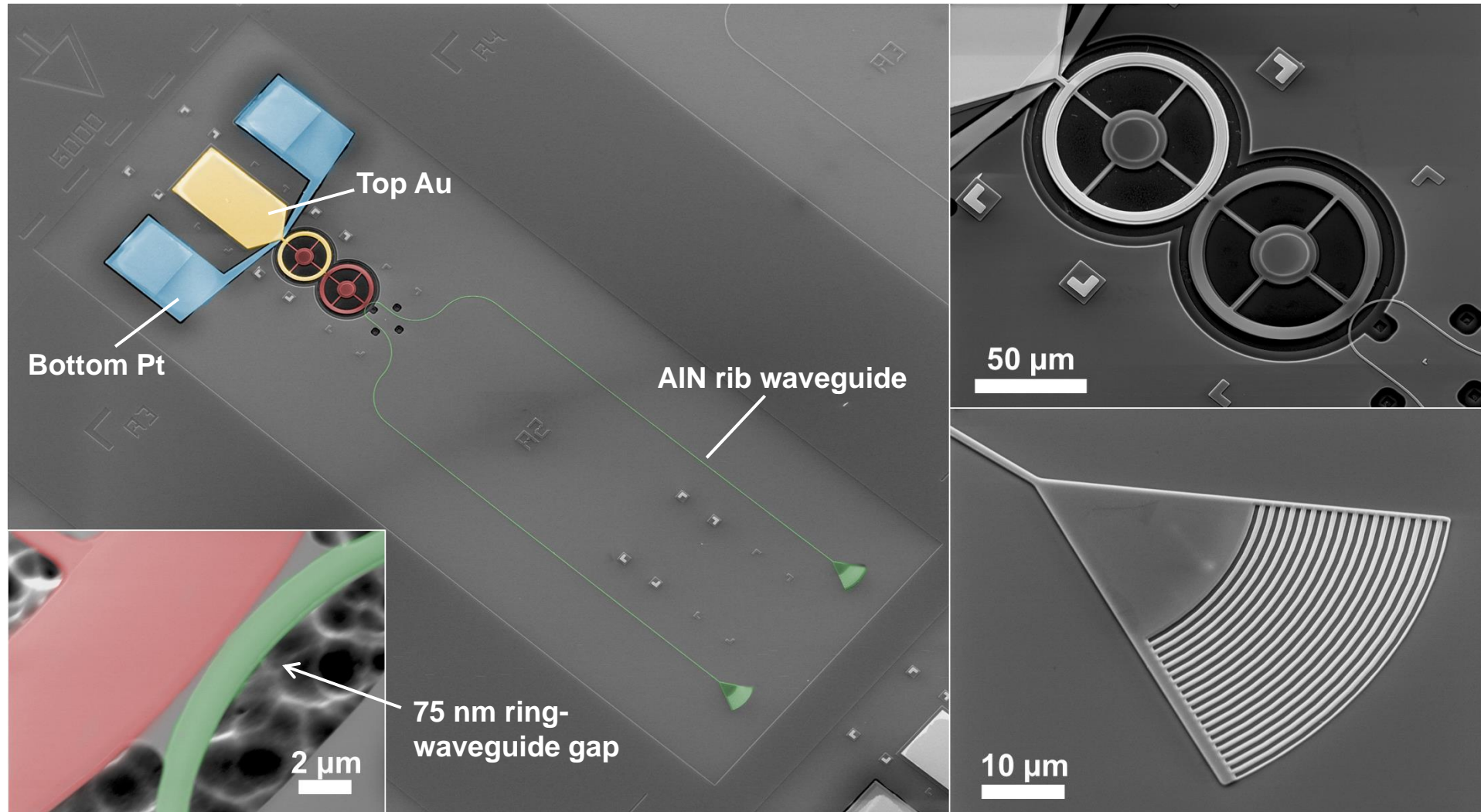
E-beam Lithography of Gaps and Gratings + 2nd Partial etch



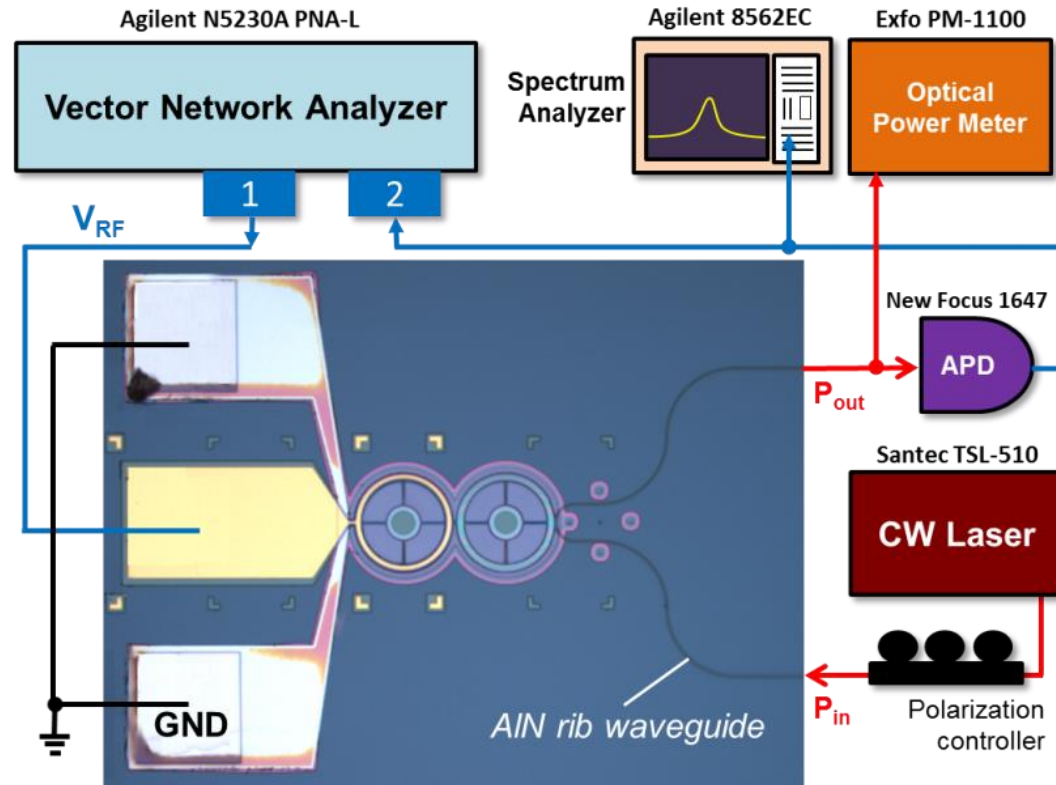
Vapor HF Release of CMR and WGM Resonators



Integrated Modulator Device



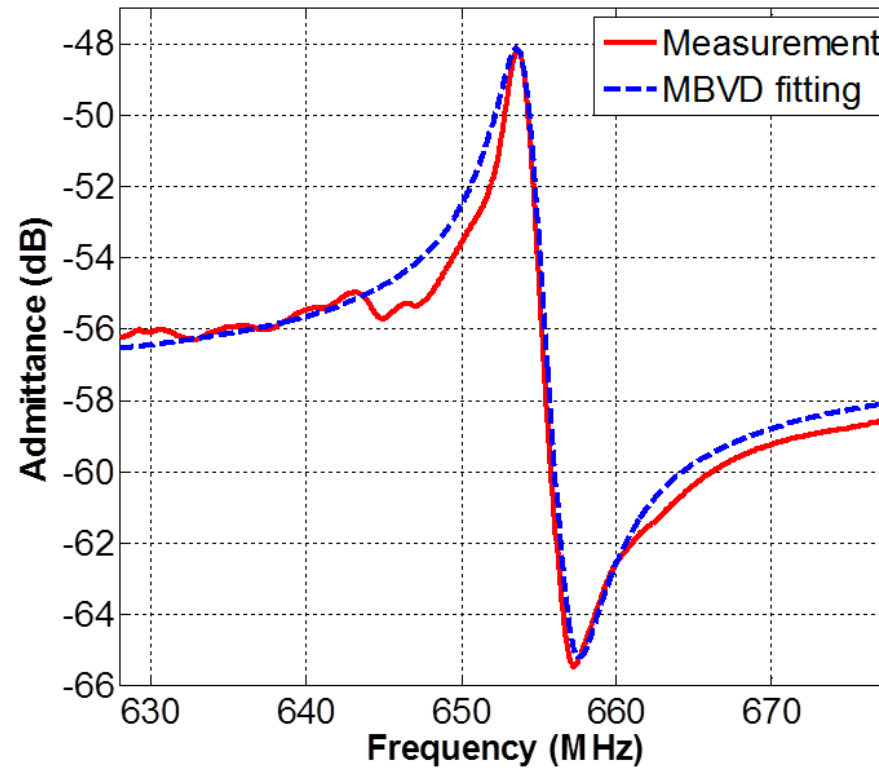
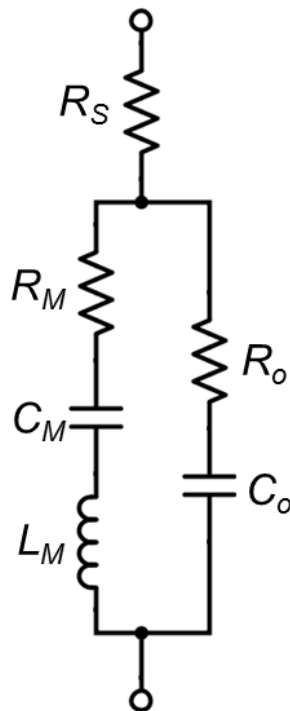
Acousto-Optic Modulator Characterization



- Device characterization is done for both types of resonator
- Acoustic resonator tested with RF ground-signal-ground probes to extract S_{11} parameters
- Optical resonator tested with fiber array
- Simultaneous probing for electro-optomechanical characterization (via S_{21} or Spectrum Analyzer)

Acoustic Resonator Response

- Modified Butterworth van Dyke (MBVD) equivalent circuit model:



Fitted parameters:

$$f_o = 653.96 \text{ MHz}$$

$$Q_{mech} = 270$$

$$k_t^2 = 1.16\%$$

$$R_S = 68 \Omega$$

$$R_M = 220 \Omega$$

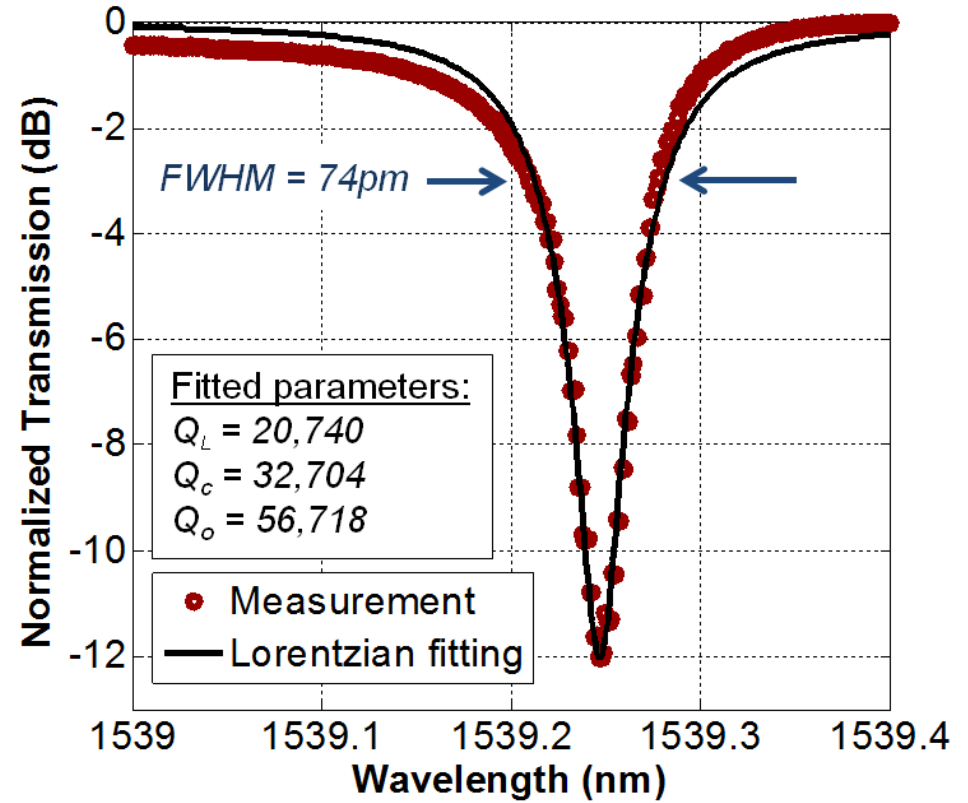
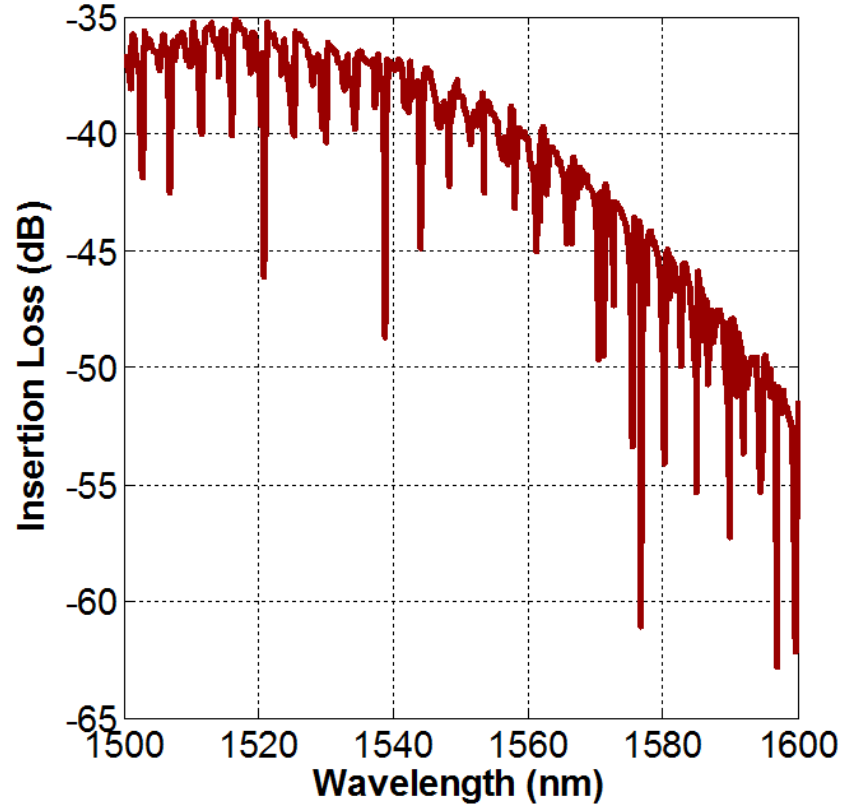
$$C_M = 3.24 \text{ fF}$$

$$L_M = 18.22 \text{ uH}$$

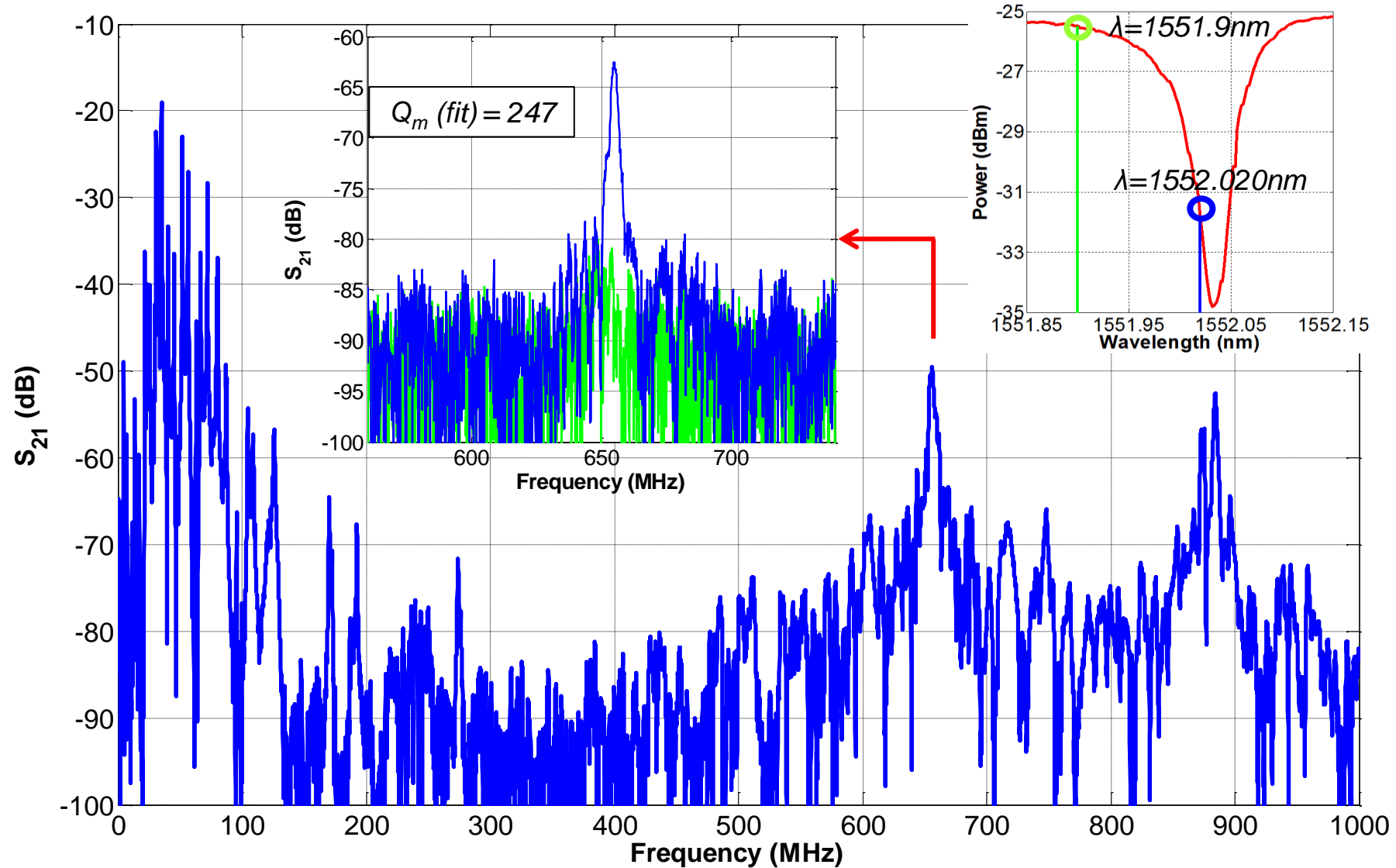
$$R_o = 100 \Omega$$

$$C_o = 345 \text{ fF}$$

Photonic Resonator Response



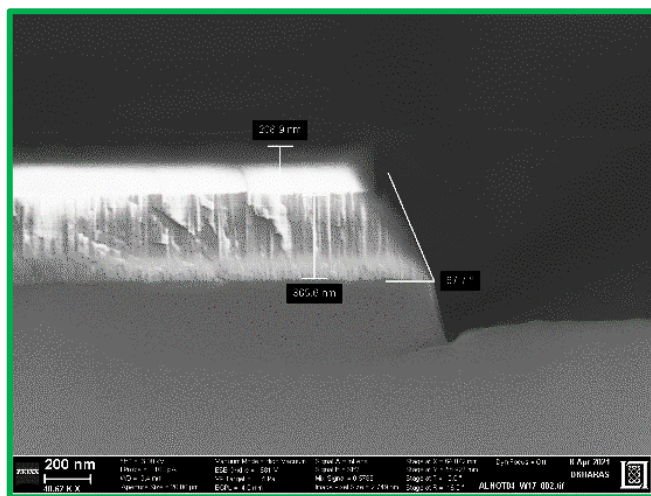
Forward Transmission (S_{21}) – Electro-Optomechanical Measurement



200-mm wafer processing – etch development

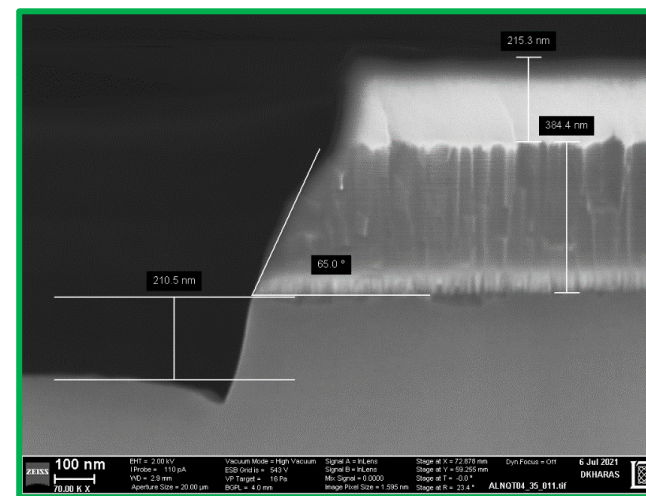
Applied Materials Centura Metal Etch

	Variables:	Best Condition:
ICP Power (W)	{1000, 1200}	1000
Bias Power (W)	{100, 125}	125
Pressure (mTorr)	{4, 6, 15}	6
Cl ₂ flow (sccm)	{0, 40, 82, 120}	120
BCl ₃ flow (sccm)	{0, 10, 20, 58, 100}	10
Ar flow (sccm)	{0, 20, 40, 80}	40
Total flow (sccm)	{100, 160, 170, 180, 220}	170
Etched Result:	Angle	~65°

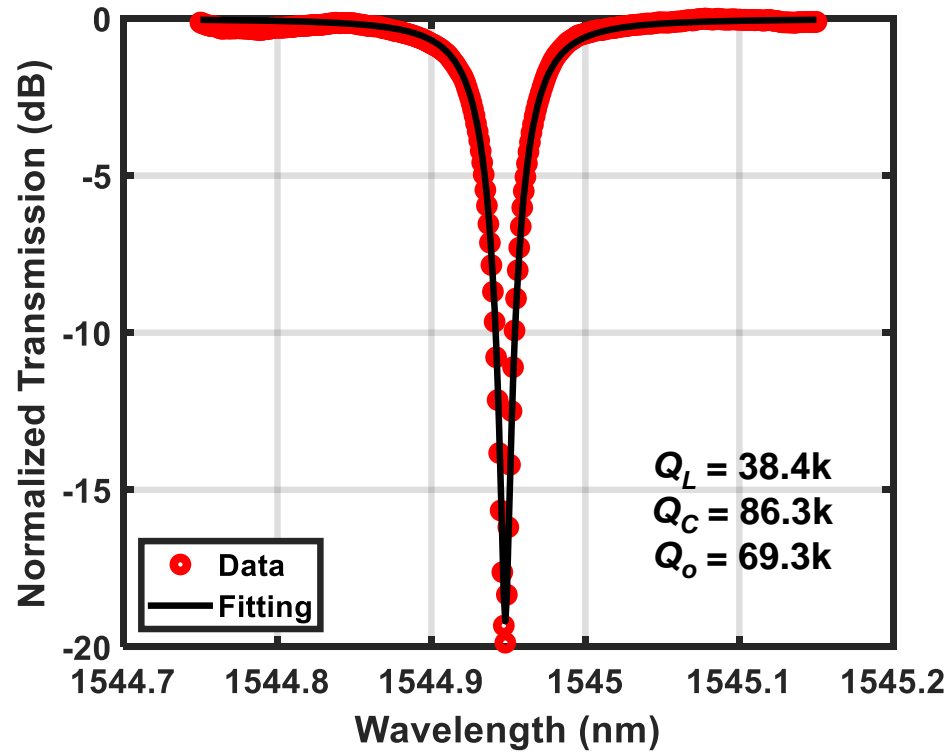


SAMCO Metal Etch

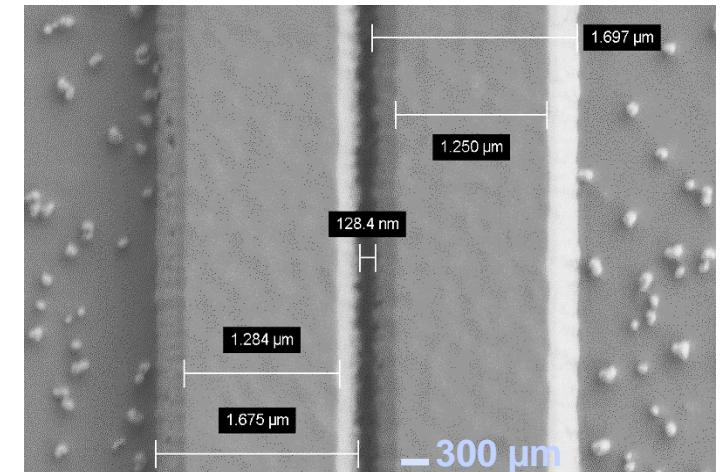
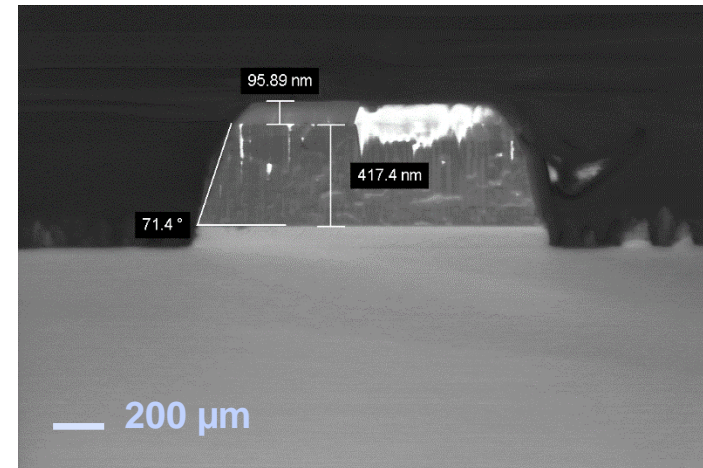
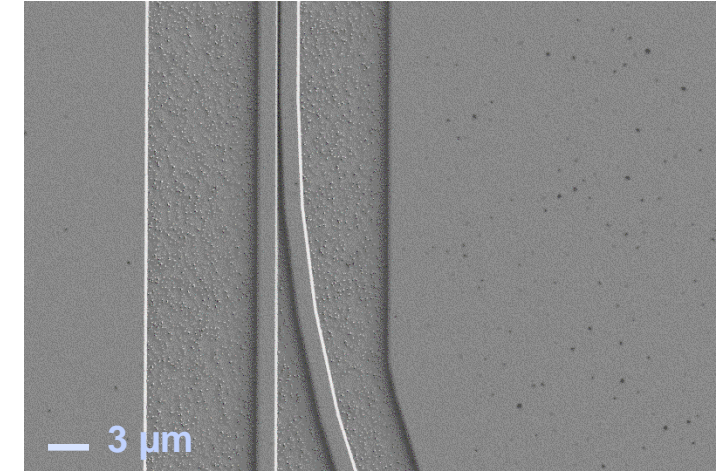
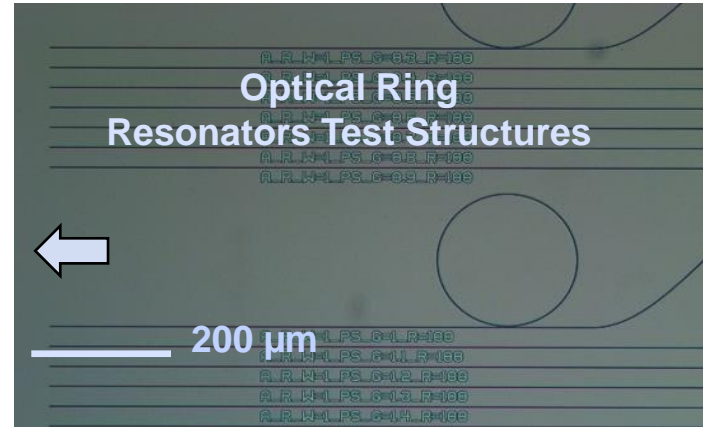
	Variables:	Best Condition:
ICP Power (W)	{600}	600
Bias Power (W)	{200}	200
Pressure (Pa)	{0.4, 0.7, 1.1}	0.4
Cl ₂ flow (sccm)	{14, 20, 30, 40, 65, 90}	40
BCl ₃ flow (sccm)	{0, 5, 10, 15, 40}	10
Ar flow (sccm)	{0, 6, 10, 15}	0
Total flow (sccm)	{20, 30, 35, 40, 50, 115}	50
Etched Result:	Angle	~65°



Initial Optical Ring Resonator Measurements



Target Q achievable through:
5-10X enhancement for disk resonator geometries
2-3X improvement from etching optimization



Conclusions

- **AlN is an excellent platform for photonic integration targeting applications in RF-Photonics as well as quantum information processing**
- **Low-loss gratings and waveguides have been demonstrated with sputtered AlN thin films**
- **Piezoelectric and photonic resonators are successfully co-fabricated to demonstrate displacement-based acousto-optic modulators**
- **Further improvements to processing will enable microwave-to-optical frequency converters in 200-mm platform**



Acknowledgements

Carnegie Mellon University:

- **Prof. Gianluca Piazza**
- **Matt Moneck**
- **Norm Gottron**
- **James Rosvanis**
- **National Science Foundation (NSF ECCS-1201659)**

Northeastern University:

- **Jack Guida**
- **Michele Pirro**
- **Prof. Matteo Rinaldi**

MITLL Quantum Transducer team:

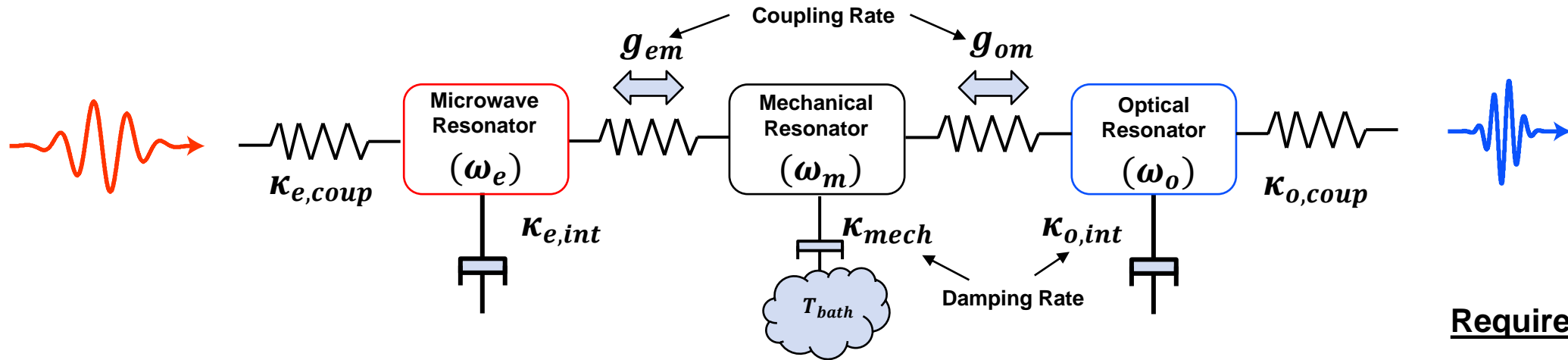
- **Dave Kharas**
- **Danna Rosenberg**
- **Alex Medeiros**
- **Matt Cook**
- **Cyrus Hirjibehedin**
- **Paul Juodawlkis**

Thank you!



Supplementary

Optical-to-Microwave Photon Conversion



Efficiency

$$\eta_e = \frac{\kappa_{e,coup}}{\kappa_{e,coup} + \kappa_{e,int}}$$

$$\eta_{mech} = \frac{4C_{em}C_{om}}{(C_{em} + C_{om} + 1)^2}$$

$$\eta_o = \frac{\kappa_{o,coup}}{\kappa_{o,coup} + \kappa_{o,int}}$$

Bandwidth

$$\Gamma_{em} = \frac{4g_{em}^2}{\kappa_{e,coup} + \kappa_{e,int}}$$

$$\Gamma_{om} = \frac{4g_{om}^2}{\kappa_{o,coup} + \kappa_{o,int}}$$

Cooperativity

$$C_{em} = \frac{\Gamma_{em}}{\kappa_{mech}}$$

$$C_{om} = \frac{\Gamma_{om}}{\kappa_{mech}}$$

Requirements

$$\kappa_{coup} \gg \kappa_{int}$$

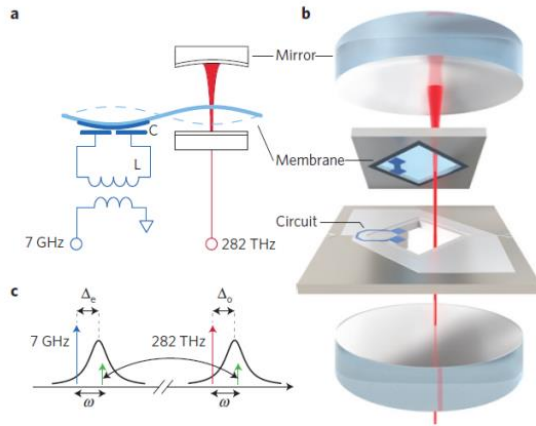
Large g

$$\kappa_{mech} \ll \Gamma$$

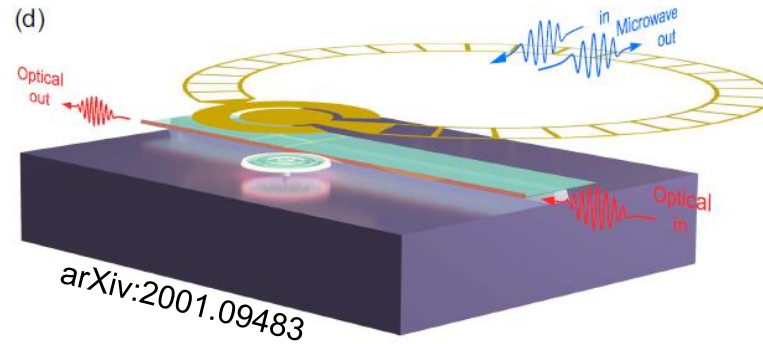
High-efficiency, high-bandwidth, low-noise conversion requires overcoupled resonators, strong coupling between resonators, and low resonator losses

Overview of Recent Work

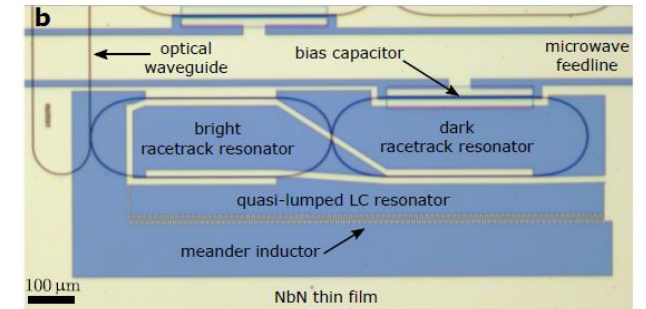
Electro-static optomechanical



Piezo optomechanical



Electro-optic



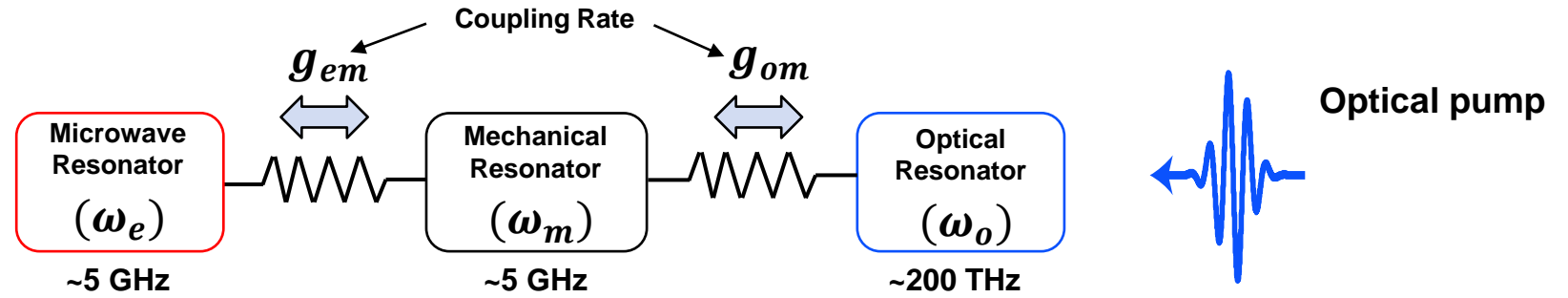
	Electro-static	Piezo-based	Electro-optic
Efficiency	47% [1]		
Coupling strength g_0	few Hz [1]	10's kHz to MHz [2,3,4]	100's Hz [5,6]
Noise			
Scalability			

1. Higginbotham et al, Nature Physics (2018)
2. Han et al, arXiv (2020)

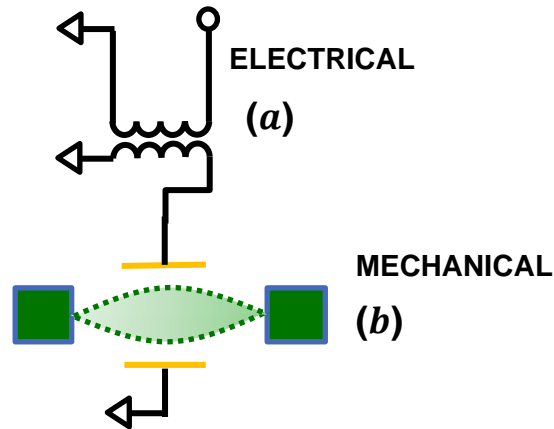
3. Forsch et al, Nature Physics (2020)
4. Mirhosseini et al, Nature (2020)

5. Fan et al, Science Adv. (2018)
6. Holzgrafe et al, arXiv (2020)

Piezo-mechanical and Opto-mechanical Coupling



Piezo-mechanical coupling



- Same frequency for mech. and elec. resonators
- Native beamsplitter interaction that swaps an excitation between the two resonators

Opto-mechanical coupling

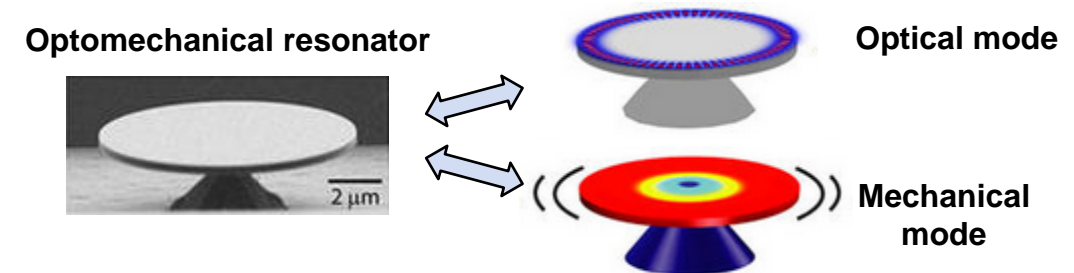


Image adapted from: <https://www.nist.gov/news-events/news/2013/08/wideband-wavelength-conversion-using-cavity-optomechanics>

- Requires pump to get beamsplitter interaction
- Coupling rate can be tuned with power
- Low $g_{0,om}$ combined with optical losses can lead to high thermal occupation, leading to noise

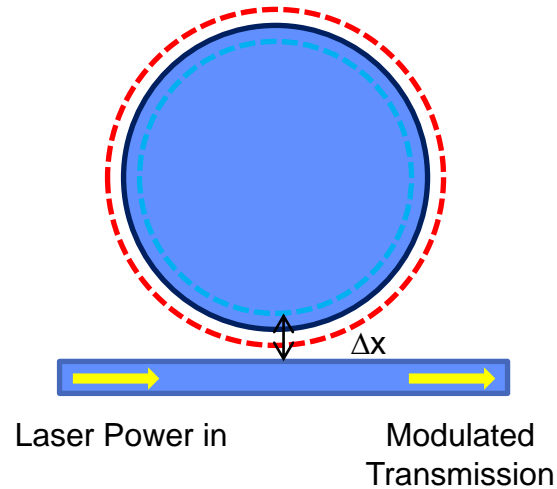
AlN as a photonic material: CMOS integrable, piezoelectric, elasto-optic effects, with low optical losses

	Si	SiO ₂	Si ₃ N ₄	GaAs	GaN	LiNbO ₃	AlN
Index (1550 nm, Ordinary)	3.47	1.45	~2.0	3.37	2.31	2.21	~2.04
Bandgap	1.12 eV	8.9 eV	5.1 eV	1.43 eV	3.4 eV	4.0 eV	6.2 eV
Optical losses (α) in integrated structure	0.3 dB/cm <i>Waveguide</i> <i>(Cardenas et al., 2009)</i>	0.007 dB/cm <i>Microtoroid resonator</i> <i>(Polman et al., 2004)</i>	0.055 dB/cm <i>Ring resonator</i> <i>(Gondarenko et al., 2009)</i>	0.5 dB/cm <i>Waveguide</i> <i>(Inoue et al., 1985)</i>	0.65 dB/cm <i>Waveguide</i> <i>(Stolz et al., 2011)</i>	2.03 dB/cm <i>Disk resonator</i> <i>(Wang et al., 2014)</i>	0.6 dB/cm <i>Ring resonator</i> <i>(Xiong et al., 2012)</i>
Piezoelectric	☒	☒	☒	d ₃₁ = 0 d ₃₃ = 0 d ₁₄ = -2.7 pC/N	d ₃₁ = -1.9 pC/N d ₃₃ = 3.7 pC/N	d ₃₁ = -1 pC/N d ₃₃ = 6 pC/N (Z-cut)	d ₃₁ = -1.98 pC/N d ₃₃ = 4.98 pC/N
Elasto-Optic	☒	☒	☒	p ₁₁ = -0.026	p ₁₁ = -0.086* (estimated)	p ₁₁ = -0.026	p ₁₁ = -0.10* (estimated)

*S. Yu. Davydov, *Semiconductors* **36**, 41-44 (2002); G. Bu, et al., *Appl. Phys. Lett.* **85**, 2157 (2004).

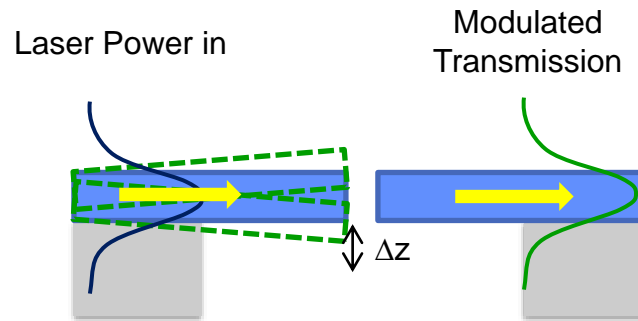
Modulation of Mechanically-Actuated Structures

i) Mechanical displacements perturbing WGM resonator



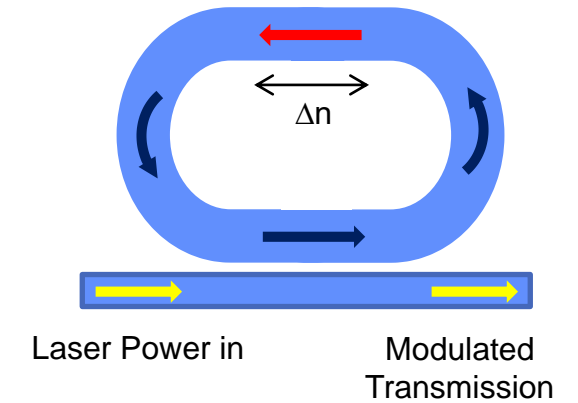
$$\Delta T(x, n) = \frac{\partial T}{\partial x} \Delta x$$

ii) Mechanical displacements perturbing waveguide end-coupling



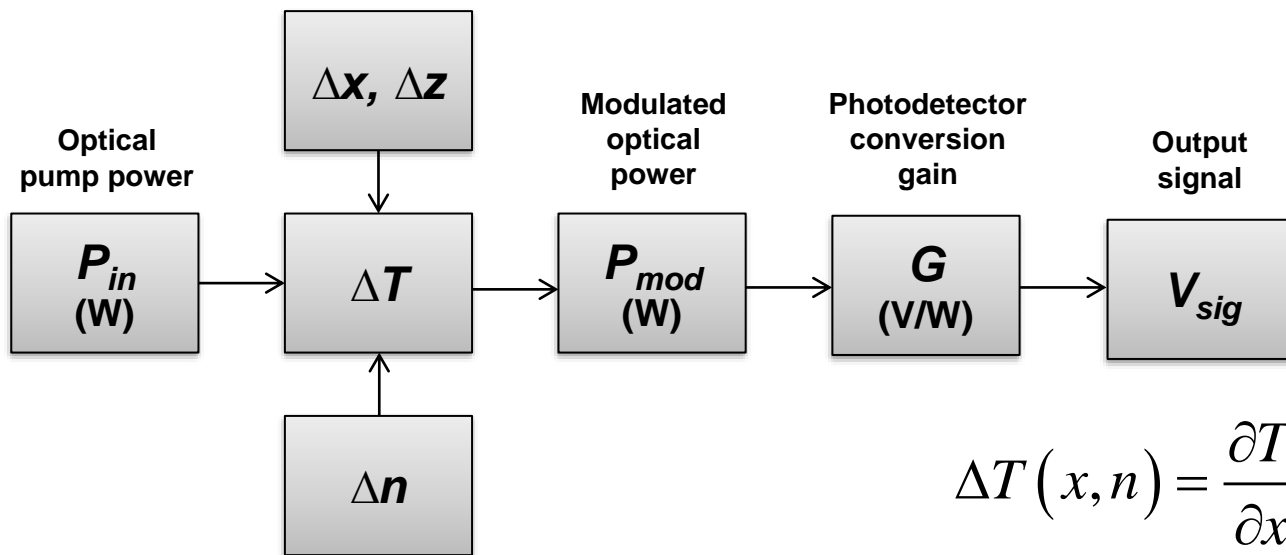
$$\Delta T(z, n) = \frac{\partial T}{\partial z} \Delta z$$

iii) Strain-induced refractive index changes



$$\Delta T(x, n) = \frac{\partial T}{\partial n} \Delta n$$

Optomechanical Modulation Model



$$\Delta T(x, n) = \frac{\partial T}{\partial x} \Delta x + \frac{\partial T}{\partial n} \Delta n = \frac{\partial T}{\partial \lambda} \left(\frac{\partial \lambda}{\partial x} \Delta x + \frac{\partial \lambda}{\partial n} \Delta n \right)$$

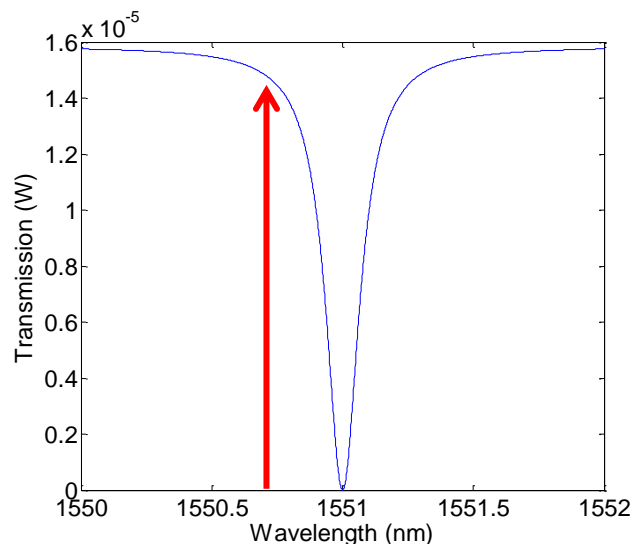
Fit data to Lorentzian:

P_{trans} = Insertion loss

Γ = FWHM

$$T(\lambda) = P_{trans} \left(1 - \frac{\Gamma^2}{4(\lambda - \lambda_o)^2 + \Gamma^2} \right)$$

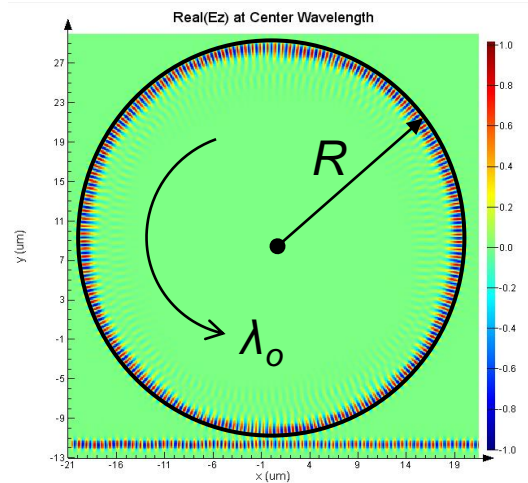
$$Q_L = \frac{\lambda_o}{\Gamma}$$



Bias laser with blue-cavity detuning and assume maximum slope of cavity Lorentzian:

$$\frac{dT}{d\lambda} = \frac{P_{trans} 8\Gamma^2 (\lambda - \lambda_o)}{[4(\lambda - \lambda_o)^2 + \Gamma^2]^2}$$

Displacement and Refractive Index Based Modulation



Resonance condition:

$$n_{eff} L = m \lambda_o$$

$$n_{eff} (2\pi R) = m \lambda_o$$

$$n_{eff} 2\pi (R + \Delta r) = m (\lambda_o + \Delta \lambda)$$

$$\frac{d\lambda}{dr} = \frac{\lambda_o}{R} = g_{om\lambda}$$

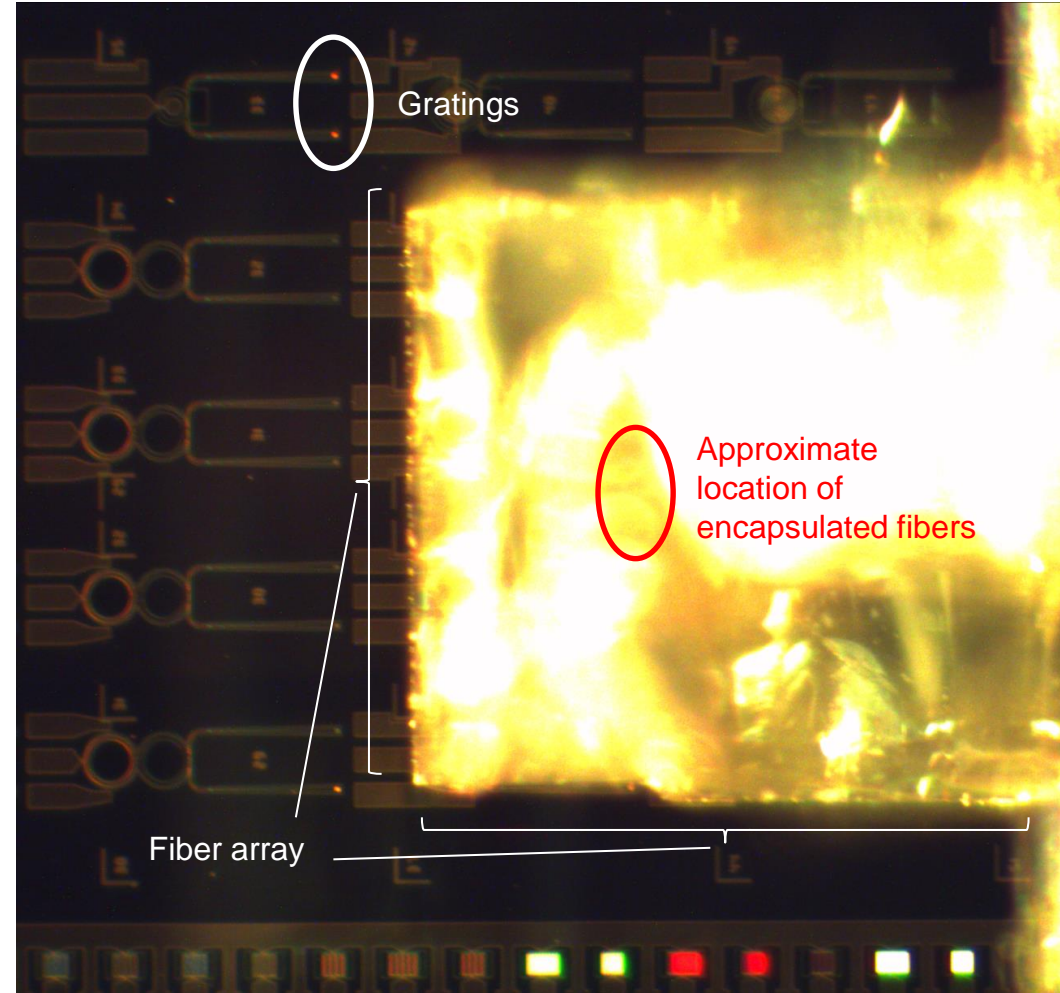
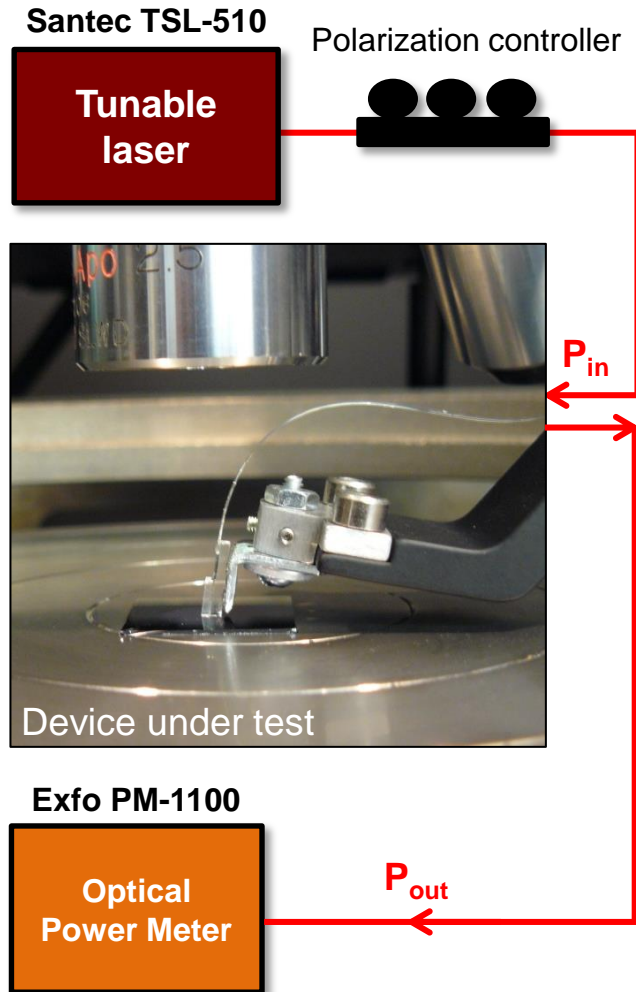
Where dr is produced by piezoelectrically induced displacements

$$(n_{eff} + \Delta n_{eff}) 2\pi R = m (\lambda_o + \Delta \lambda)$$

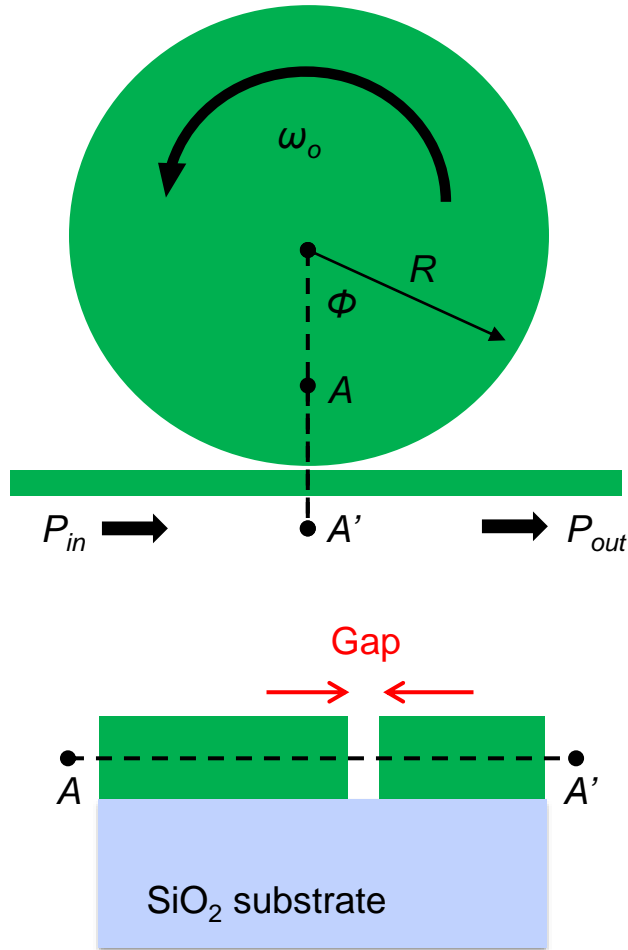
$$\frac{d\lambda}{dn_{eff}} = \frac{\lambda_o}{n_{eff}}$$

Where dn_{eff} is produced by piezoelectrically generated strain

Test Setup



Photonic Resonator Coupling



Waveguide-Resonator coupling:

$$T(\omega) = \frac{P_{out}}{P_{in}} = \left| \frac{j2(\omega - \omega_0) + \frac{1}{Q_o} - \frac{1}{Q_c}}{j2(\omega - \omega_0) + \frac{1}{Q_o} + \frac{1}{Q_c}} \right|^2 \quad \& \quad \frac{1}{Q_L} = \frac{1}{Q_o} + \frac{1}{Q_c}$$

Regimes of operation:

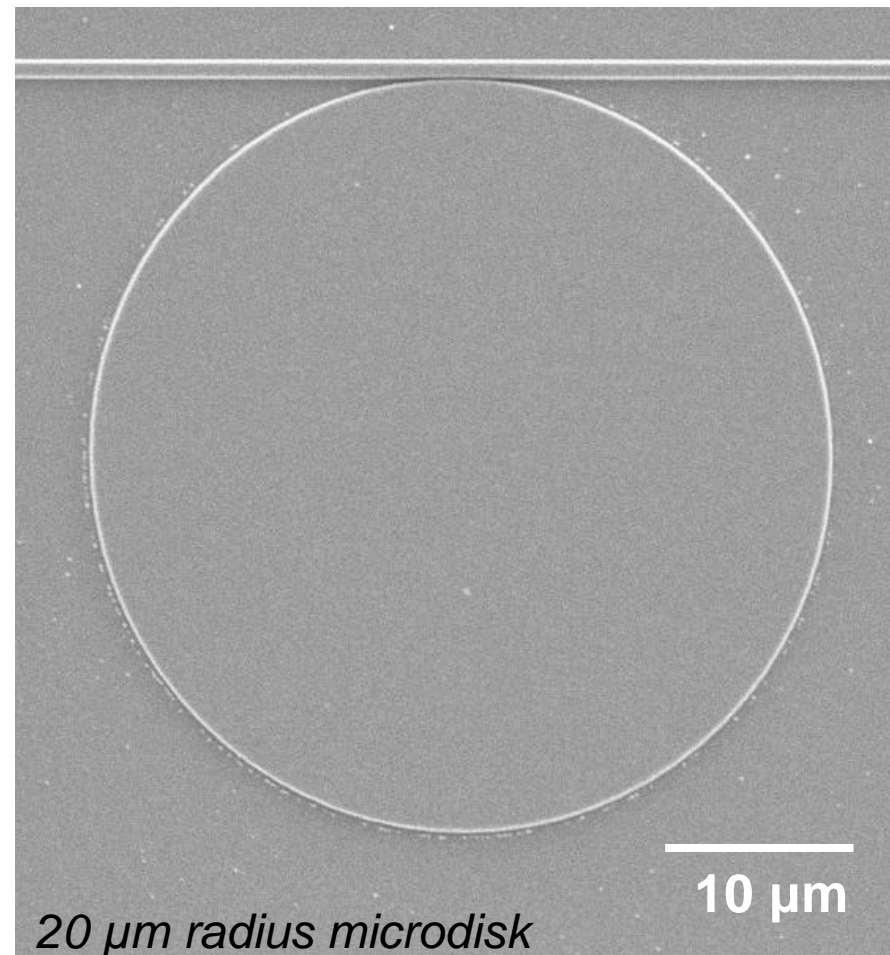
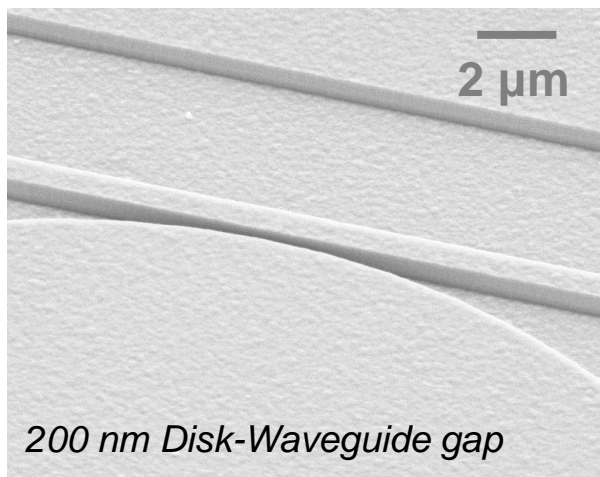
- i) $Q_c > Q_o$: Undercoupled
- ii) $Q_c = Q_o$: Critically coupled ←
- iii) $Q_c < Q_o$: Overcoupled

Attenuation losses:

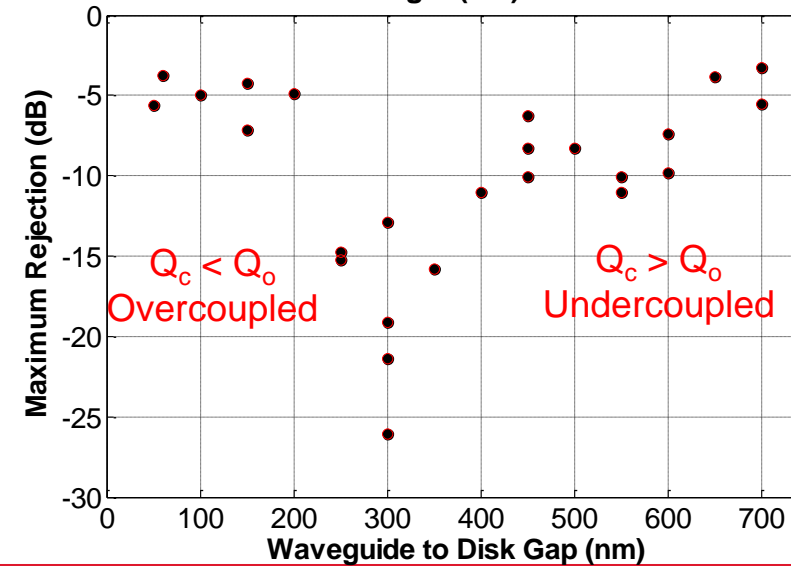
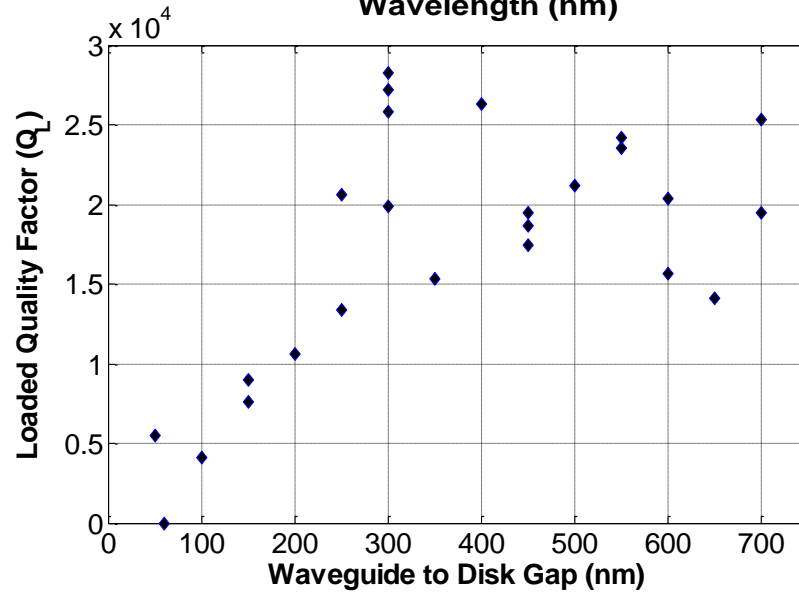
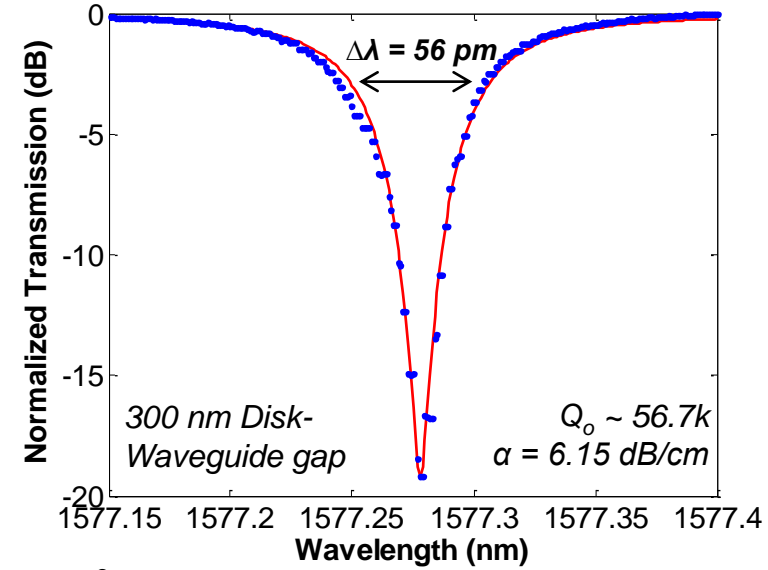
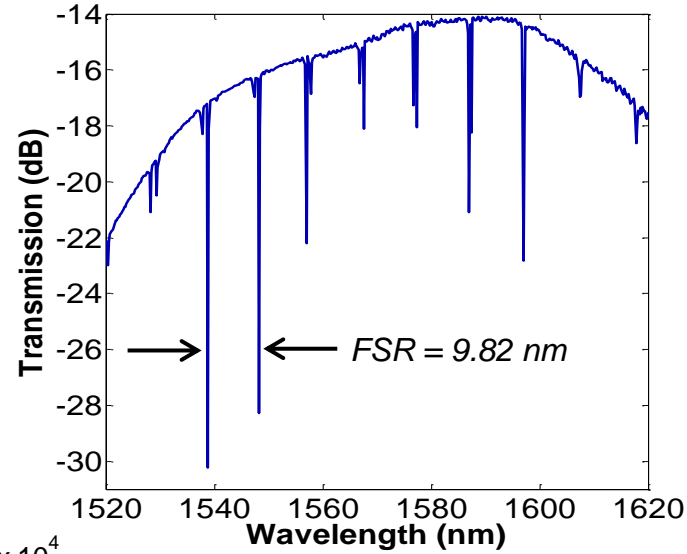
$$n_g \approx \frac{\lambda_o^2}{(FSR)(L)} \quad \longrightarrow \quad Q_L = \frac{1}{2} Q_o = \frac{\pi n_g}{\lambda_o \alpha_{disk}}$$

Vary Gap Widths to Microdisks

Fix: $R = 20\ \mu\text{m}$, Bus WG = 850 nm,
Gap: 50 nm – 700 nm in 50 nm increments

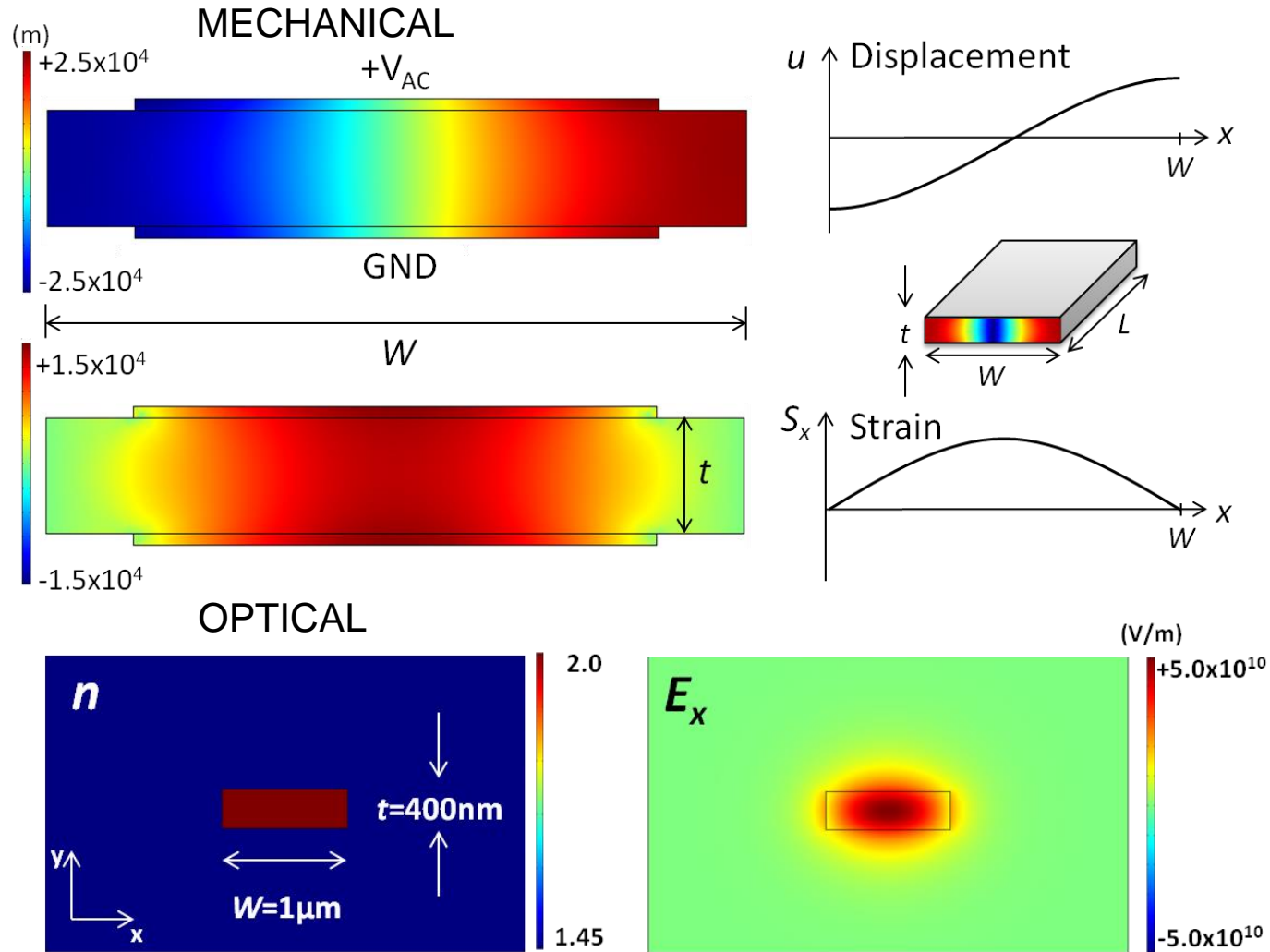


Experimental Results



Elasto-optic modulation

- Consider a thin rectangular plate cross-section:



“Single finger”
contour mode
resonator
(CMR)



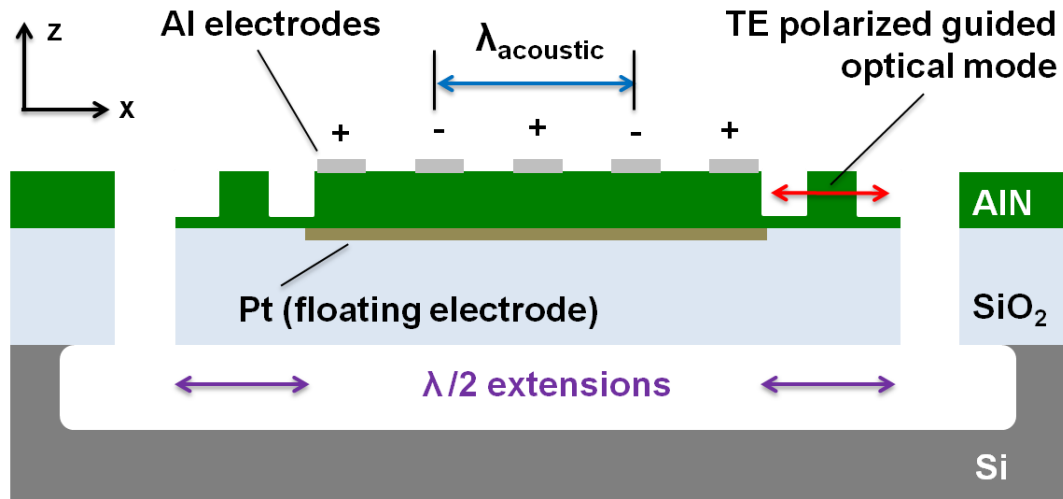
OVERLAP:
Strain $\rightarrow \Delta n$ via
elasto-optic (p)
coefficients



Guided in
waveguides, or
photonic
resonator



Device geometry

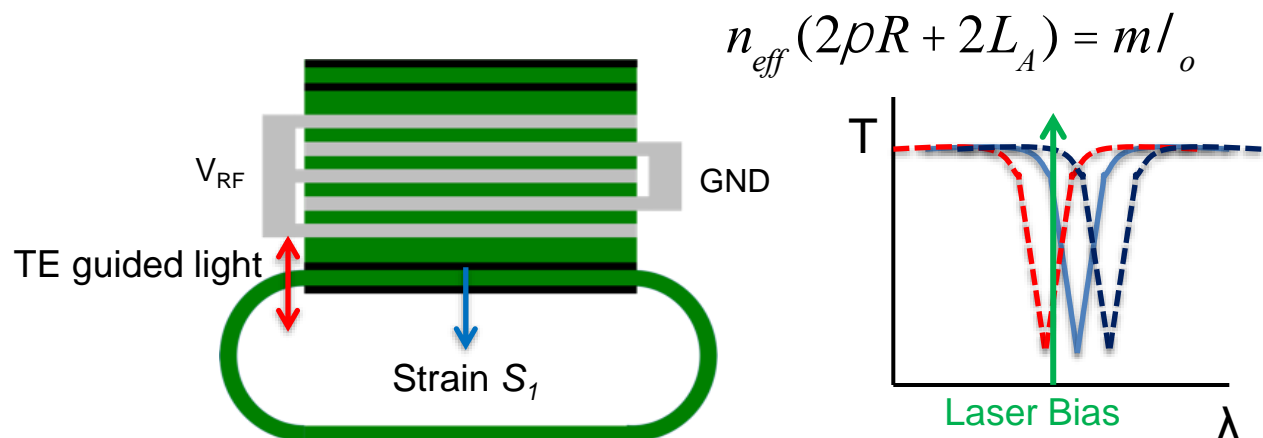


- Extended CMR generates lateral strains (S_1)
- Refractive index change for TE mode
 - AIN $p_{11} = -0.1^*$:

$$\Delta n_1 = -\frac{1}{2} n_1^3 p_{11} S_1$$

*Davydov, *Semiconductors* **36**, 2002

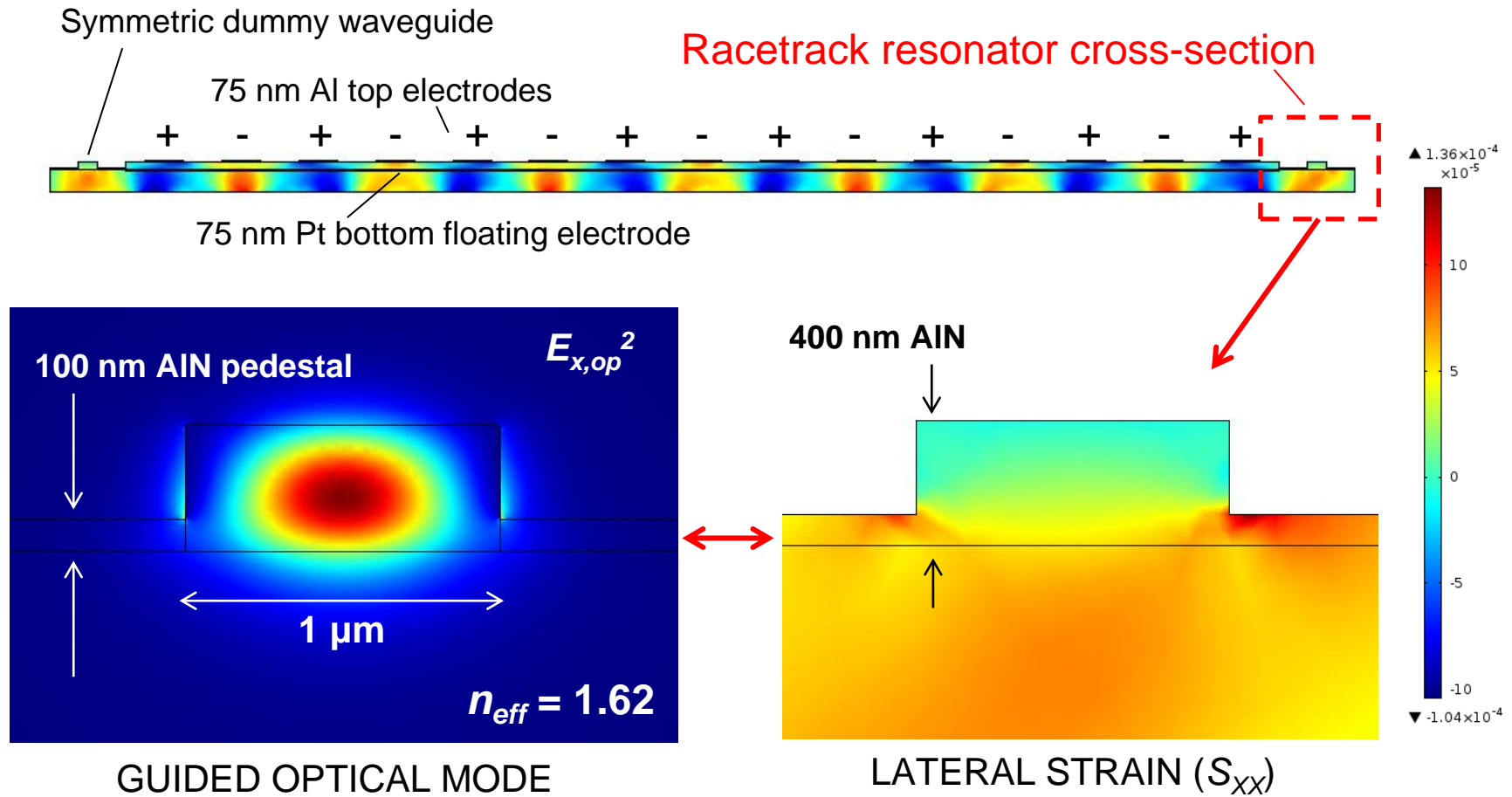
- Enhance sensitivity to strain by incorporating waveguide into a photonic racetrack resonator:



- Optical intensity modulation:

$$P_{\text{mod}} = \frac{dT}{dI} \cdot \frac{dI}{dn_{\text{eff}}} \cdot \Delta n_{\text{eff}}$$

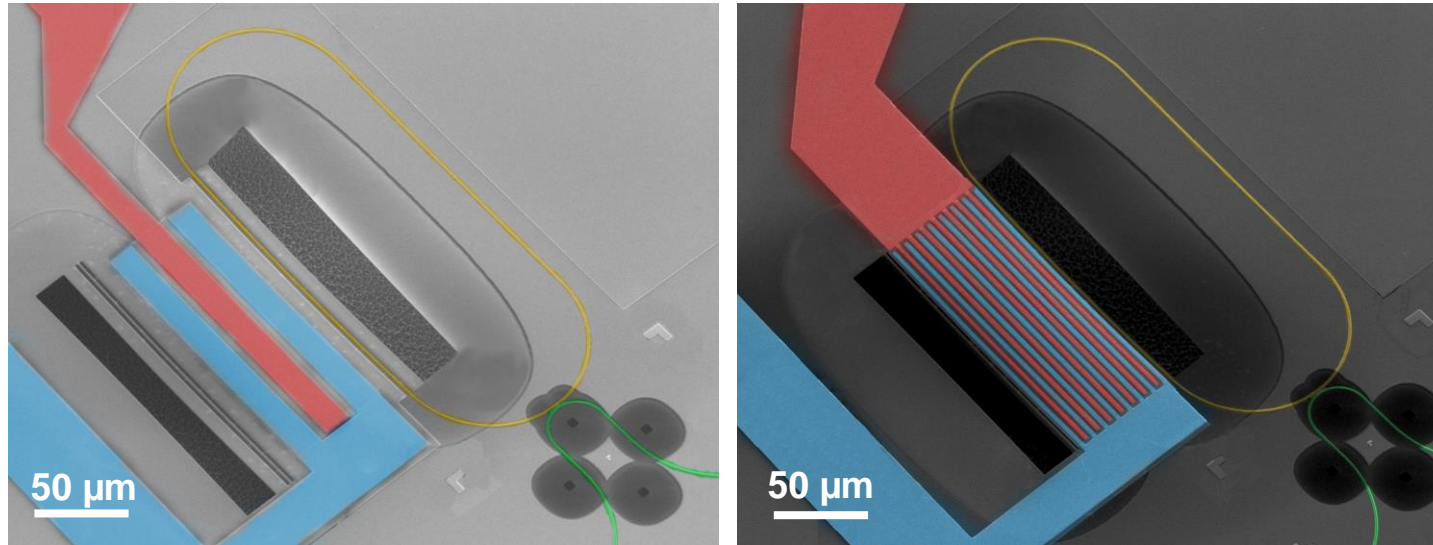
Optical mode overlap



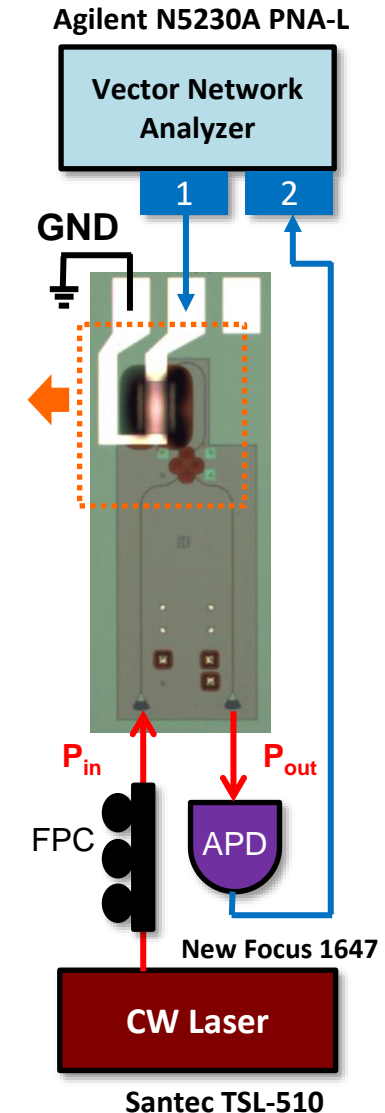
- Estimation of effective strain:

$$S_{1,eff} = \frac{\iint S_1 E_{x,op}^2 dx dz}{\iint E_{x,op}^2 dx dz}$$

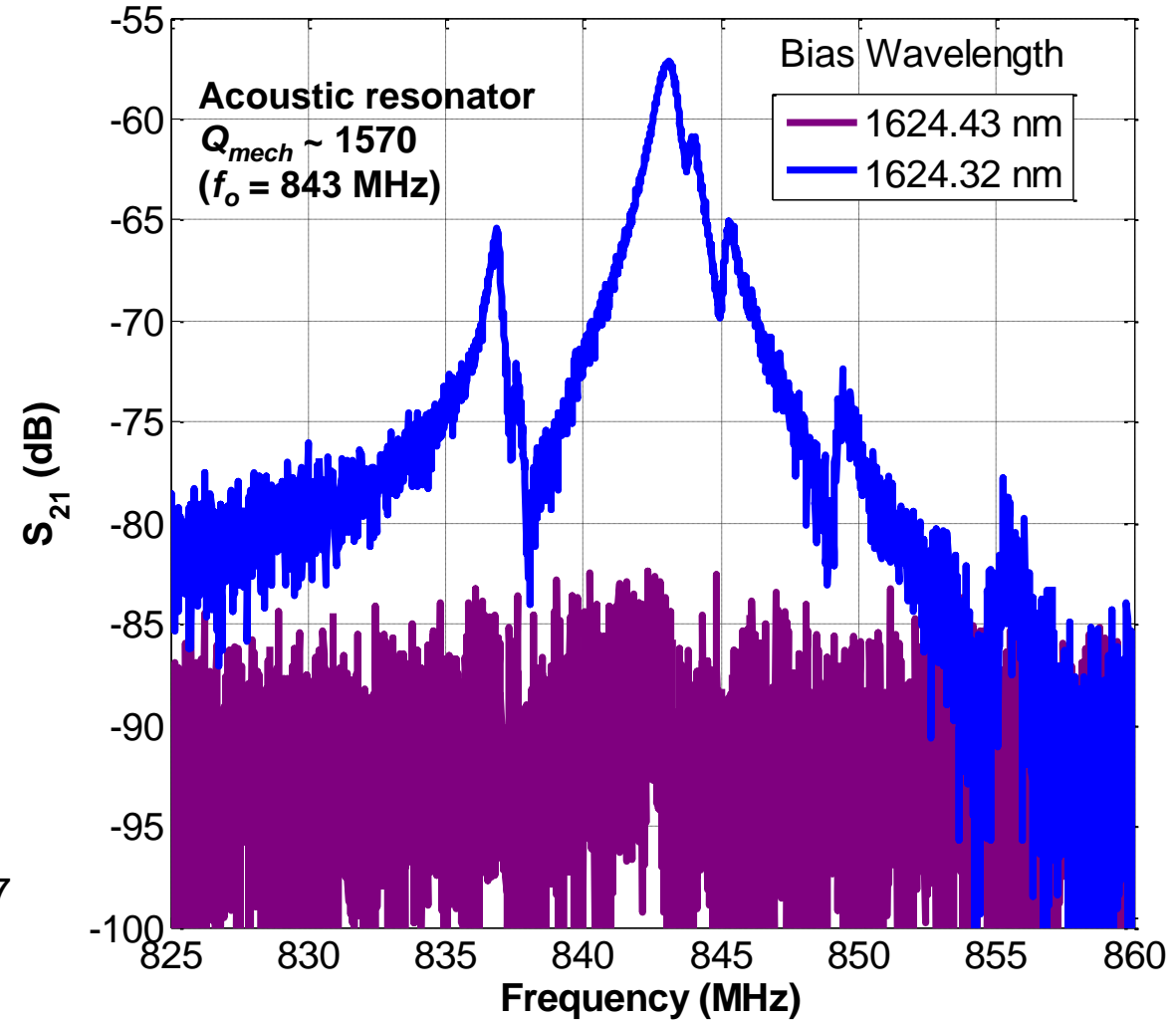
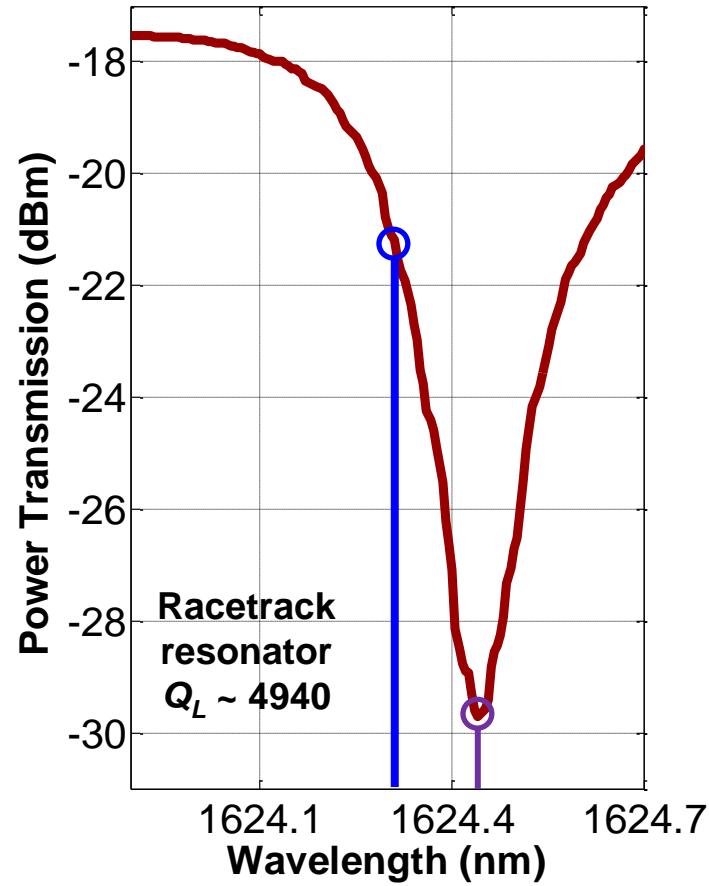
Fabricated devices and characterization



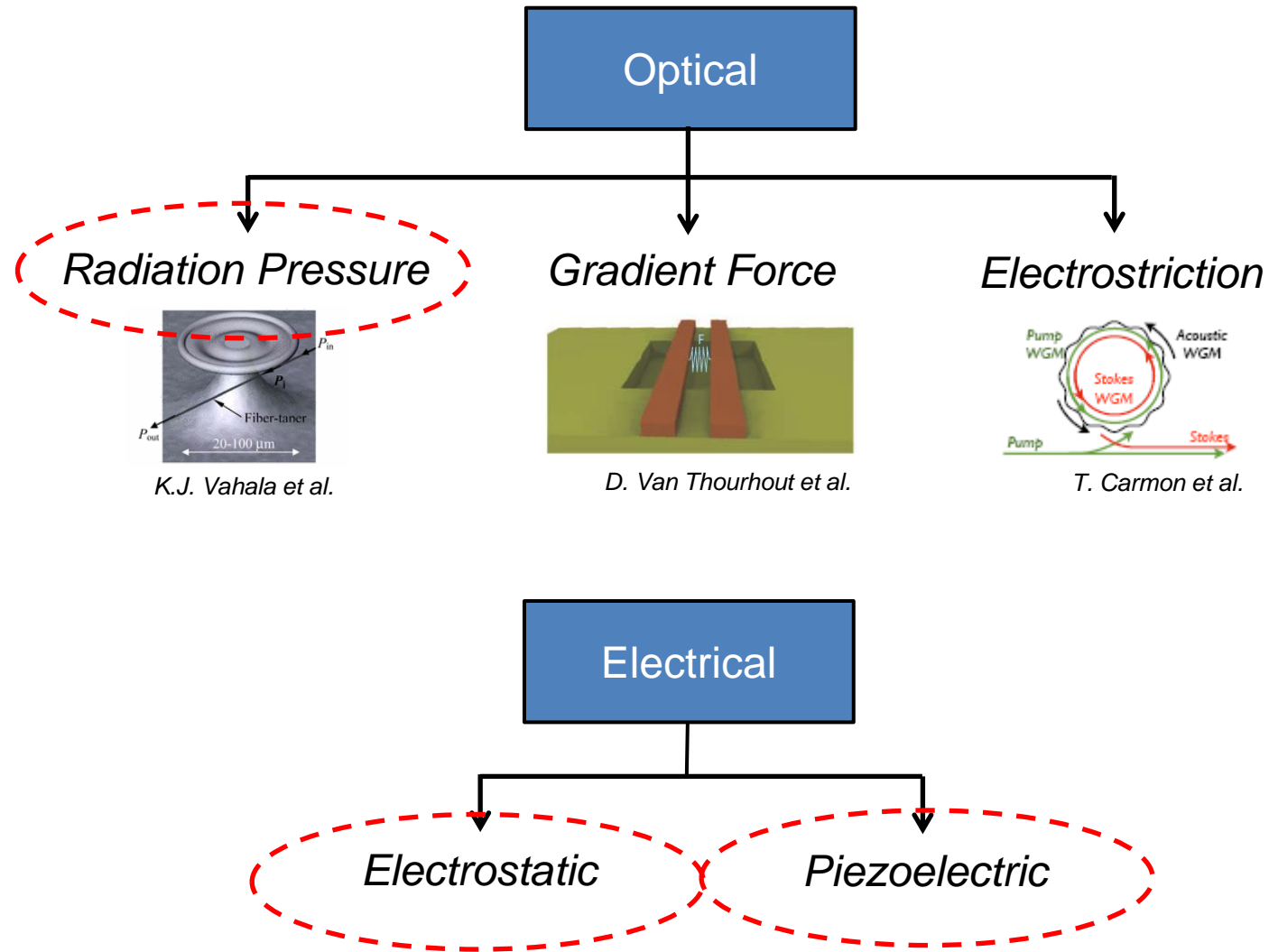
- Similar processing and testing procedure to displacement-based modulator
- Acoustic resonators fabricated with $\lambda = 40 \mu\text{m}$ and $\lambda = 8 \mu\text{m}$
- Design is extendable to smaller wavelengths (higher frequencies) of interest for microwave-optical conversion



S_{21} elasto-optic device response

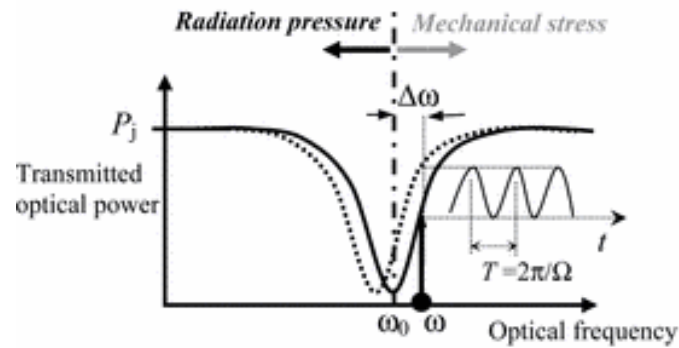
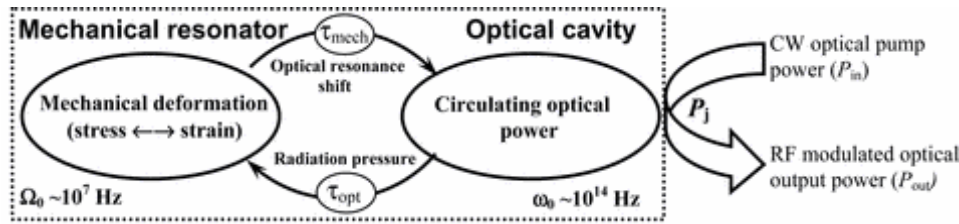
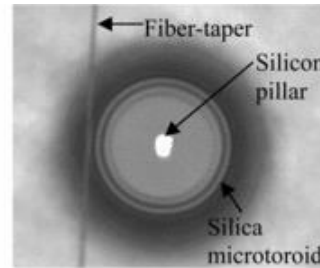
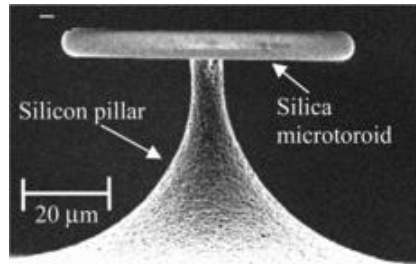


Optomechanical Device Actuation

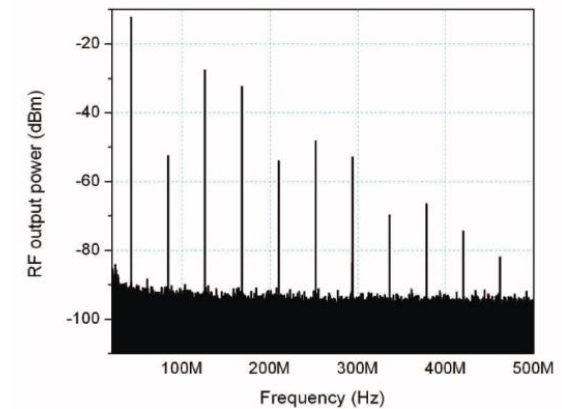
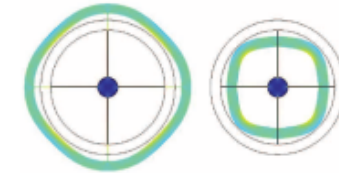
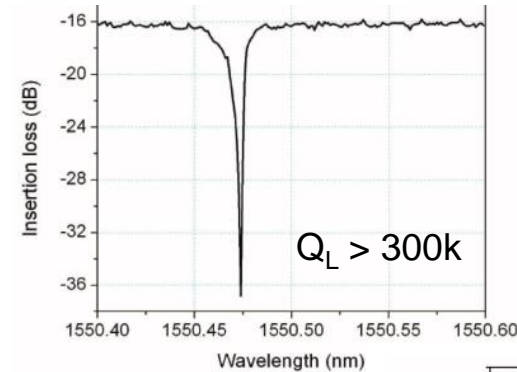
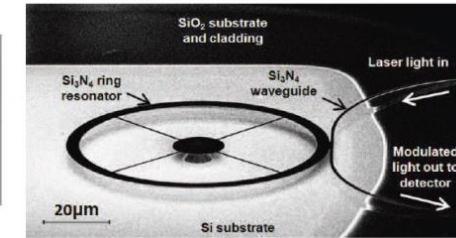
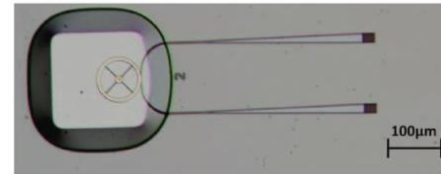


i) Radiation Pressure Driven:

Silica microtoroid optomechanical oscillator
(Hossein-Zadeh et al., *Phys. Rev. A* **74**, 2005):

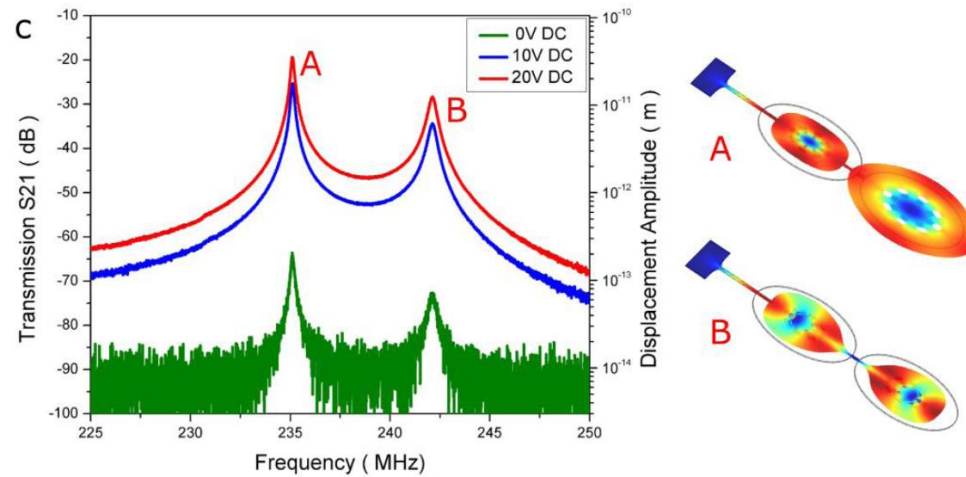
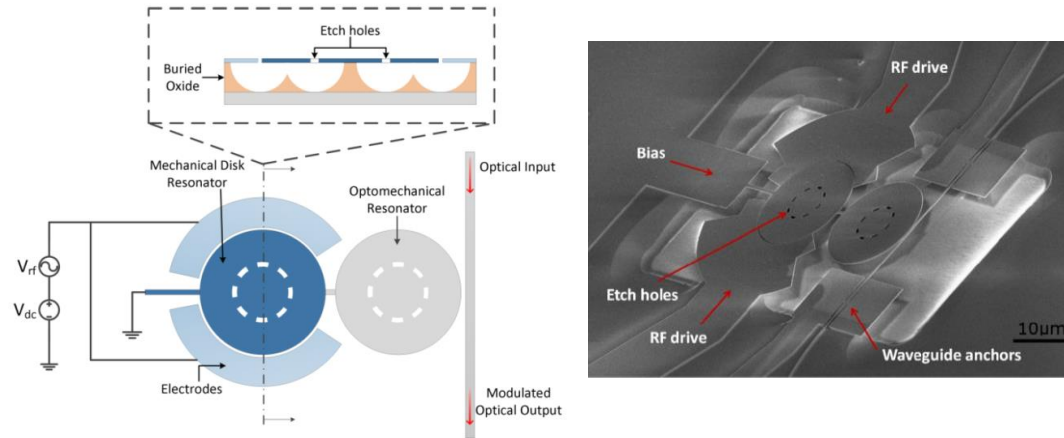


Silicon nitride optomechanical oscillator
(Tallur et al., *Opt. Express* **19**, 2011):



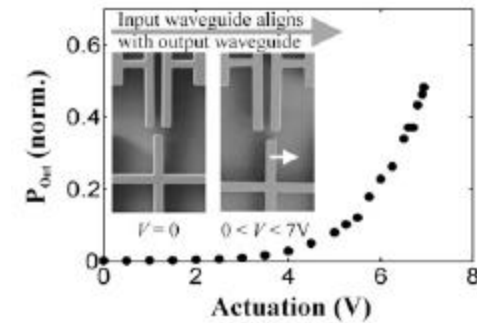
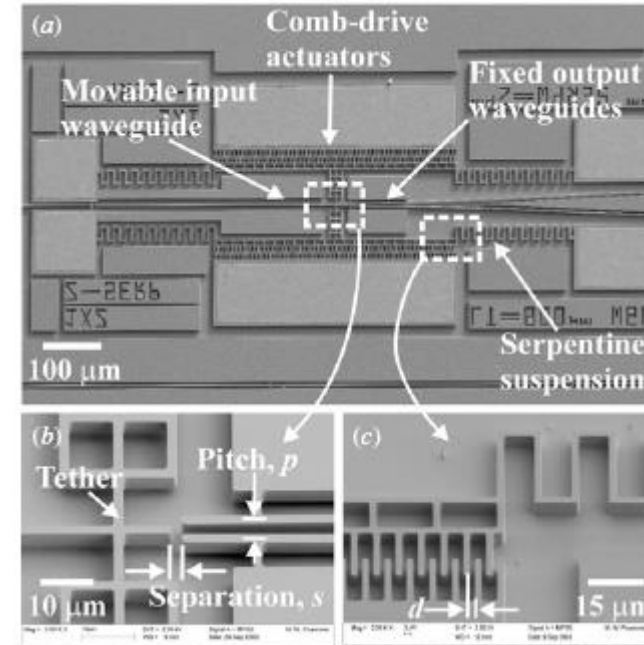
ii) Electrostatically Driven:

Silicon microdisk resonators
(Sridaran & Bhave, *Opt. Express* **19**, 2011):



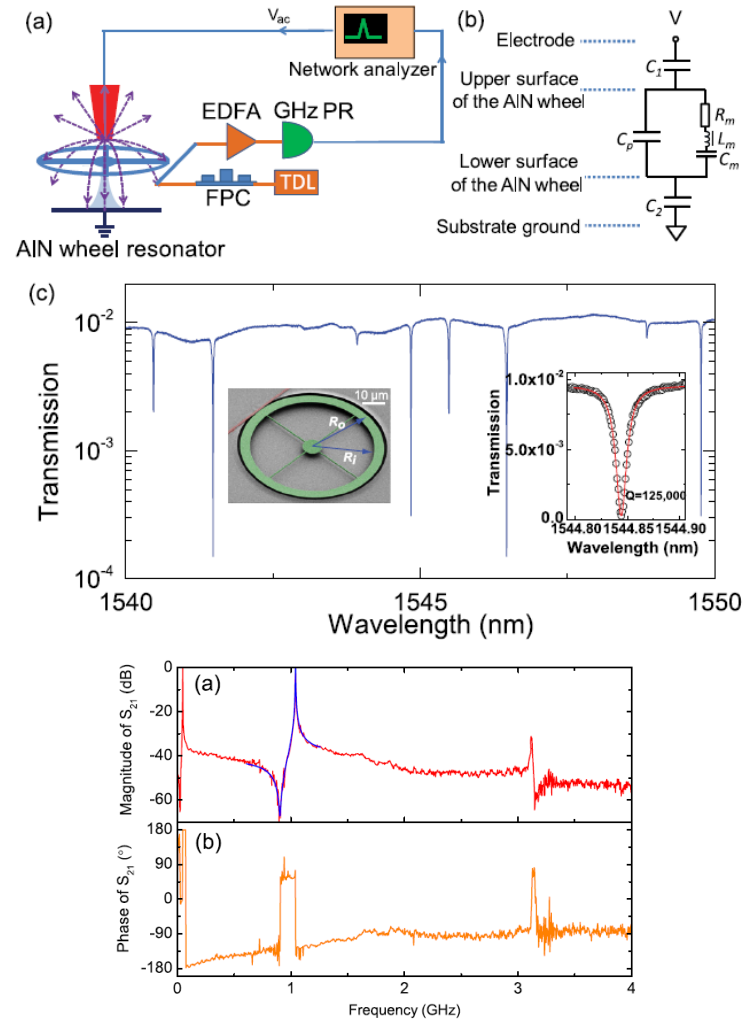
Difficult to scale >1GHz

End-coupled Indium Phosphide Waveguides
(Preussner et al., *J. Micromech. Microeng.* **16**, 2006):

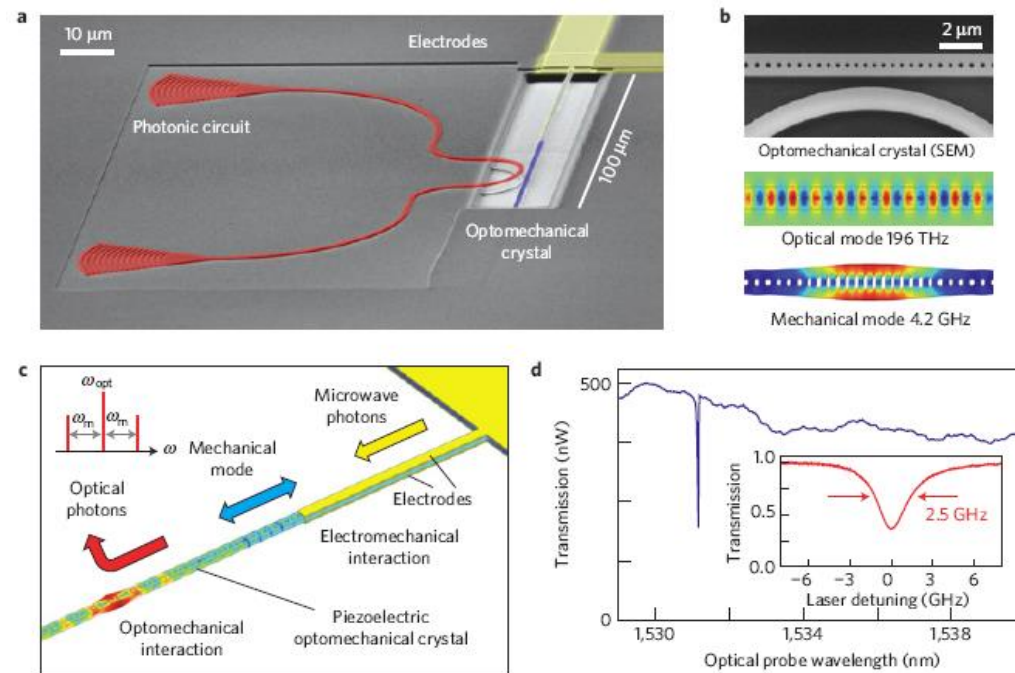


iii) Piezoelectrically Driven:

AlN ring actuated with suspended RF probe:
 (Xiong et al., *Appl. Phys. Lett.* **102**, 2013):

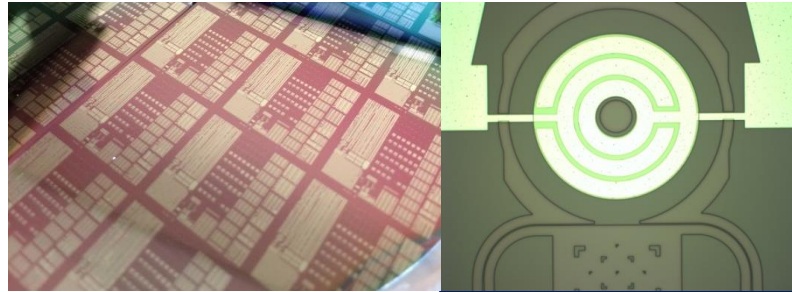


AlN optomechanical crystal:
 (Bochmann et al., *Nat. Physics* **9**, 2013):

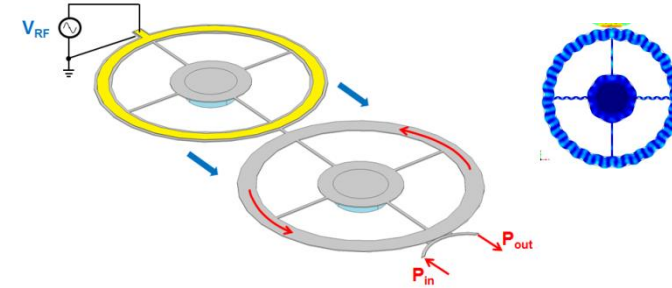


Development Overview

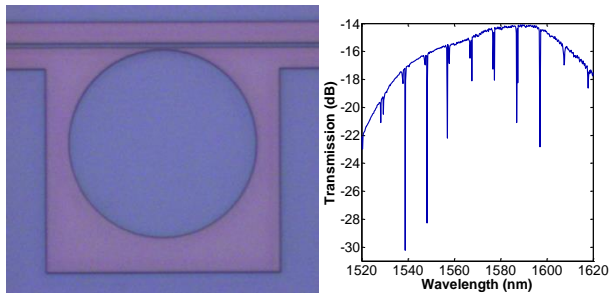
(III) Fabrication process development



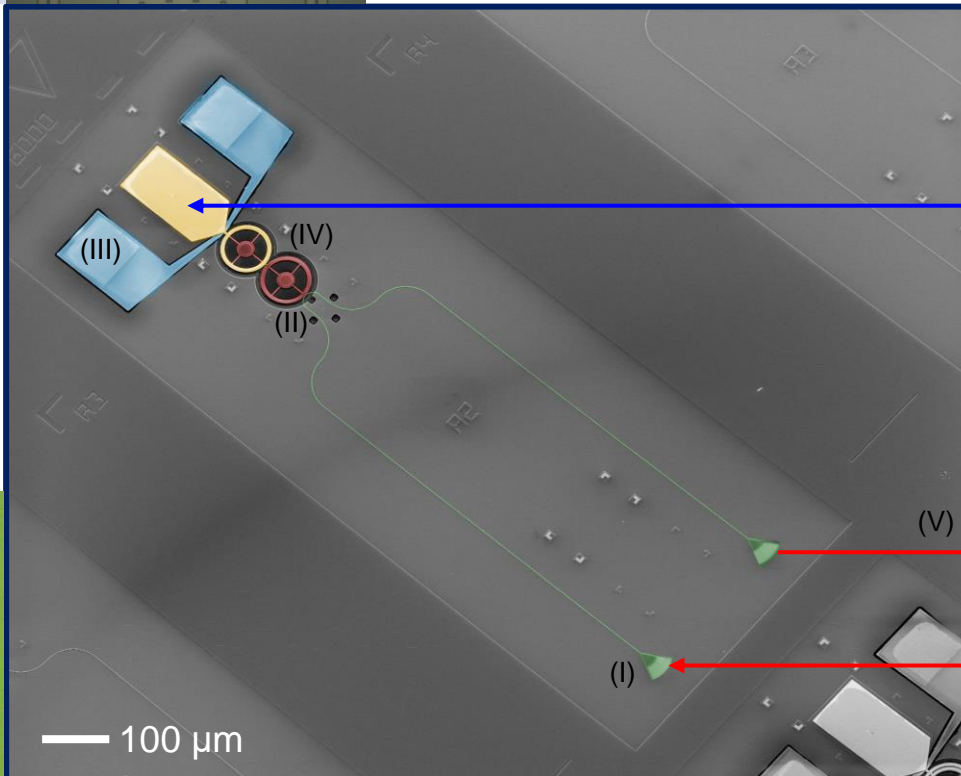
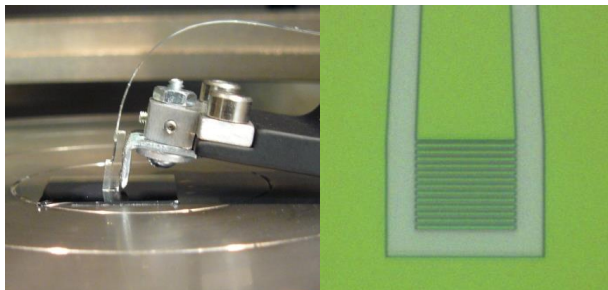
(IV) Piezoelectric acousto-optic modulator



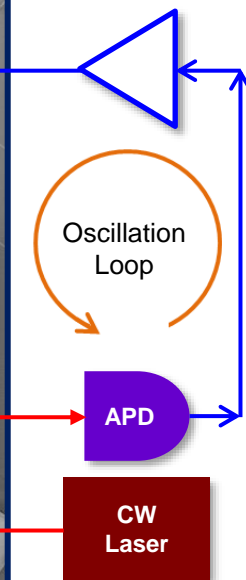
(II) Photonic resonator



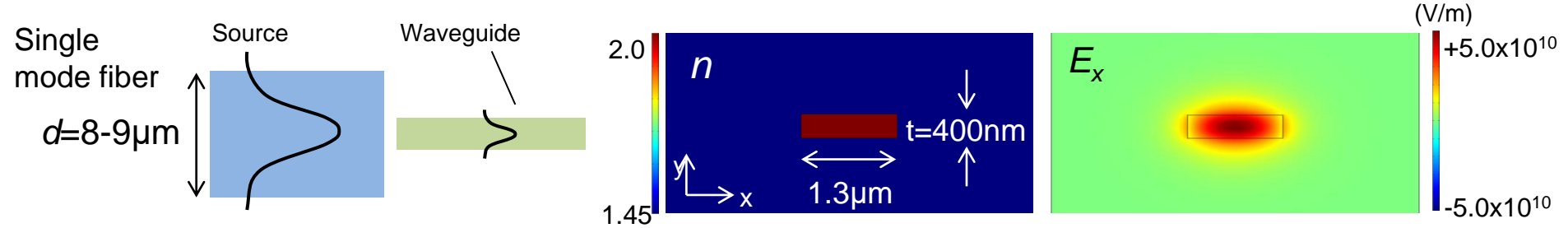
(I) AlN grating coupler



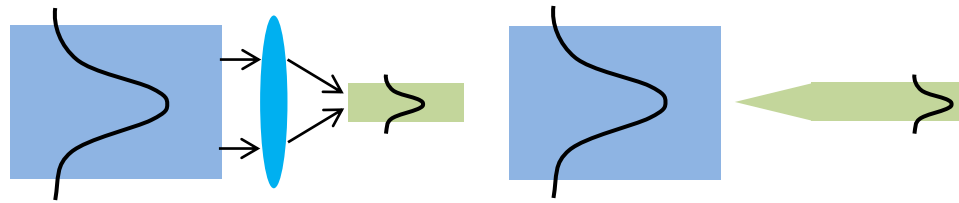
(V) Opto-acoustic oscillator



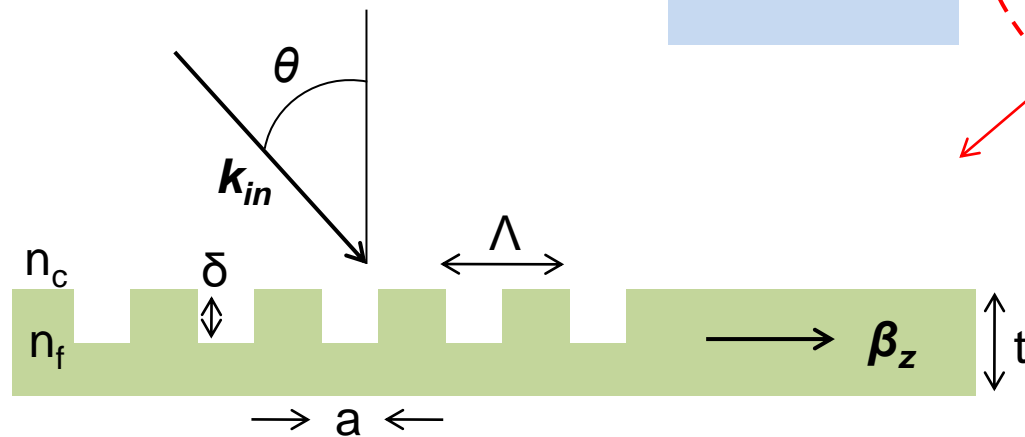
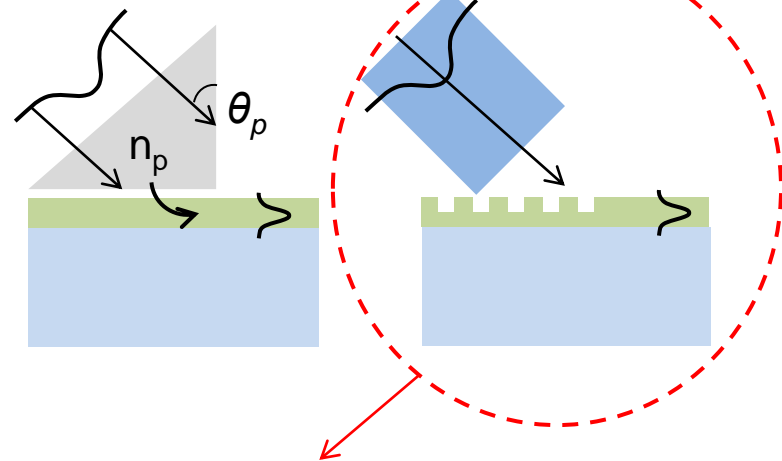
Light Coupling



Edge coupling:

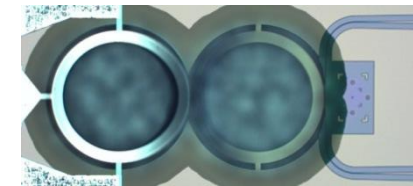
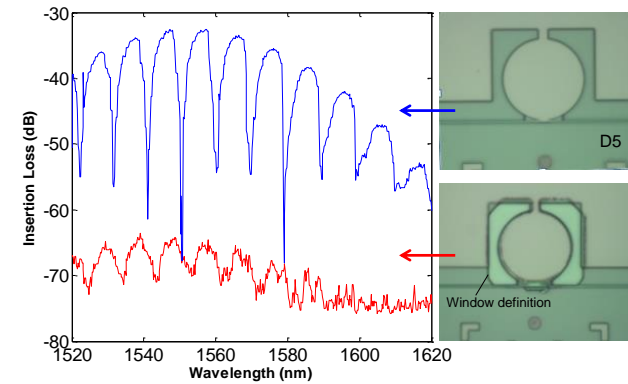
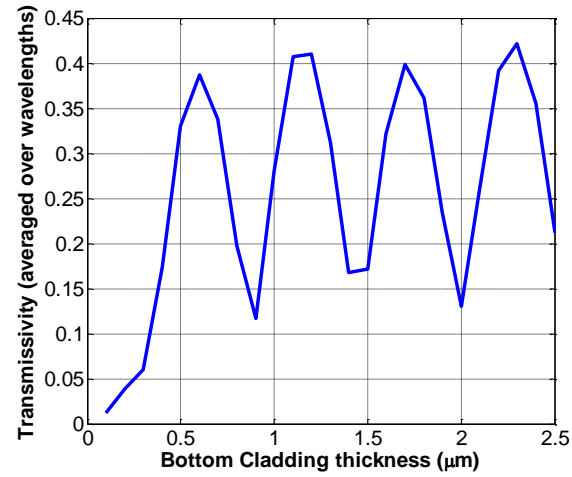
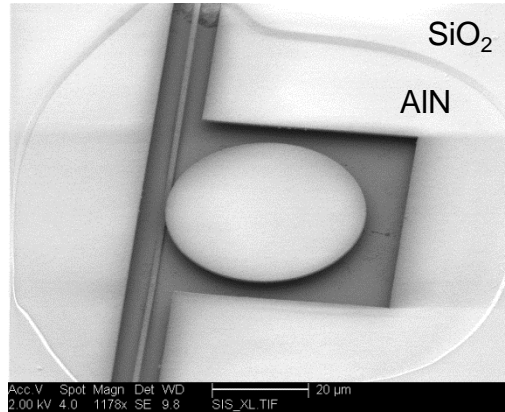


Surface coupling:

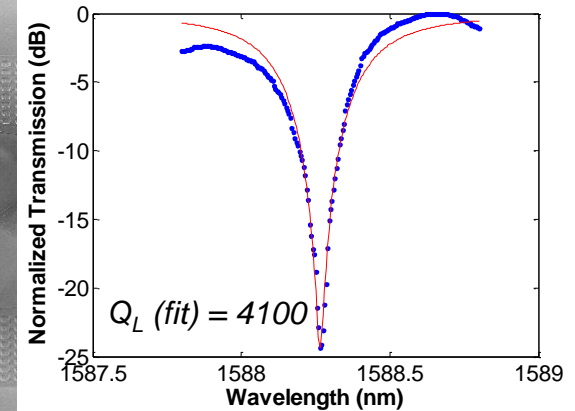
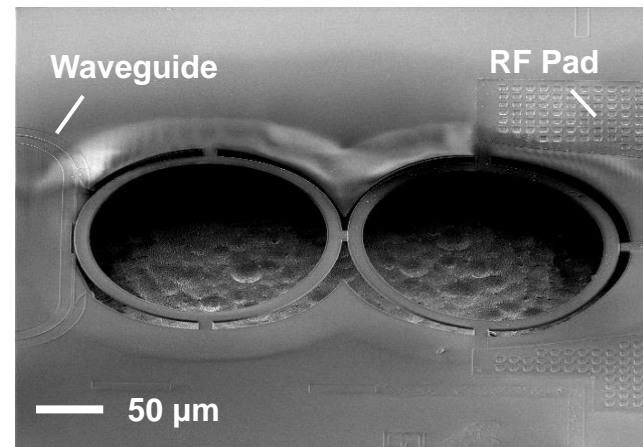
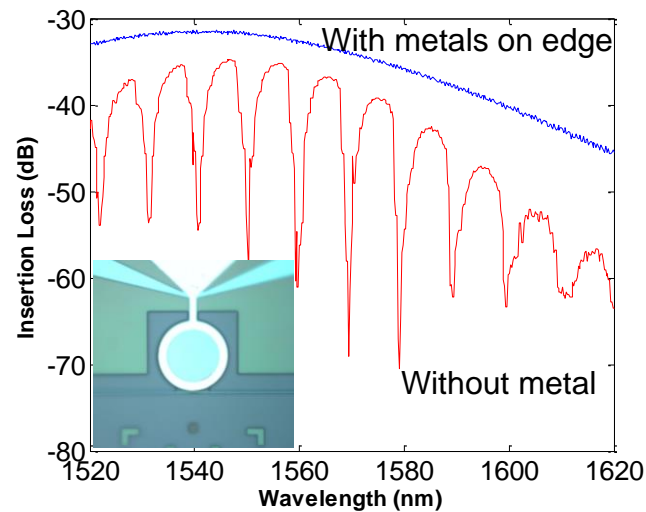


Integration Challenges

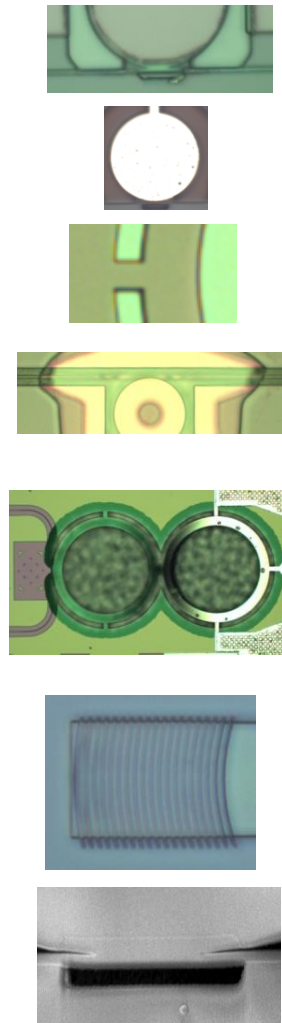
- Oxide etching and release



- Electrode patterning and AlN etching

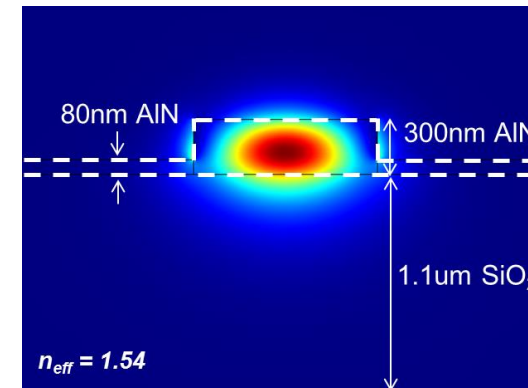


Process Modifications – Partial Etch Method

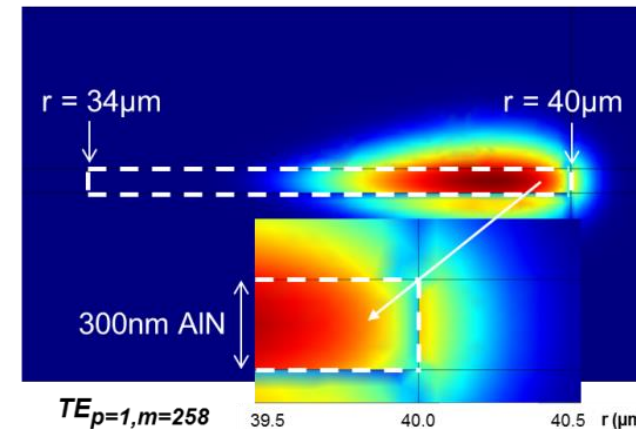


<u>Identified Issue:</u>	<u>Solution:</u>
Release window	Complete release with HF etch – using partially etched AlN as a hard mask
Metals	Primary focus on Dual-Ring or Dual-Disk structures (separated excitation)
Anchors	Change anchor points – increase number symmetrically, but reduce width
Buckling	Use a curved/recessed waveguide at the point of approach [cannot have more than 40 μm suspension]
Stress	Removal of oxide with wet release should relieve uncontrolled stress in oxide & use a thicker top metal to ensure step coverage
Oxide removal	Partial etch will keep gratings protected; Wet release at the end will automatically remove any PECVD oxide (if required as a hard mask)
WGM Coupling	Performing release in a single step at the end with HF avoids any effects from release window; May need to focus on the use of sub-100nm gaps

- Fix 300 nm AlN thickness
- Select partial etch slab thickness for rib waveguides and gratings: 80 nm



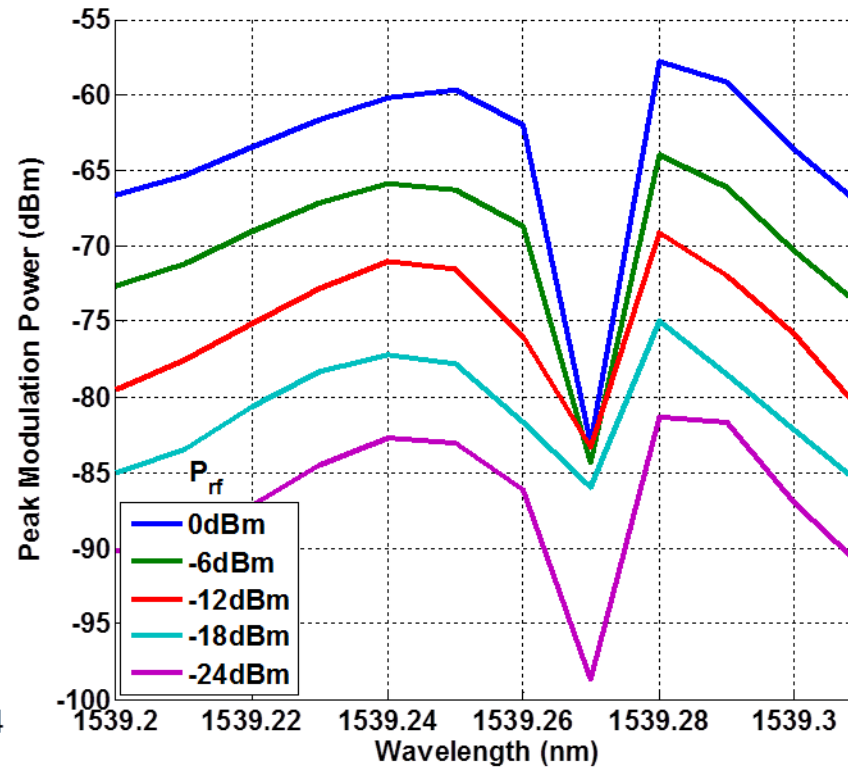
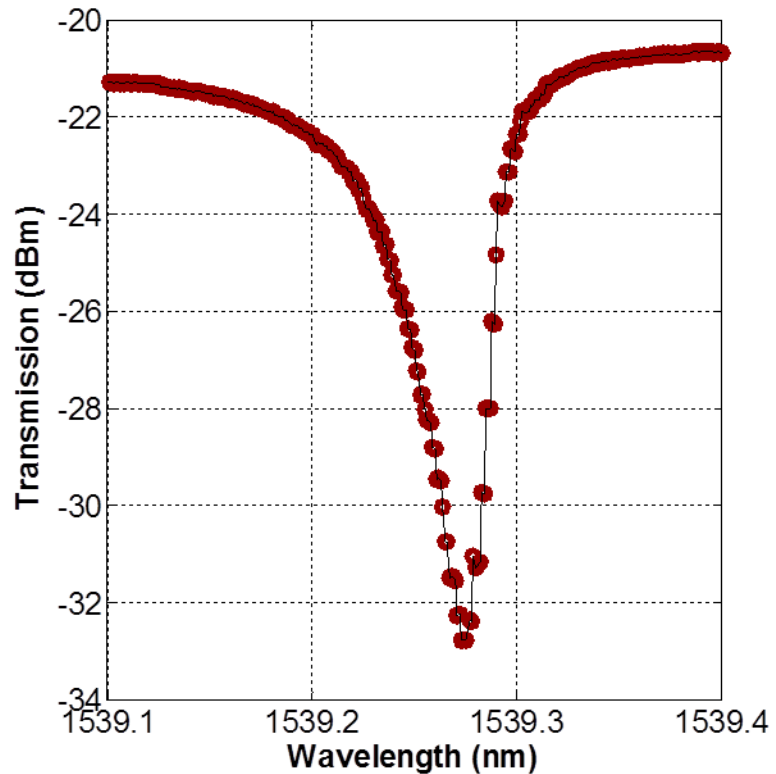
- Set WGM $R_{\text{out}} = 40 \mu\text{m}$, and thick ring width = 6 μm



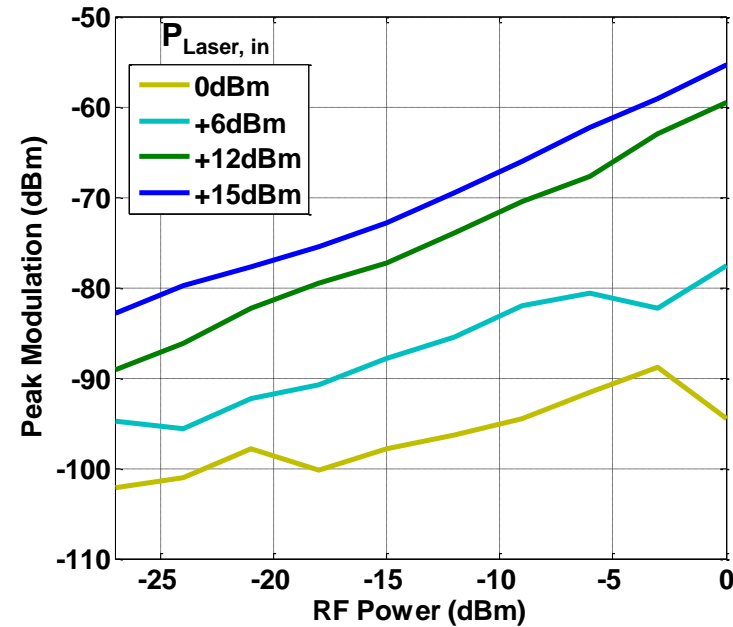
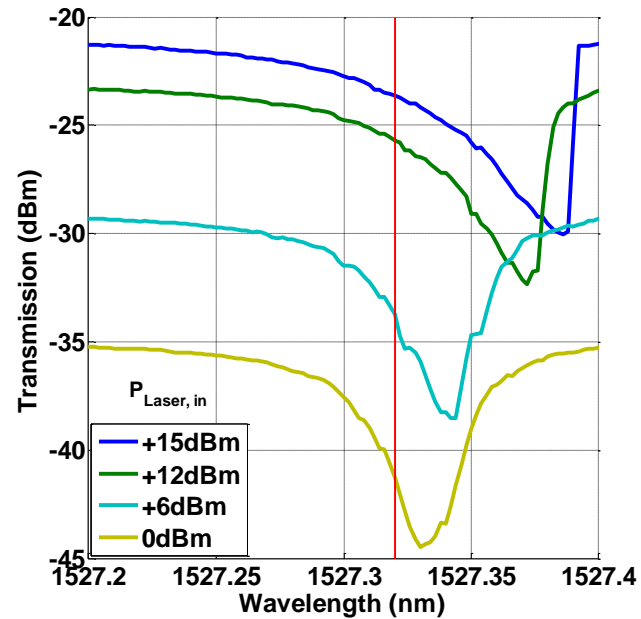
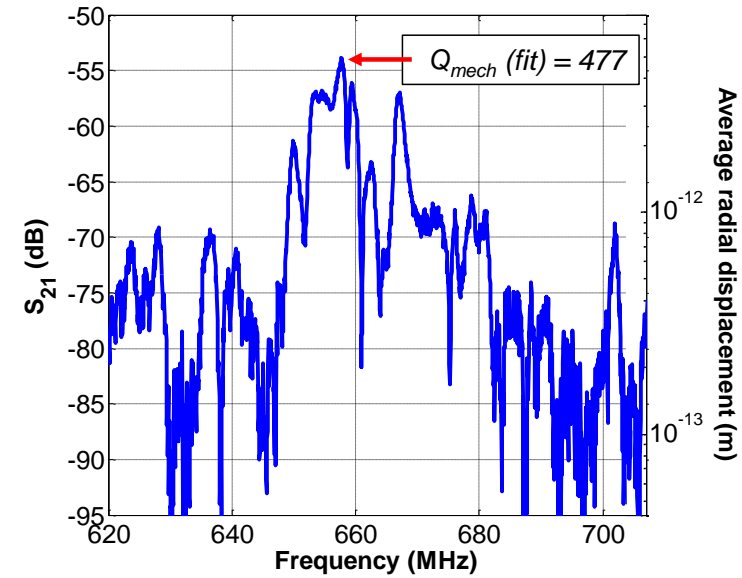
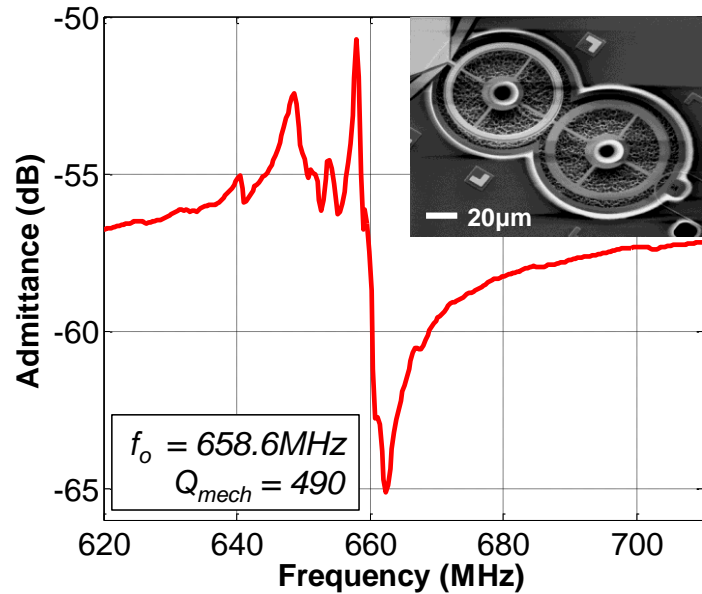
Power Sweeping – Peak Modulation

- VNA operated in CW at $f_{res,mech}$, Output on spectrum analyzer
- Increase Δr with applied P_{rf}

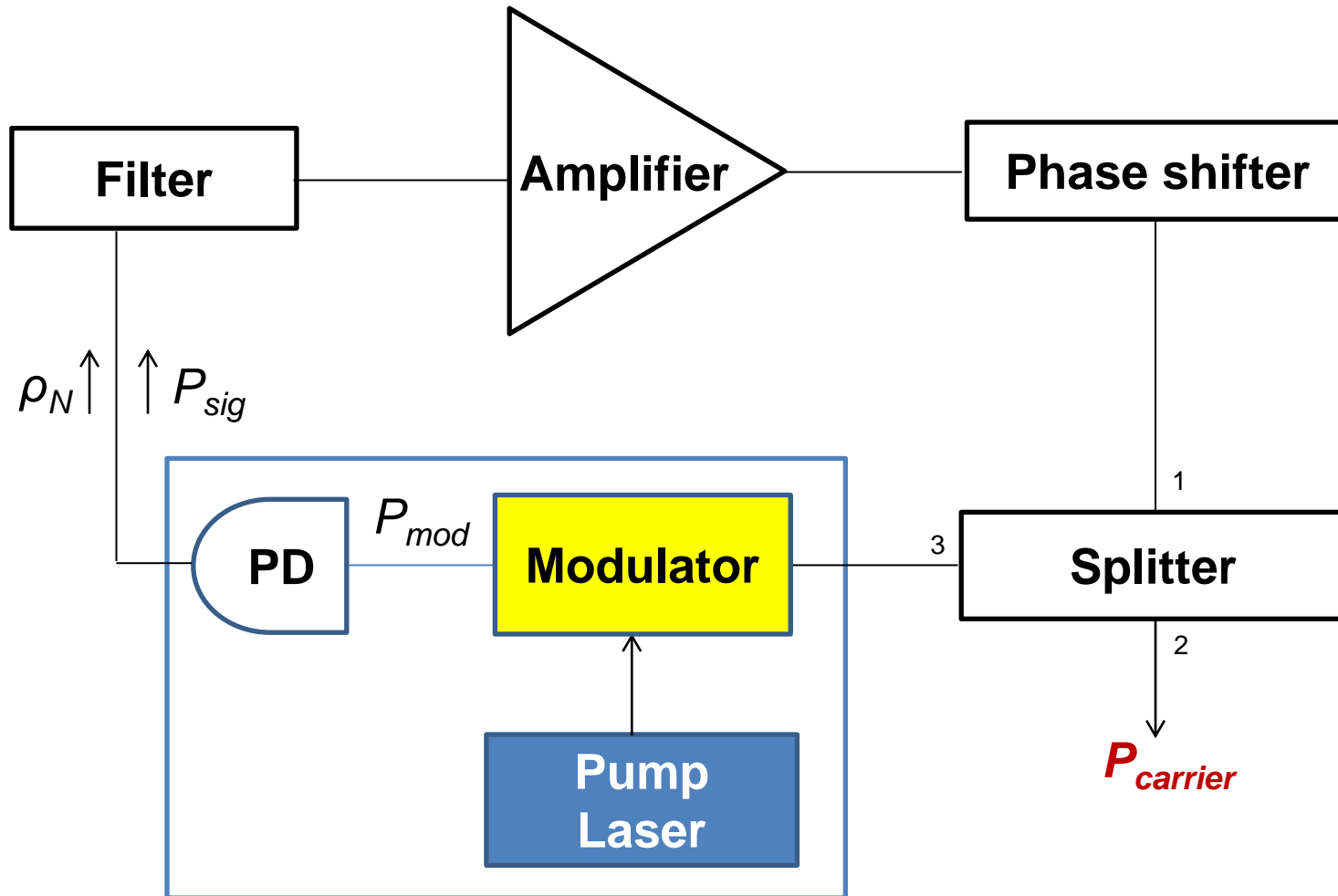
Optical: $P_{mod} = \frac{dT}{d\lambda} \cdot \frac{d\lambda}{dr} \cdot \Delta r$ Electrical: $P_{sig} = \frac{(P_{mod} \cdot G)^2}{Z_o}$



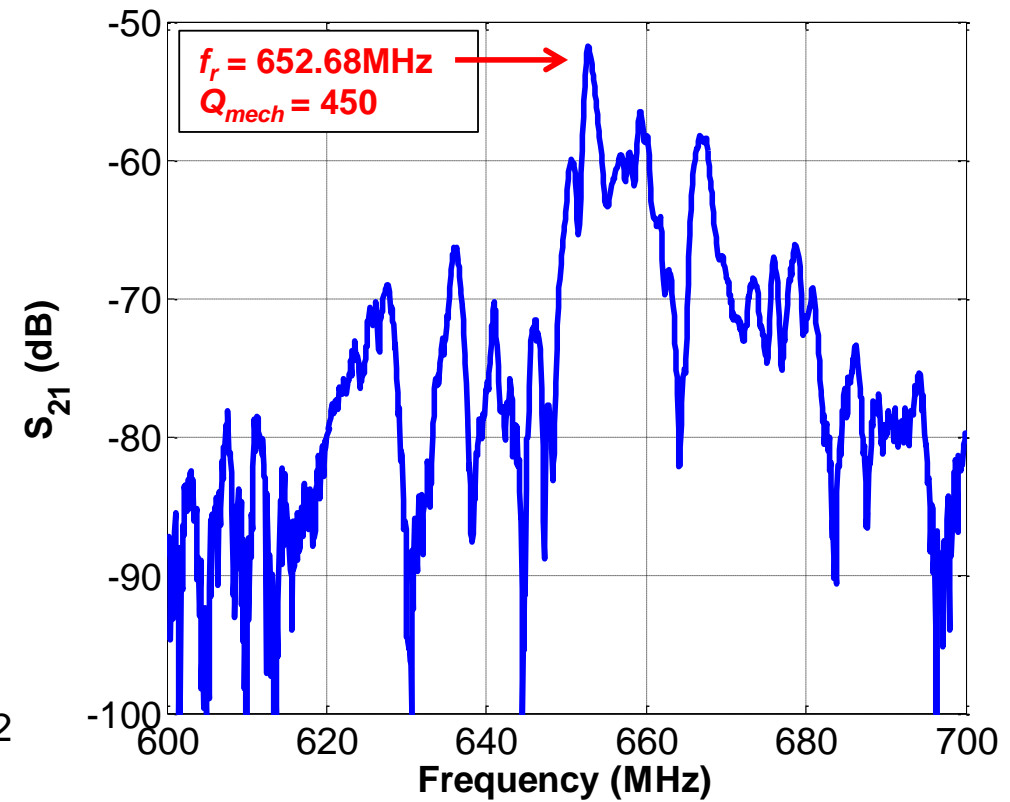
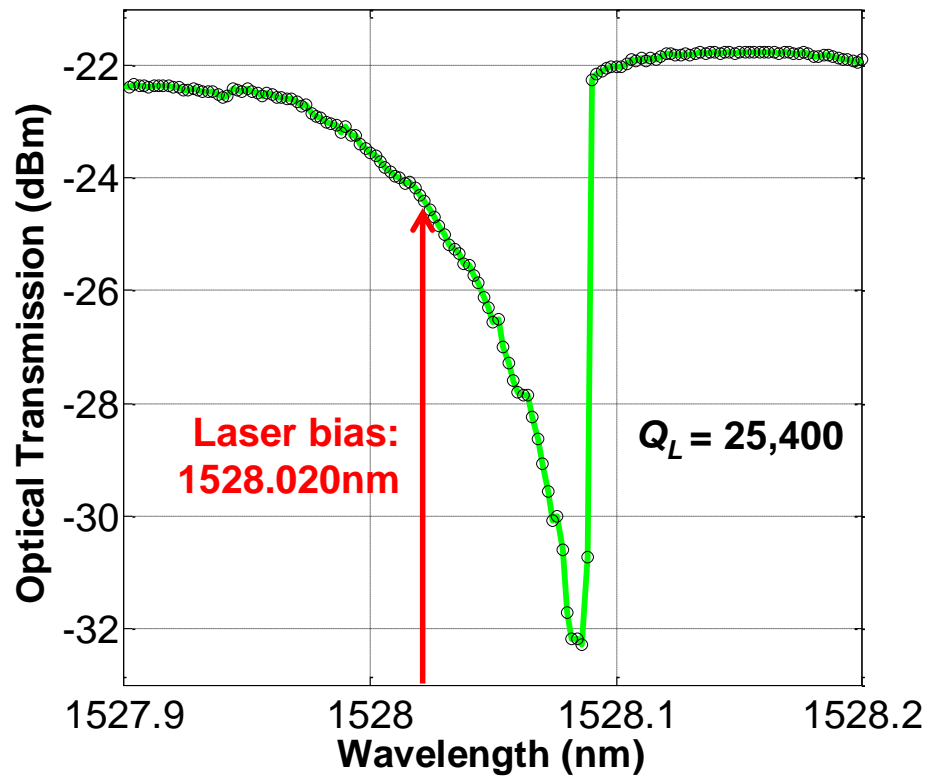
Additional XeF₂ Release



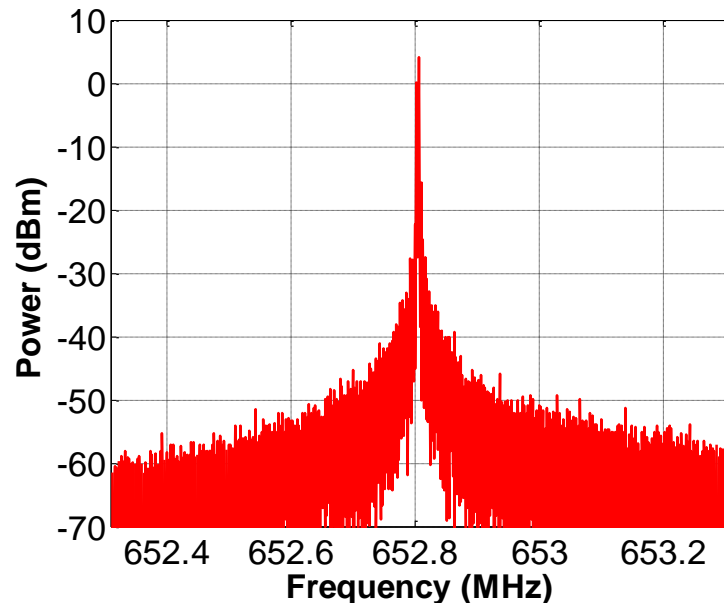
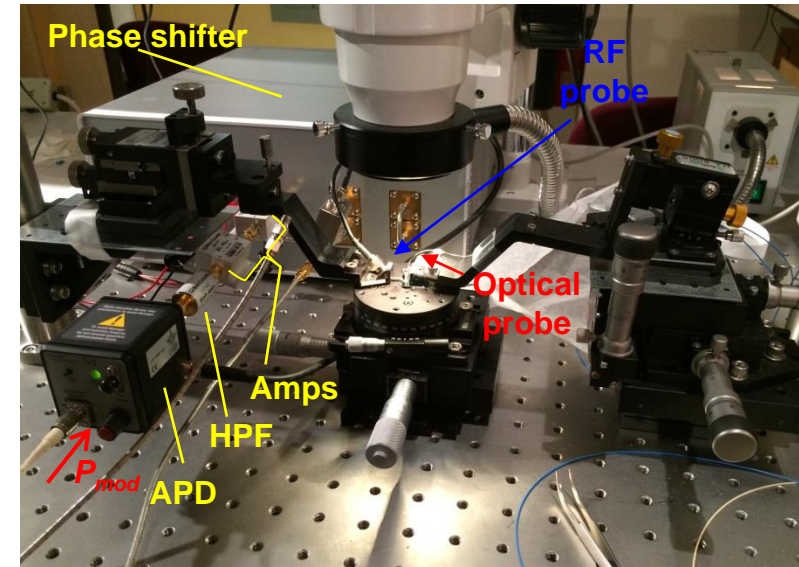
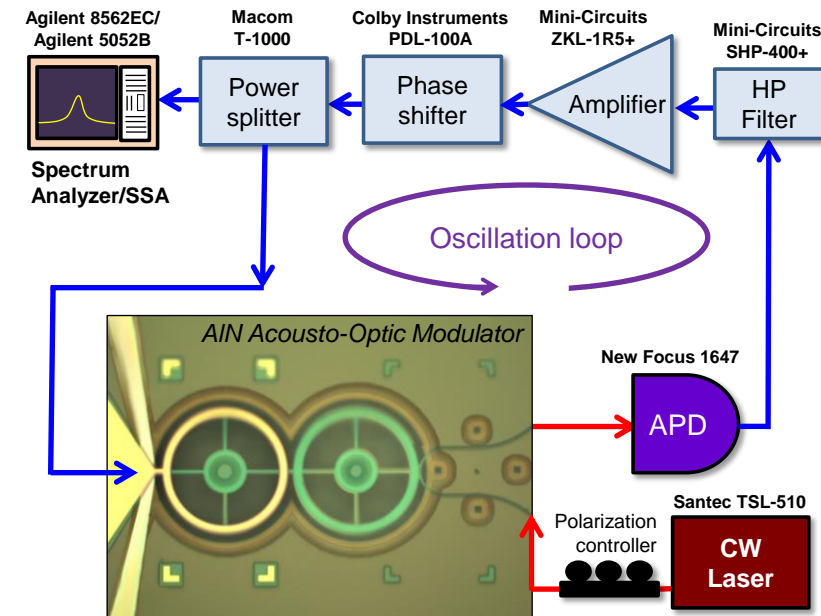
Opto-Acoustic Oscillator Loop



Operating conditions



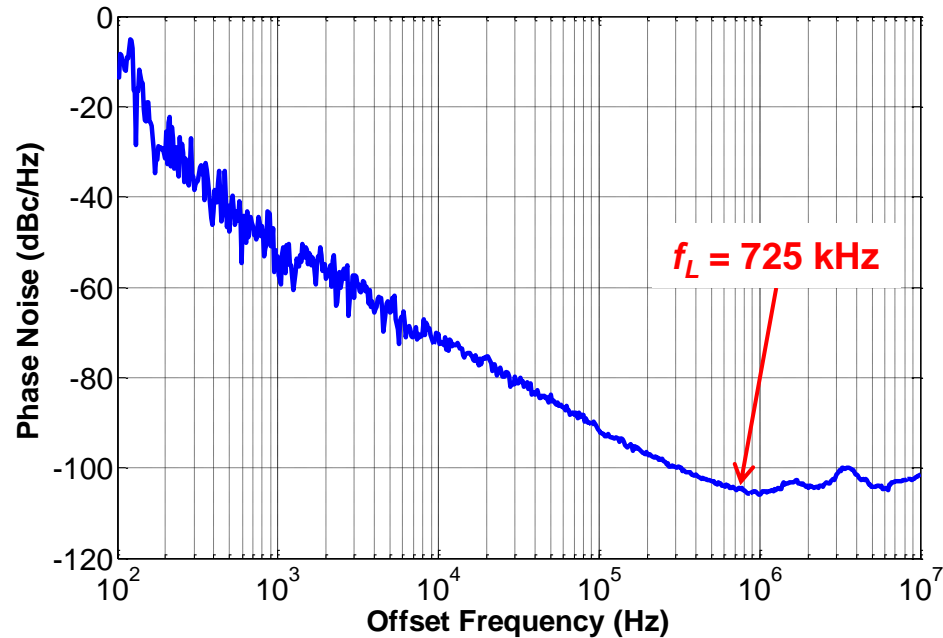
Opto-Acoustic Oscillation



- Circuit built with coaxial SMA components satisfies Barkhausen criteria
- Gain provided by 2 cascaded RF amplifiers, producing a net gain of ~66 dB
- High Pass Filter (HPF) used to exclude low frequency spurious modes in S_{21} transmission

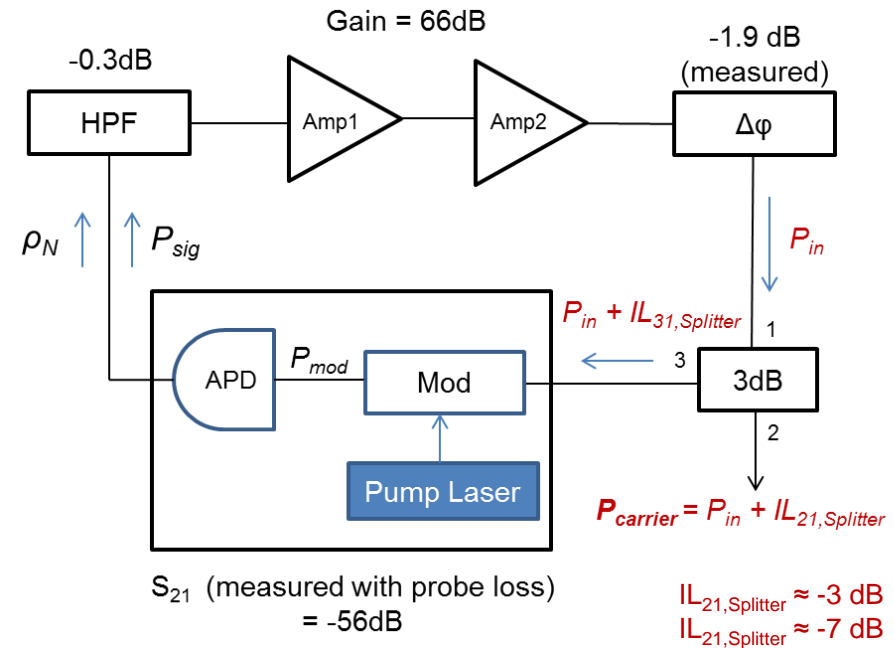
Phase Noise Measurement

Phase noise measured for $f_{\text{carrier}} = 652.8 \text{ MHz}$
with $P_{\text{carrier}} = +6.51 \text{ dBm}$



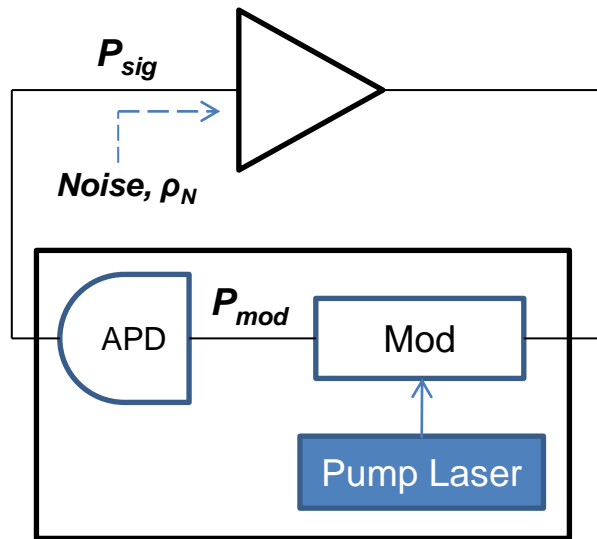
- 10kHz offset = -72 dBc/Hz
- Noise floor = -106 dBc/Hz
- Leeson corner frequency:
 $f_L = (f_{\text{carrier}}/2Q_{\text{mech}}) \approx 725 \text{ kHz}$
(matches experiment)

Schematic of the loop as tested:



- Individual components were measured for loss contributions
- Some additional losses present in the connections – but this provides us an estimate for P_{sig}

Phase Noise Model



- Starting from the Leeson formula:

$$S_{\phi}(f) = \left[1 + \frac{1}{f^2} \left(\frac{\nu_o}{2Q_{mech}} \right)^2 \right] S_{\psi}(f)$$

- Describe $S_{\psi}(f)$:

$$S_{\psi}(f) = \frac{\overline{v_n^2} / \Delta f}{v_{sig}^2} = \frac{\left(\frac{1}{2} \right) \rho_N R_{PD}}{P_{sig} R_{PD}} = \frac{\rho_N}{2P_{sig}}$$

- ρ_N is the additive noise, originating at the photodetector:

$$\rho_N = \text{Thermal noise} + \text{Shot noise} + \text{Laser RIN}$$

$$\rho_N = (4k_B T \cdot NF) + (2eMF_A \sqrt{P_{sig} R_{PD}}) + (N_{RIN} P_{sig})$$

Where:

- k_B : Boltzmann's constant
- T : Ambient temperature
- e : electron charge
- M : APD multiplication factor
- F_A : APD excess noise factor
- R_{PD} : APD load resistor
- N_{RIN} : Laser Relative Intensity Noise
- NF : Amplifier Noise Factor
- A : Amplifier Gain

Main Contributions to Phase Noise

- Using losses in the loop, estimate: $P_{sig} = -54.29$ dBm

- Assuming: $T = 293\text{K}$
 $NF = 3.05\text{dB}$
 $F_A = 5$ (New Focus 1647)
 $F_A = M^x$ ($x \sim 0.7$ for InGaAs)
 $R_{PD} = 50\Omega$
 $N_{RIN} = -145$ dB/Hz for Laser
(Santec TSL-510)

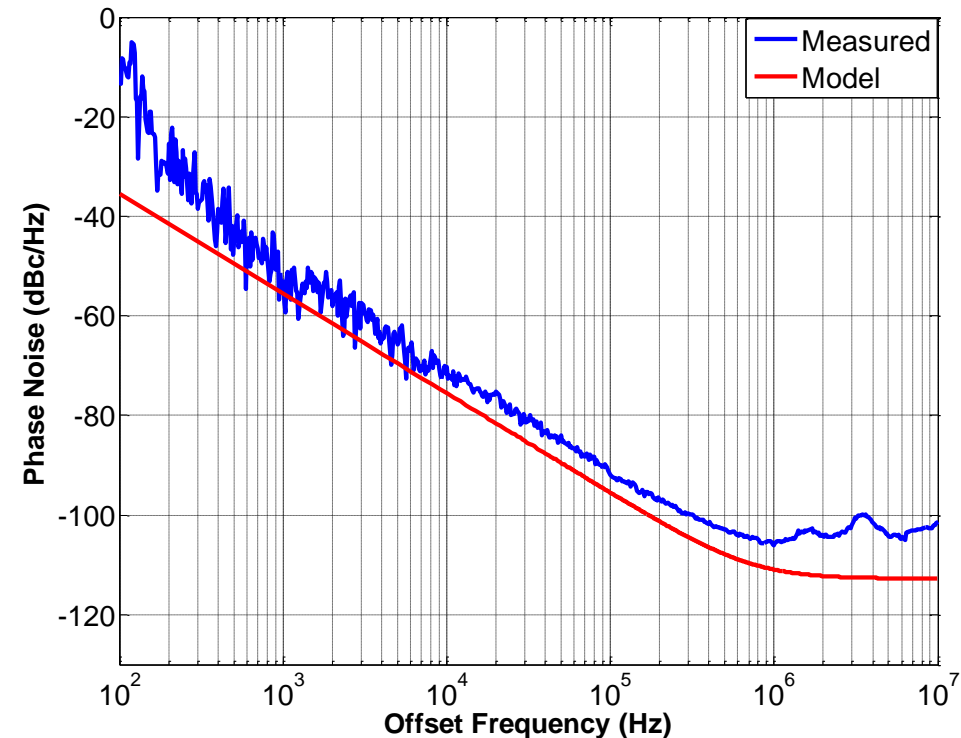
- Evaluation of ρ_N contributors:

$$Thermal = 3.26 \times 10^{-20} \text{ W/Hz}$$

$$Shot = 6.88 \times 10^{-21} \text{ W/Hz}$$

$$RIN = 1.17 \times 10^{-23} \text{ W/Hz}$$

- Net $\rho_N = 3.95 \times 10^{-20}$ W/Hz, producing a noise floor of -113 dBc/Hz
- Low photocurrent generated by P_{sig} causes thermal noise contribution to dominate



Modulator Analytical Transfer Function

- Description of modulation capability:

$$P_{\text{mod}} = \frac{dT}{d\lambda} \cdot \frac{d\lambda}{dr} \cdot \Delta r$$

$$= P_{\text{trans}} H_{\text{cav}} \cdot g_{\text{om}\lambda} \cdot \eta_{\text{om}} V_{\text{rms}}$$

Transmission losses ← P_{trans} ← H_{cav} ← $g_{\text{om}\lambda}$ ← η_{om} ← V_{rms} ← Input voltage

Transfer function Optomechanical coupling Piezo-optomechanical transduction

$$H_{\text{cav}} = \frac{8\Gamma^2(\lambda - \lambda_o)}{[4(\lambda - \lambda_o)^2 + \Gamma^2]^2}$$

$$g_{\text{om}\lambda} = \frac{\lambda_o}{R_{\text{out}}}$$

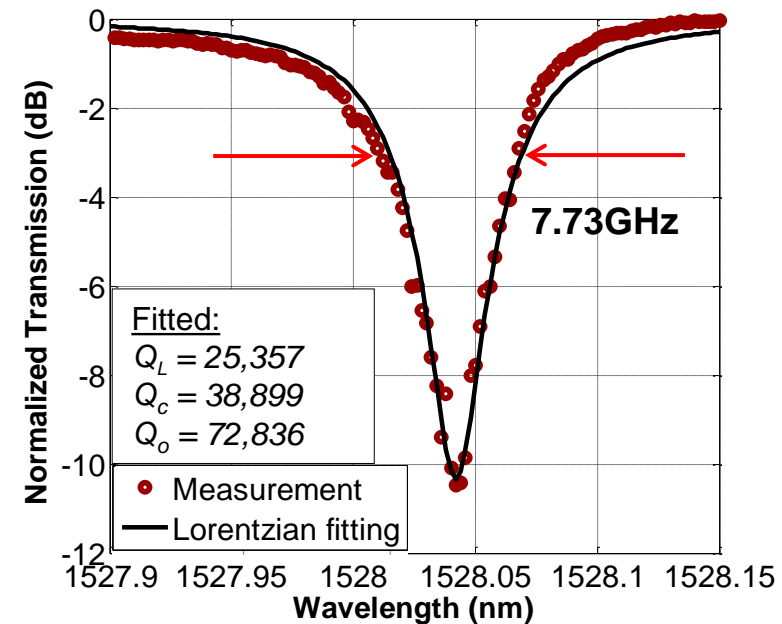
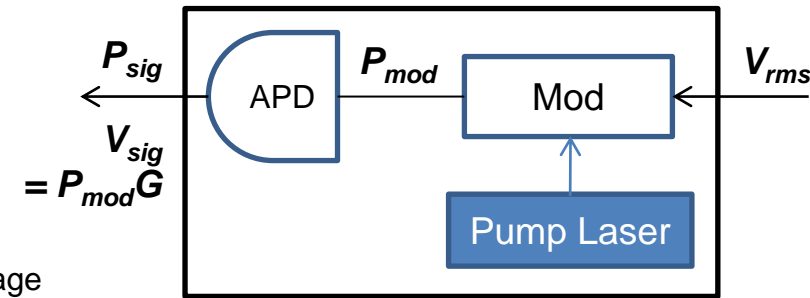
- Device tested for P_{trans} at a level of -22dBm

- For our WGM resonator, $\Gamma = 60$ pm

- ↳ • We can extract a simplified expression for S_{21} of the modulator ($G = \text{APD gain}$):

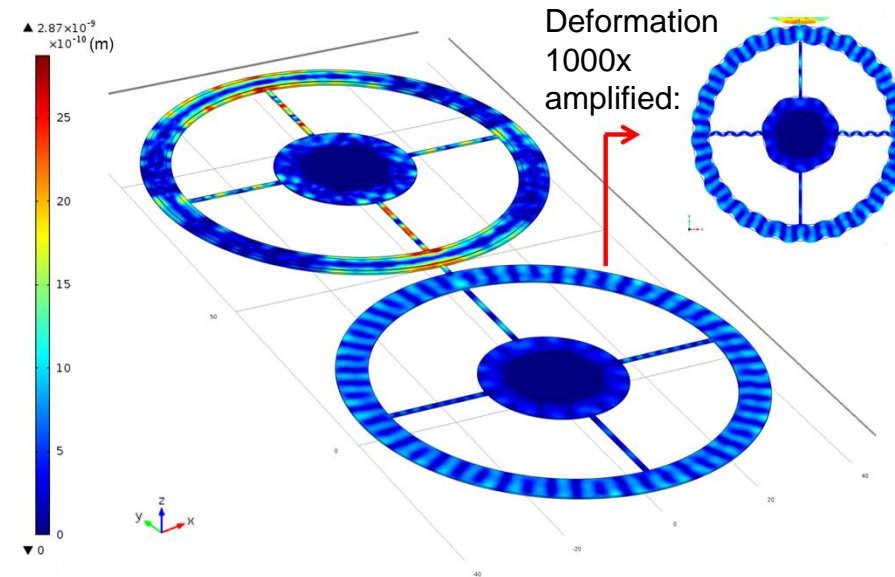
$$S_{21,\text{dB}} = 20\log(P_{\text{trans}} H_{\text{cav}} g_{\text{om}\lambda} \eta_{\text{om}} G)$$

- ➡ • For the measured $S_{21} = -56\text{dB}$, this yields $\eta_{\text{om}} = 26$ pm/V



Piezo-Optomechanical Transduction Capability

- FEM simulations confirm the η_{om} transduction capability is diminished due to mismatch in the modes of the CM and WGM rings
- This produces displacement in the WGM ring, in which Δr does not correspond to that of the radial contour mode, but rather generates an average displacement Δr_{avg}



- By re-designing the ring geometries to exploit the electromechanical coupling (η) in the CMR:

$$\eta = 2d_{31}E_{eq} \left(2\pi R_{avg} \right)$$

- Fully coupled into WGM:

$$\Delta r = Q_{mech} \left(\frac{F_{piezo}}{m_{eff} \Omega_{mech}^2} \right) = Q_{mech} \left(\frac{2d_{31}E_{eq} \left(2\pi R_{avg} \right) V_{rms}}{m_{eff} \Omega_{mech}^2} \right)$$

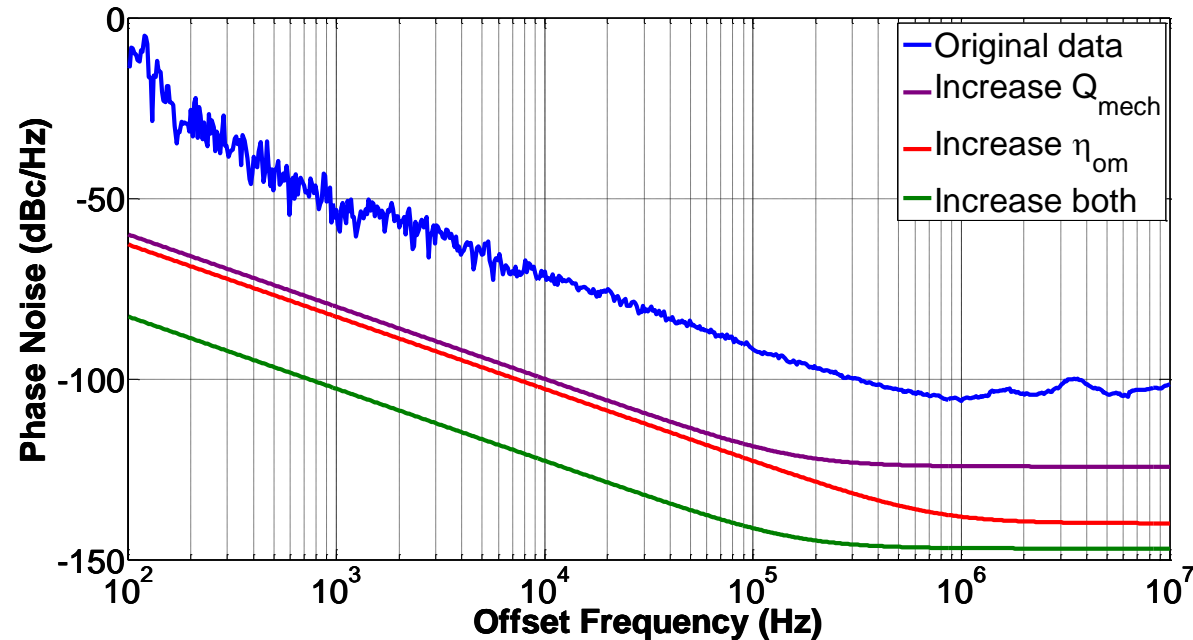
- Resulting in effective η_{om} capability:

$$\eta_{om} = Q_{mech} \left(\frac{4\pi d_{31}E_{eq} R_{avg}}{m_{eff} \Omega_{mech}^2} \right)$$

2-3 orders of magnitude higher than that currently produced

PN Expectation with Improvements to η_{om}

- All other factors remaining the same ($Q_{opt} = 25,000$, Optical transmission losses, $P_{carrier}$, Mismatch losses at input), compute η_{om}

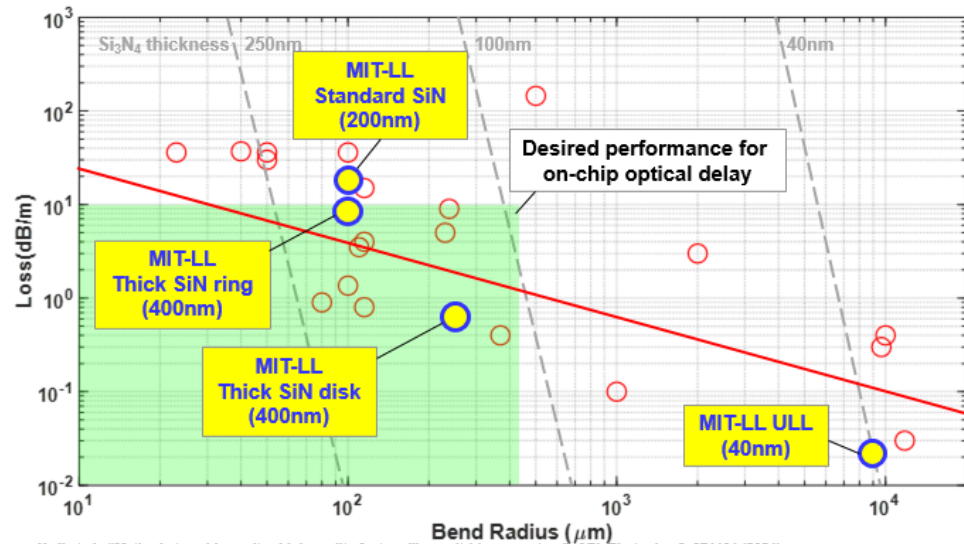


	Initial			
η_{om}	26 pm/V			
P_{trans}	-22.5 dBm			
G	14,000 V/W			
Q_{mech}	450			
P_{sig}	-54.2 dBm			
Noise floor	-113 dBc/Hz			
ρ_N Dominant contribution	Thermal			

- Improvements in the S_{21} can also be attained by tuning a host of parameters:
 - P_{trans} (determined by gratings)
 - Q_{opt} – Generate S_{21} gain
 - 50Ω matching

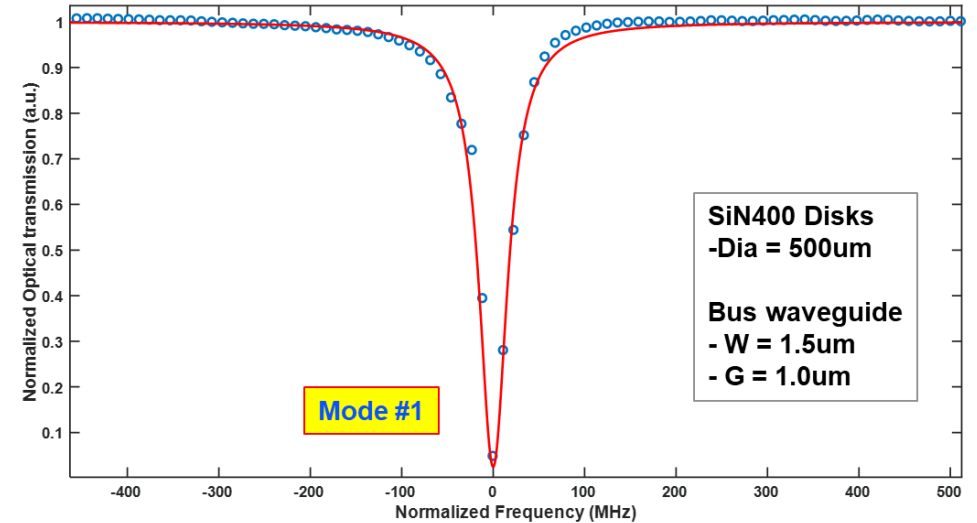
Optical resonators using 400 nm thick LPCVD SiN

Comparison of MIT-LL Optical Delay Technology to State-of-the-Art LPCVD Si₃N₄



X. Ji et al., "Methods to achieve ultra-high quality factor silicon nitride resonators", APL Photonics 6, 071101 (2021)
 W. Jin et al., "Hertz-linewidth semiconductor lasers using CMOS-ready ultra-high-Q microresonators", Nature Photonics 15, 346-353 (2021)
 J. Liu et al., "High-yield, wafer-scale fabrication of ultralow-loss, dispersion-engineered silicon nitride photonic circuits", Nature Communications 12, 2236 (2021)

Zoomed in showing detailed Q near 1.8467375e5 GHz (wavelength = 1623.362nm) QTMECH03SL W24_Dev1



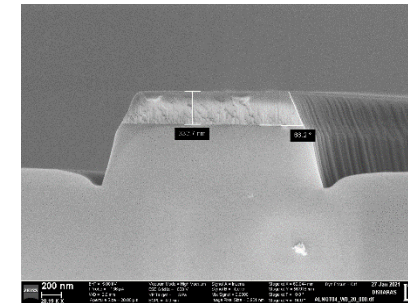
Mode #	Q _{bus-disk}	Q _{unloaded}	FSR (GHz)	ng
1	8.3943e6	11.542e6	100.06	1.90739

DISTRIBUTION STATEMENT C. Distribution authorized to U.S. Government agencies and their contractors – NOT APPROVED FOR PUBLIC RELEASE

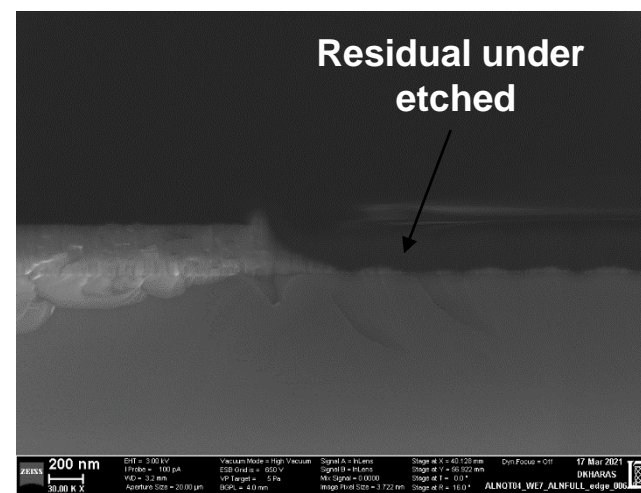
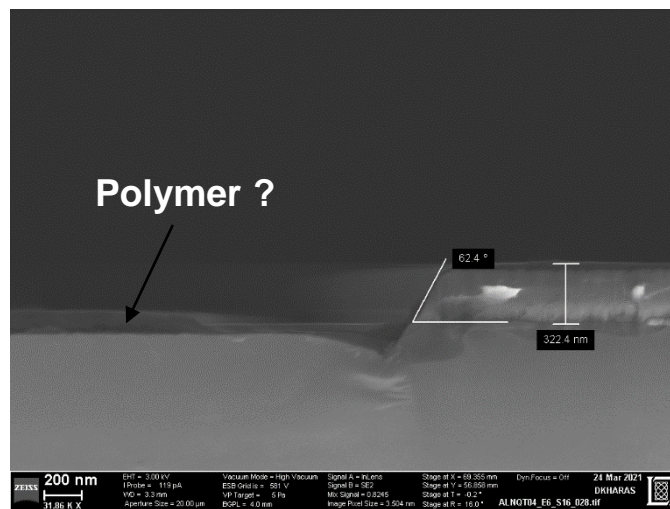
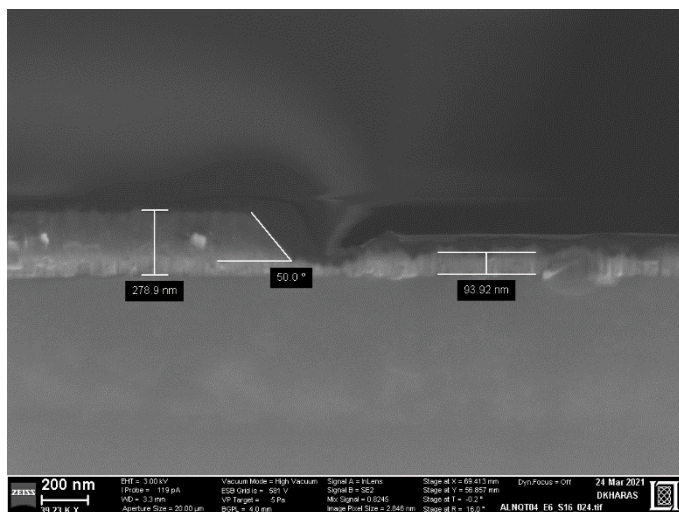
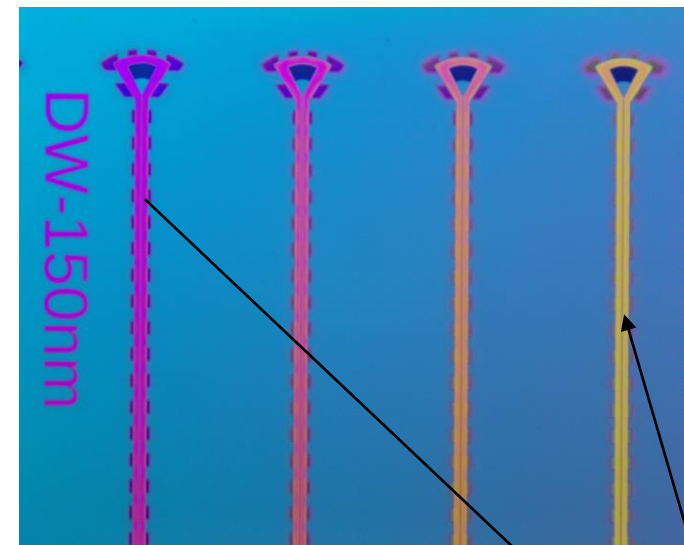
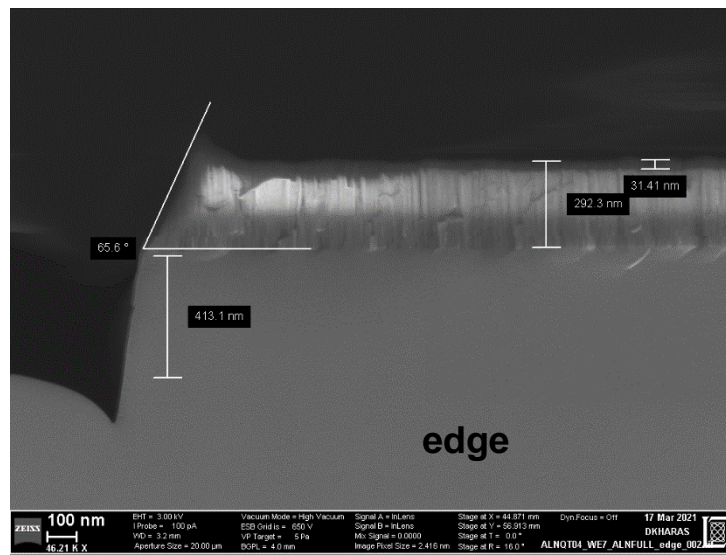
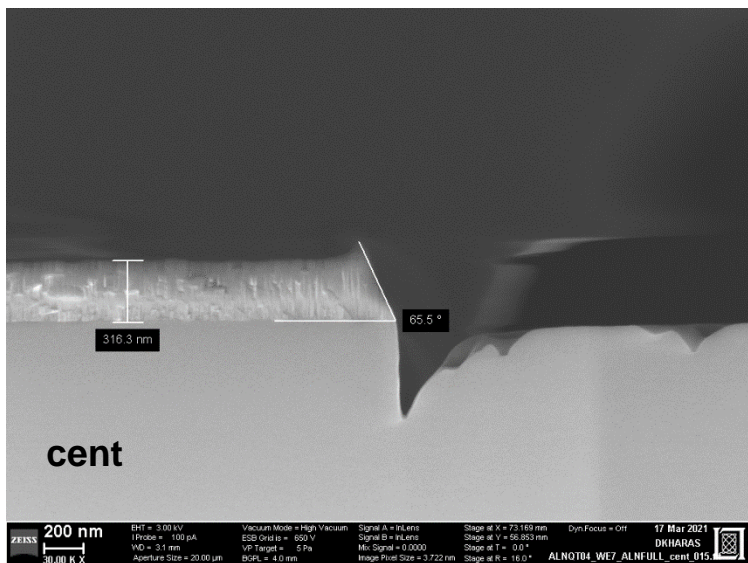
LINCOLN LABO
MASSACHUSETTS INSTITUTE OF TECHNOLOGY

EB-ALNWG01

- Etched several wafers using an oxide hard mask and EB-ALNWG01 Aluminum Nitride etch.
 - Wafer 0 (AINQT03 -20) & ALNQT04 wafers 1 & 4,
- 300-400nm Aluminum Nitride sputtered by OEM group
- 300 nm oxide hard mask needed
- Patterning using JSR 500nm resist w 65nm BARC
- Oxide open using EBA-SIPWGOX28 (15 sec Barc etch, and 50 sec Oxide etch)
 - Etch was developed as part of the IONPH008X aluminum oxide improvement DOE, where we tried to have an oxide opening etch with good JSR selectivity and reduced polymer formation.
 - OX ER ~6.7nm/sec, JSR ER ~4.1nm/sec
- Aluminum Nitride etch EB-ALNWG01
 - Etch seems to slow down with time and not clear at the bottom
 - Etch is sloped 65 deg, shows micro trenching at edges
 - Accelerated etch into silicon is seen.
 - Etch is not uniform across the wafer surface-some evidence of polymer residues on surface. Mottled surface appearance in places, perhaps where oxide hard-mask thickness variability on the surface or polymer residues?
 - ALN ER ~1.65-2.4 nm/sec
 - Ox HM ER ~1.3 nm/sec



- Etched several wafers using an oxide hard mask and EB-ALNWG01 Aluminum Nitride etch.
 - ALNQT04 wafers 16, 17 (ALNQT03 E6, E7) and ALNQT04 w3,
- Wafers were had ALN deposited at Northeastern University, and wafer 3 had OEM ALN.
- 200 nm oxide hard mask used on wafer 16 and 17, but insufficient used 300 nm sequel oxide on wafer 3
- Patterning using JSR 500nm resist w 65nm BARC
- Oxide open using EBA-SIPWGOX28 (15 sec Barc etch, and 35 sec Oxide etch)
- Aluminum Nitride etch EB-ALNWG02
 - Etch seems to slow down with time and not clear at the bottom
 - Etch is sloped 65 deg, shows micro trenching at edges
 - Accelerated etch into silicon is not seen to the same extent as 01 etch
 - OEM and NE ALN appear to etch at different rates,
 - NE ALN etched at ~2 nm/sec,
 - OEM ALN ER ~1.4 -1.9 nm/sec
 - Ox HM ER ~1.36 - 1.6 nm/sec
 - Resist consumption rate ~ 3.3 nm/sec (averaged across all steps)



Variable Etch depth And color



AIN baseline etch recipe – EB-ALNWG01

EB-ALNWG01.rcp

File Help

Step:	Step 1	Step 2	Step 3	Step 4
StepName:	STAB1	TIN-TI	MAIN	DECHUCK
Chamber Selection:	-B-----	-B-----	-B-----	-B----12345
Step end control:	By Time	By Time	By Time	By Time
Maximum step time:	10.0 seconds	5.5 seconds	180.0 seconds	5.0 seconds
Endpoint Selection:	No Endpoint	No Endpoint	External Endpoint	No Endpoint
EndpointParams:			Algorithm ID: 3 Min Endpoint Time: 100 Secs	
Pressure Control:	Servo to xxx mTorr	Servo to xxx mTorr	Servo to xxx mTorr	No Pressure Control
Pressure:	10 mTorr	10 mTorr	6 mTorr	mTorr
Bias Power:	0	100	125	0
RFMode:	0	0	0	0
DC Bias Limit:	-1000 to 0	-1000 to 0	-1000 to 0	-1000 to 0
Source Peak Power:	0 W	1200 W	1000 W	0 W
Process Position:	N/A	N/A	N/A	N/A
Temperature:	14.0 °C	14.0 °C	14.0 °C	1.0 °C
Gas1:	BCL3 0	BCL3 0	BCL3 20	N2-20 10
Gas2:	CL2 80	CL2 80	CL2 120	
Gas3:	N2-20 0	N2-20 0	N2-20 0	
Gas4:	ARB 40	ARB 40	ARB 40	



Ideas to try for improving sidewall angle

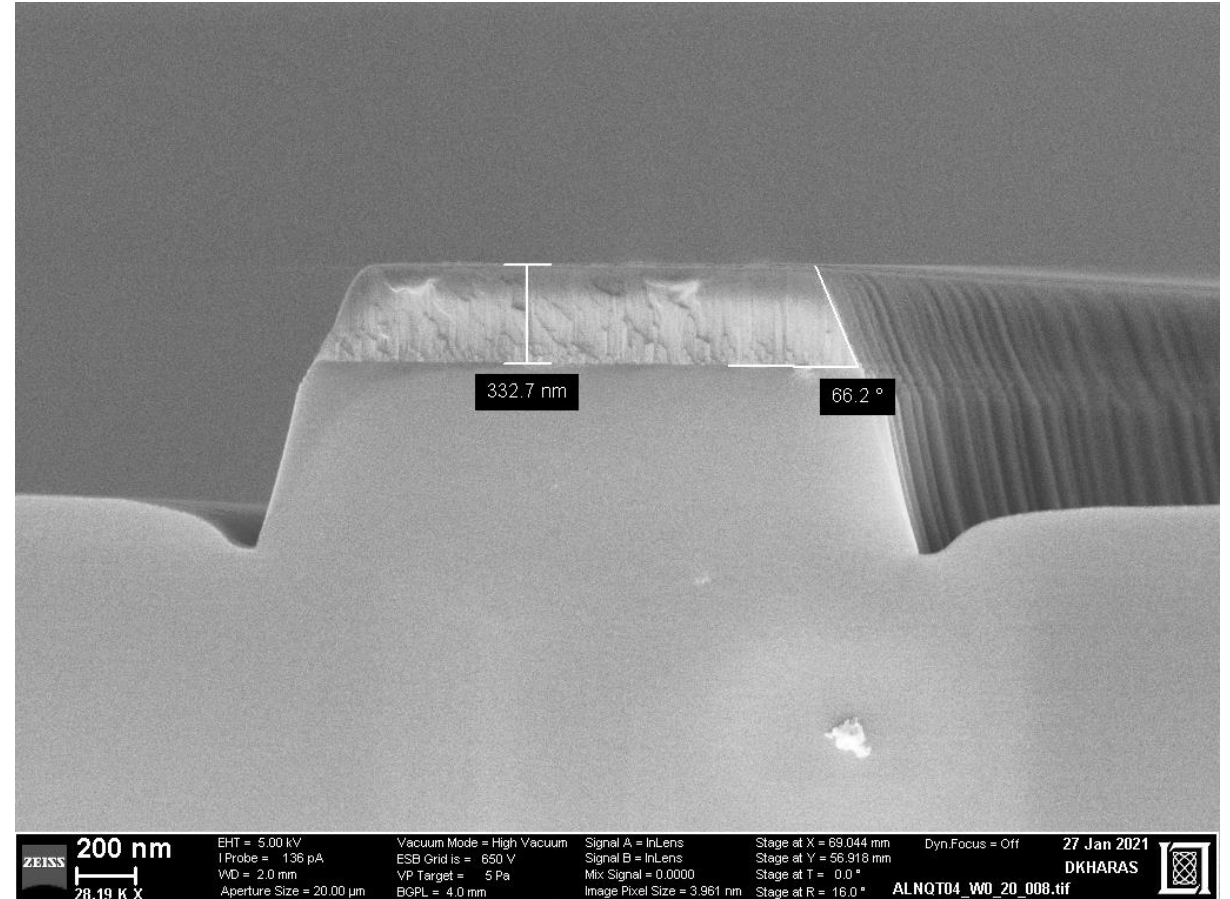
- **Low chamber pressure (maybe can try 4 mT if the plasma can stabilize)**
- **High ICP power**
- **Changing the Cl₂/BCl₃ blend (typically higher flow on BCl₃ than Cl₂, blended in seems to help the etch rate and selectivity for III-V's)**
- **Minimizing Ar flow unless we have a lot of re-deposition on the substrate (Ar is physical and might hurt the SiO₂ selectivity)**

Recipe 1: EB-ALNWG01

Main etch: (1/27/21)

- 6 mT
- 1000 W source (ICP)
- 20 sccm BCl₃
- 120 sccm Cl₂
- 40 sccm Ar
- 125 W bias

- Wafer: AINQT04_W0 (slot 20)



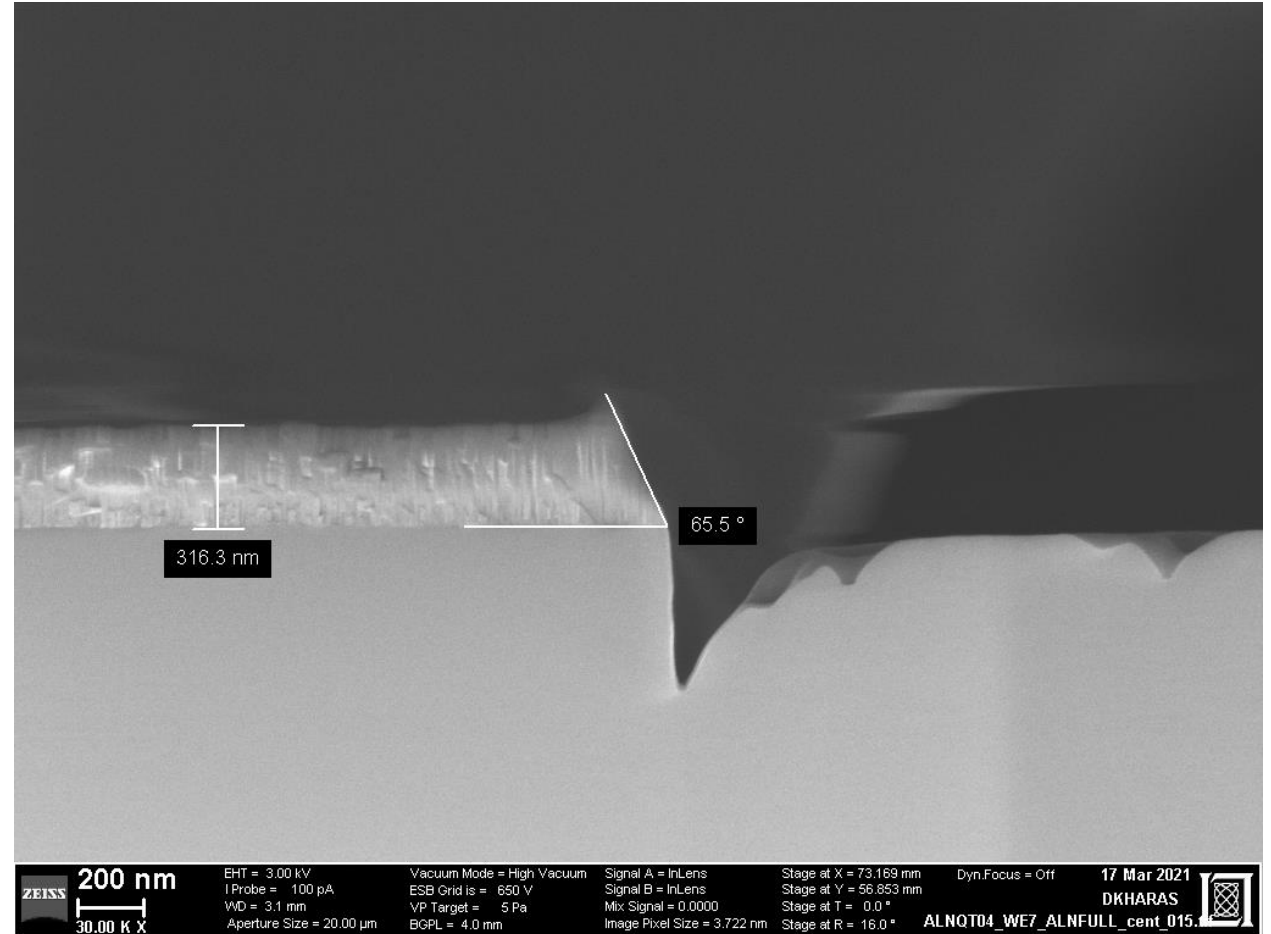
Recipe 2: EB-ALNWG02

Main etch: (2/3/21)

- 4 mT
- 1200 W source (ICP)
- 20 sccm BCl₃
- 80 sccm Cl₂
- 40 sccm Ar
- 125 W bias

- Lower pressure, higher power → no effect on slope, negative impact on selectivity

- Wafer: AINQT03_E7

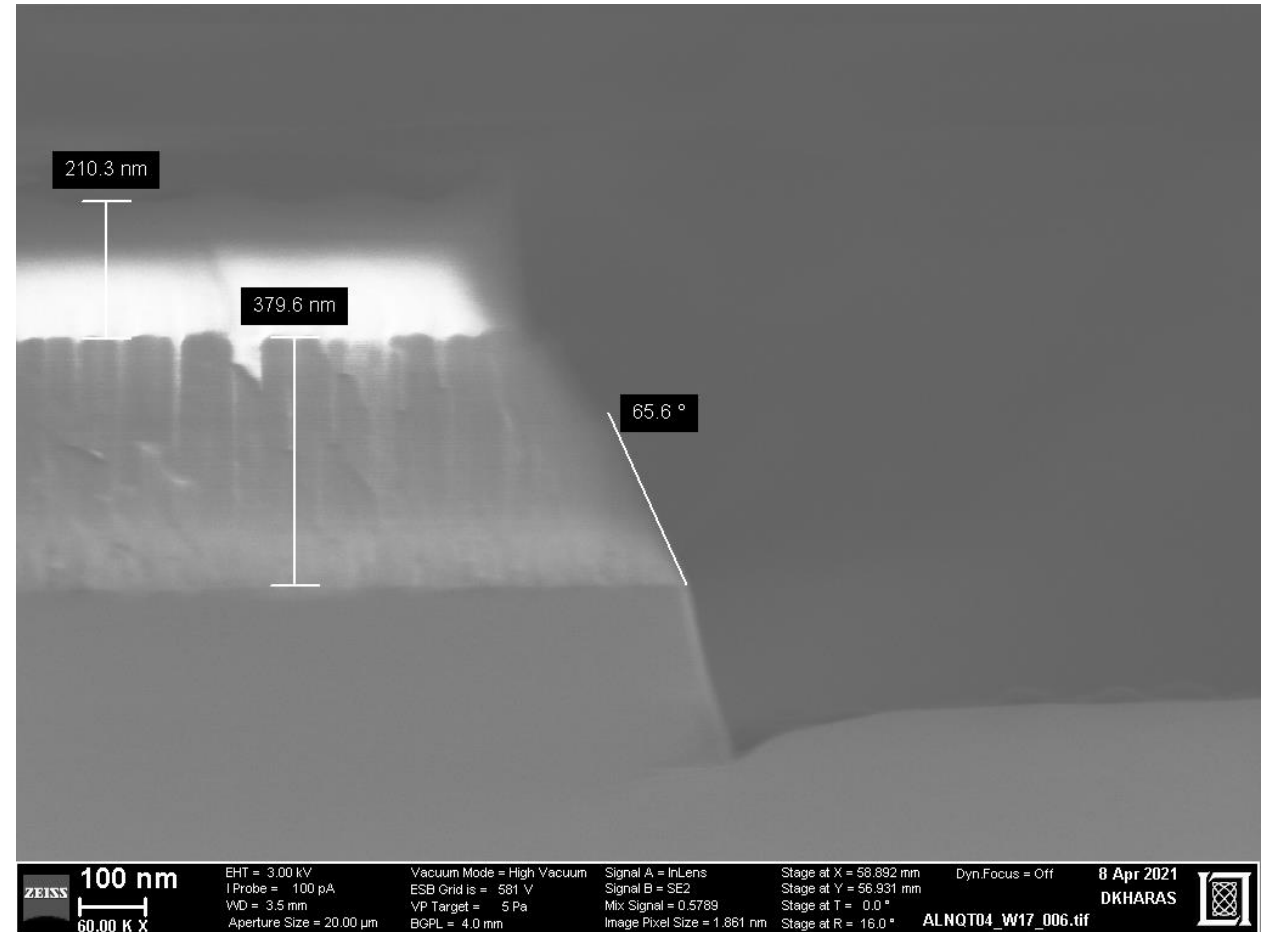


Recipe 3

Main etch: (4/2/21)

- 6 mT
- 1000 W source (ICP)
- 10 sccm BCl₃
- 120 sccm Cl₂
- 40 sccm Ar
- 125 W bias

- Wafer: AINQT04_W17

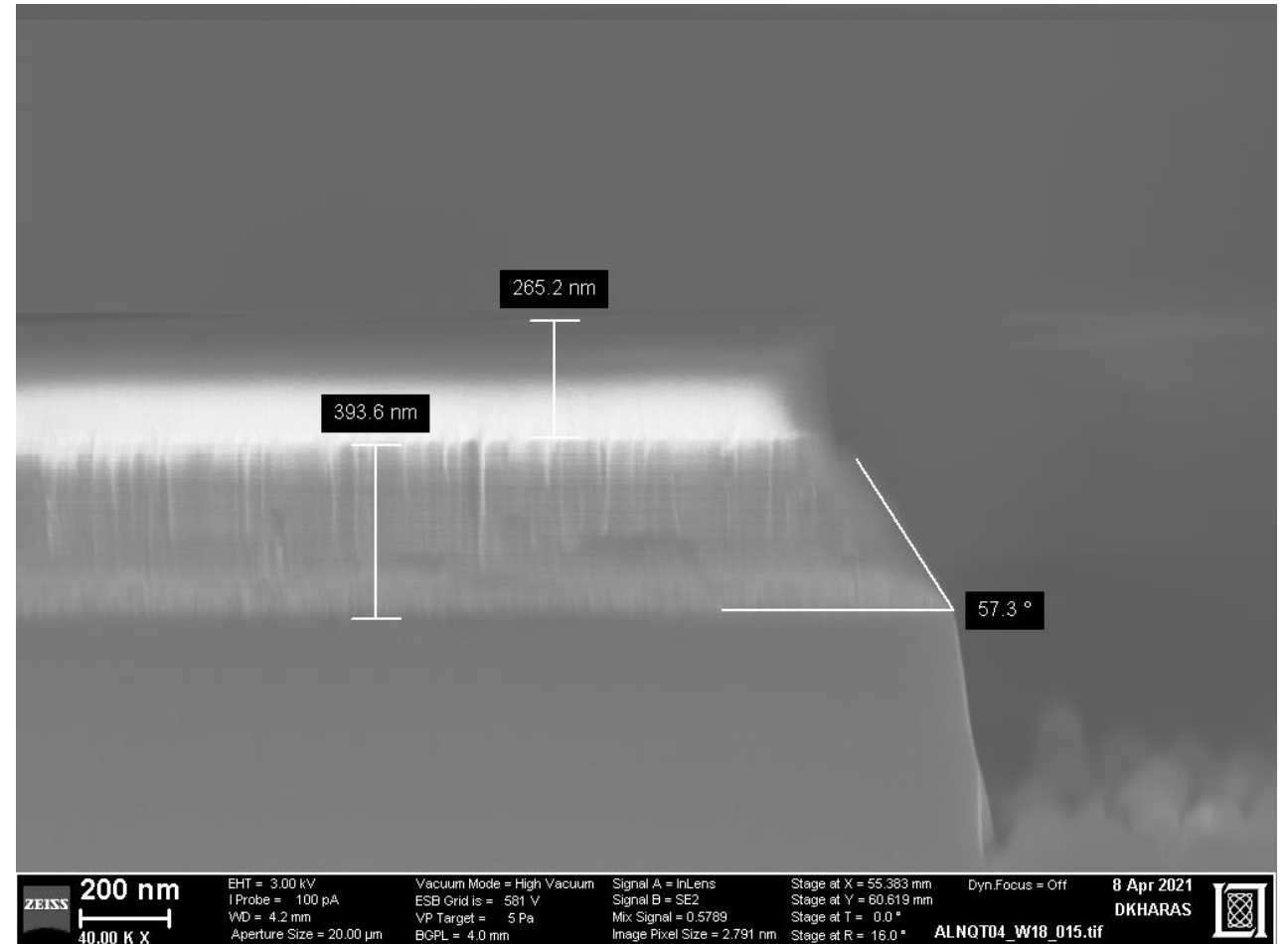


Recipe 4

Main etch: (4/2/21)

- 6 mT
- 1000 W source (ICP)
- 0 sccm BCl₃
- 120 sccm Cl₂
- 40 sccm Ar
- 125 W bias

- Wafer: AINQT04_W18



Recipe 5

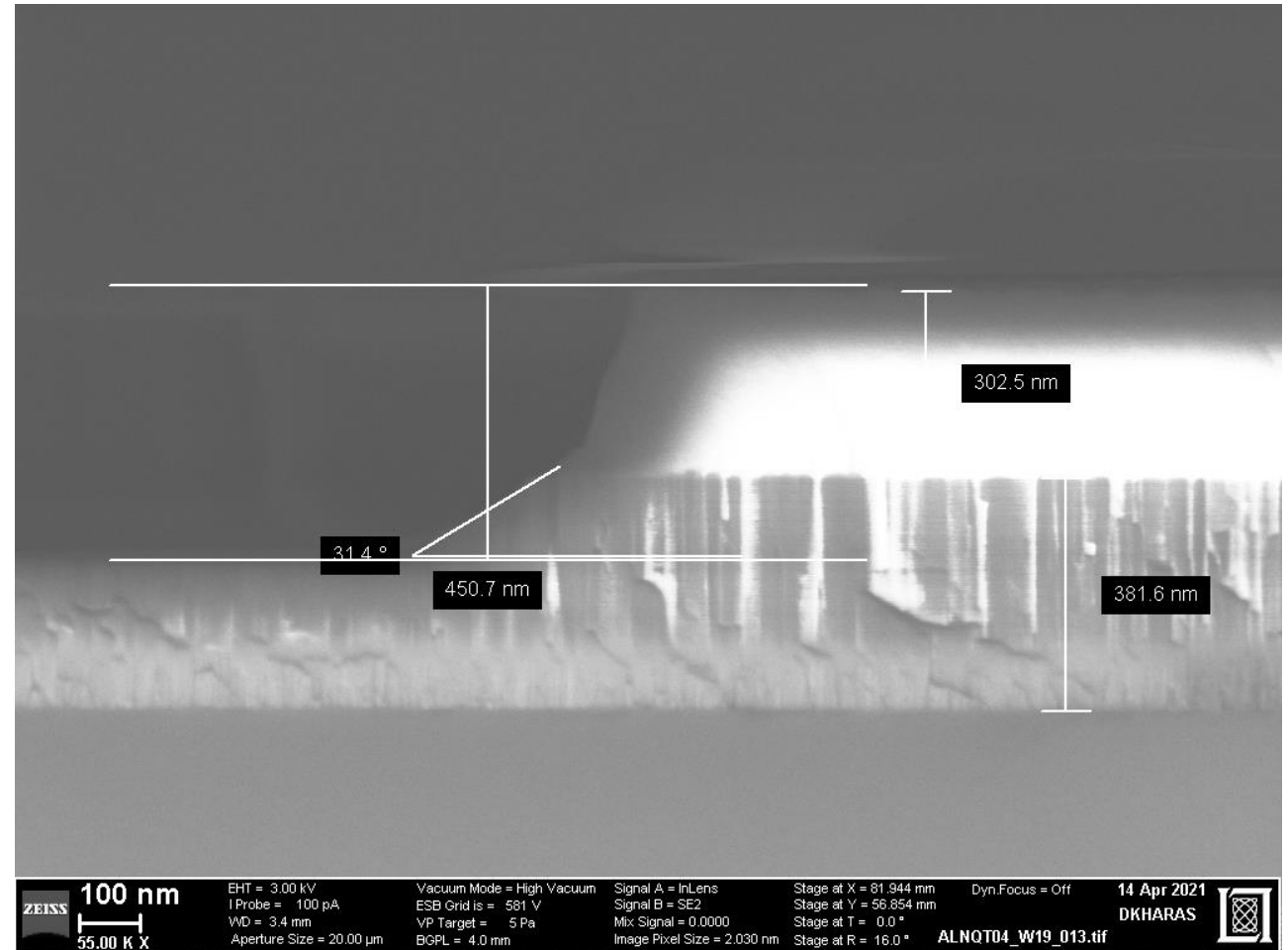
Main etch: (4/15/21)

- 6 mT
- 1000 W source (ICP)
- 58 sccm BCl₃
- 82 sccm Cl₂
- 40 sccm Ar
- 125 W bias

Adapting from Al in C400:

- Bias – 250 ICP – 250
- Pressure - .4Pa Pos – 100%
- Cl₂ – 14sccm / AR – 6sccm / BCl₃ – 10sccm

• **Wafer: AINQT04_W19**

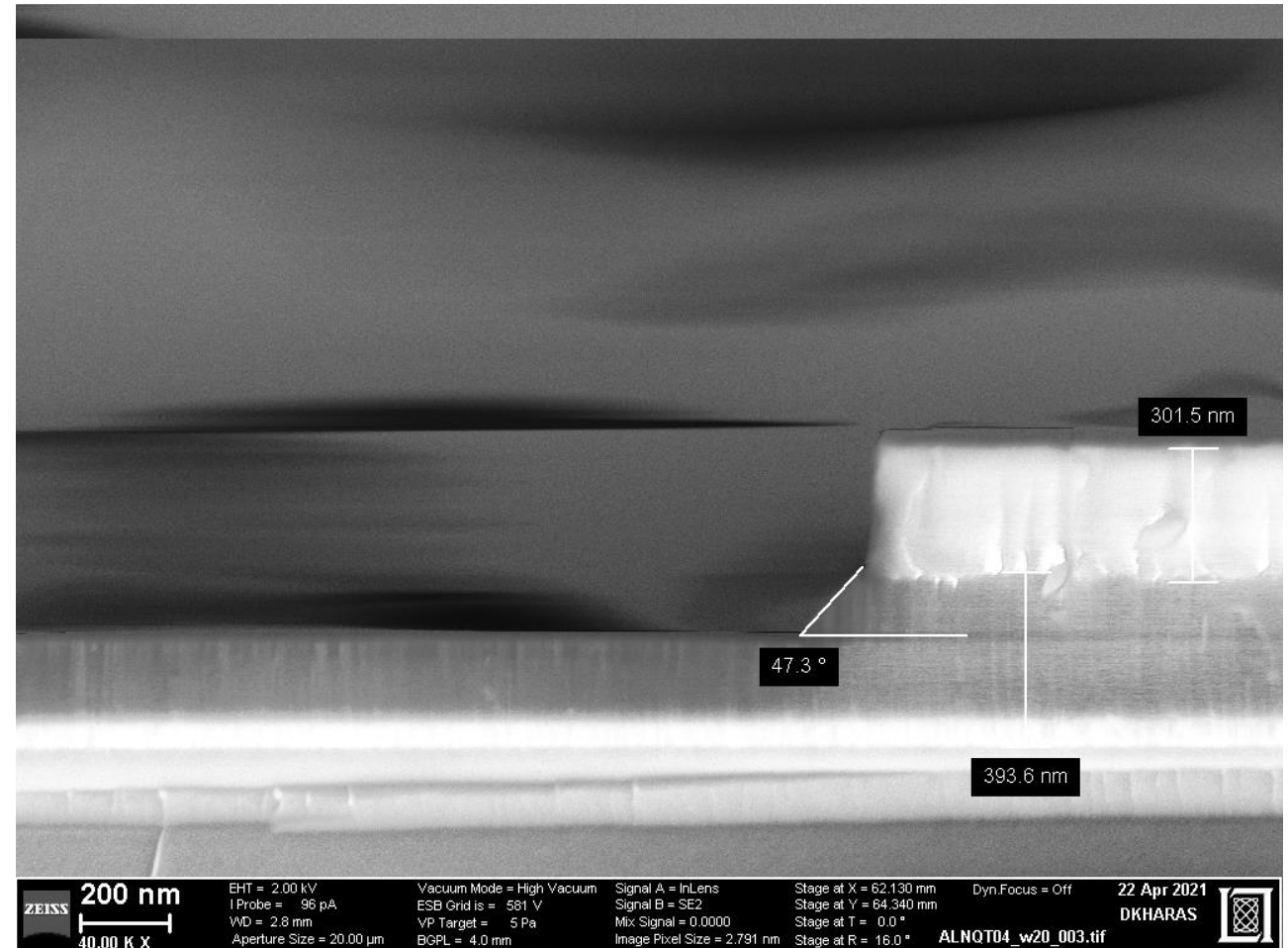


Recipe 6

Main etch: (4/22/21)

- 6 mT
- 1000 W source (ICP)
- 20 sccm BCl₃
- 40 sccm Cl₂
- 40 sccm Ar
- 125 W bias

- Wafer: AINQT04_W20



Recipe 7

Main etch: (4/26/21)

- 15 mT
- 1000 W source (ICP)
- 20 sccm BCl₃
- 120 sccm Cl₂
- 40 sccm Ar
- 125 W bias

- Wafer: AINQT04_W21



AMAT Etch Trials grouped by Variable

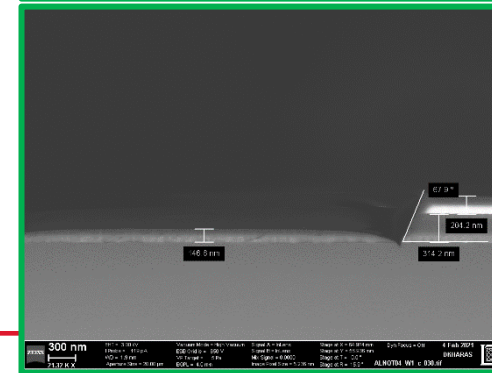
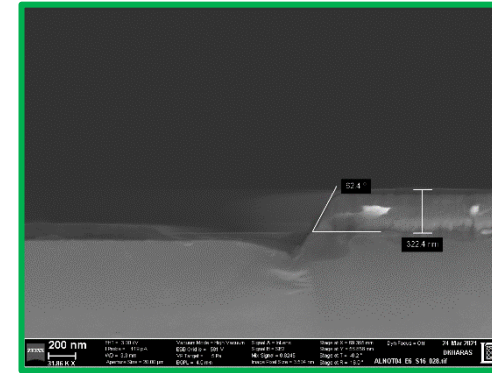
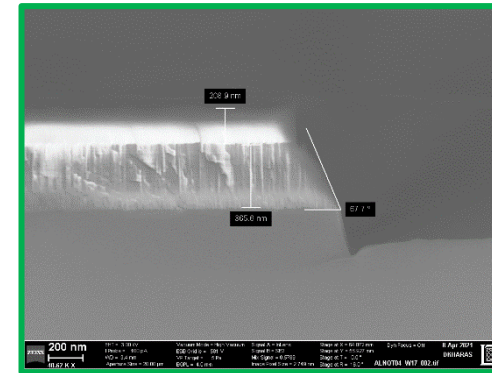
Applied Materials Centura Etcher					
fixed power, reduced BC13					
Wafer ID	wafer_1,4	26	17	18	
Recipe variant	WG01 POR	POR	WG01_V1	WG01_V2	
ICP	1000	1000	1000	1000	
BIAS	125	125	125	125	
Press	6	6	6	6	
CI2	120	120	120	120	
BCI3	20	20	10	0	
Ar	40	40	40	40	
total flow	180	180	170	160	
CI2/BCI3 ratio	6	6	12	6	
etch angle	66	50.4	66	57	
etch time	120	50	100	100	
depth	160	228	380	397	
Etch rate		4.56	3.80	3.97	
			etched through	etched through	
			worse		
			Increase P	decrease P	
Wafer ID	wafer_1,4	26	21	E6,E7	
Recipe variant	WG01 POR	POR	WG01_V5	WG02	
ICP	1000	1000	1000	1200	
BIAS	125	125	125	125	
Press	6	6	15	4	
CI2	120	120	120	80	
BCI3	20	20	20	20	
Ar	40	40	40	40	
total flow	180	180	180	140	
CI2/BCI3 ratio	6	6	6	4	
etch angle	66	50.4	47	66	
etch time	120	50	50	25	
depth	160	228	263	53	
Etch rate	1.33	4.56	5.26	2.12	
		WG0X14	reduces etch angle	maintains etch angle	
			resist only	resist only	
			0.44	0.34	
			1.02		
			higher bias	lower bias	higher bias and icp
Wafer ID	wafer_1,4	26	B22	B25	B24
Recipe variant	WG01 POR	POR	WG01_V6	WG01_V9	WG01_V8
ICP	1000	1000	1000	700	1200
BIAS	125	125	200	50	200
Press	6	6	6	6	6
CI2	120	120	120	120	120
BCI3	20	20	20	20	20
Ar	40	40	40	40	80
total flow	180	180	180	180	220
CI2/BCI3 ratio	6	6	6	6	6
etch angle	66	50.4	57	56	59
etch time	120	50	50	100	50
depth	160	228	350	253	338
Etch rate	1.33	4.56	7.00	2.53	6.76

reduced CI2, increasing BC13		
20	19	27
WG01_V4	WG01_V3	EB-ALOX36
1000	1000	1200
125	125	100
6	6	4
40	82	0
20	58	100
40	40	0
100	180	100
2	1.41	
47	39	47
50	50	70
134	163	63
2.68	3.26	0.90
		higher BCL3 worse

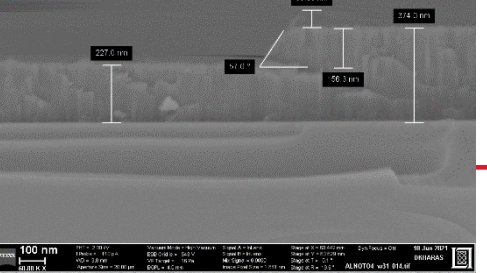
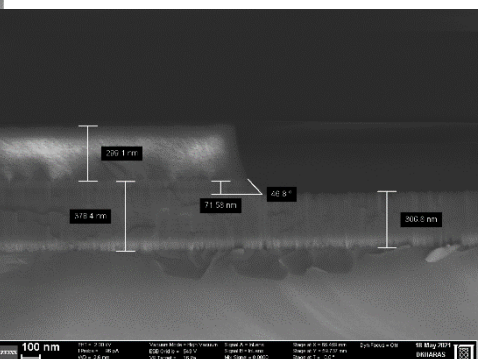
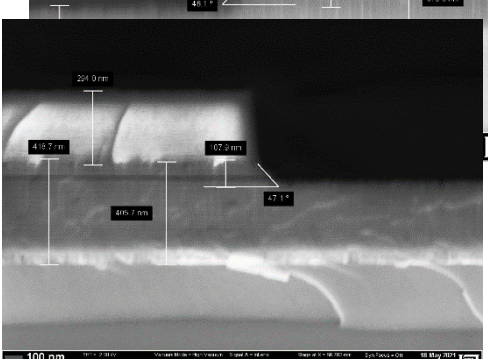
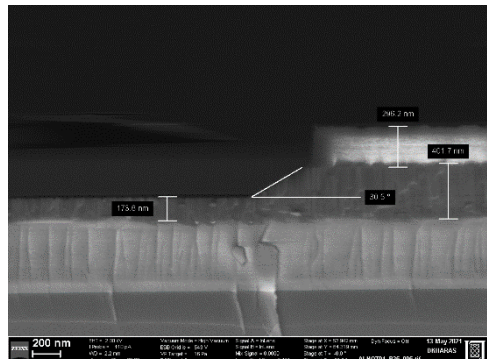
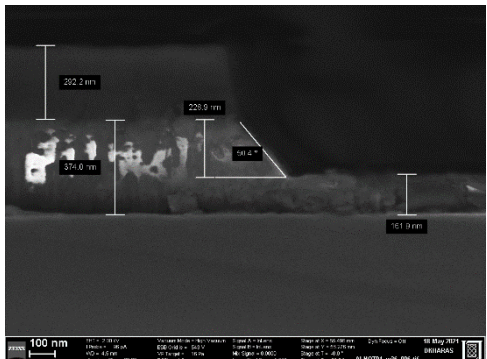
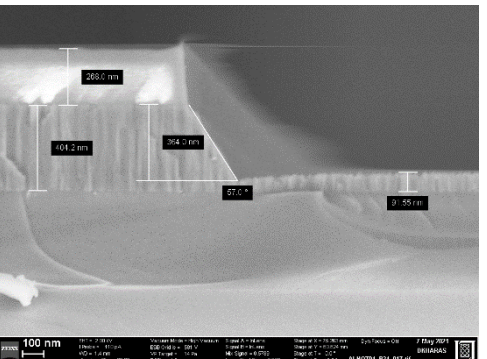
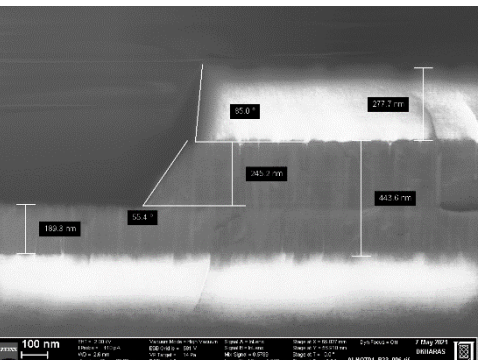
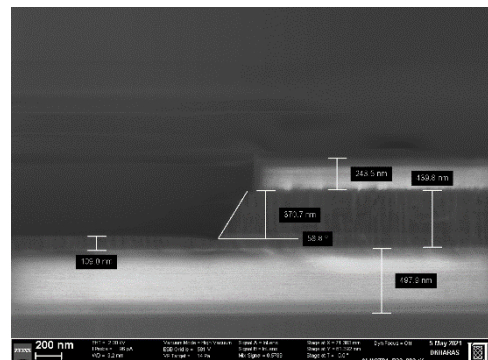
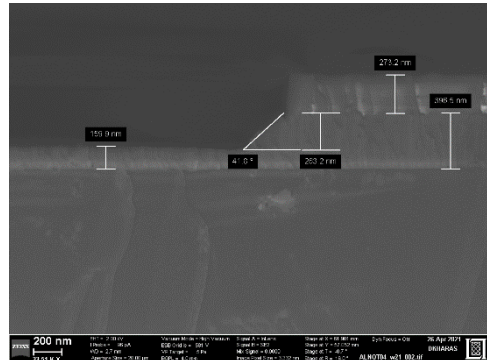
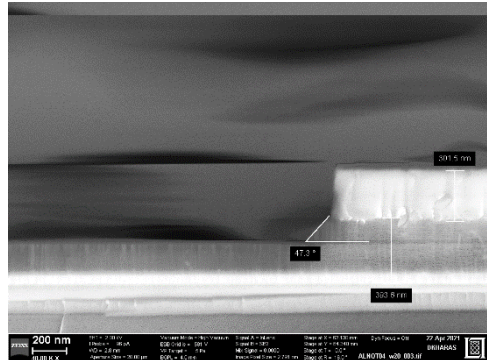
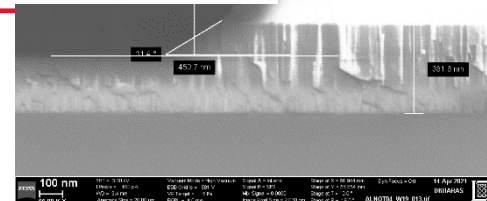
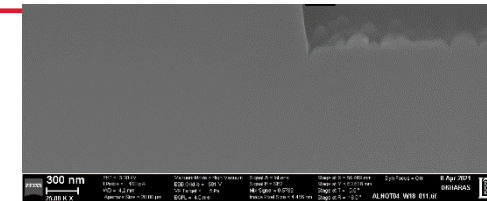
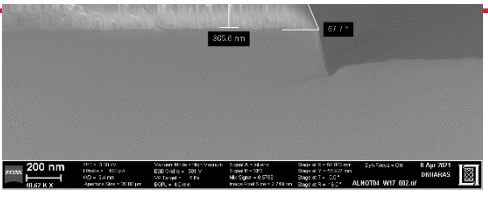
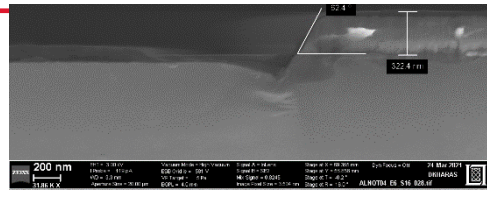
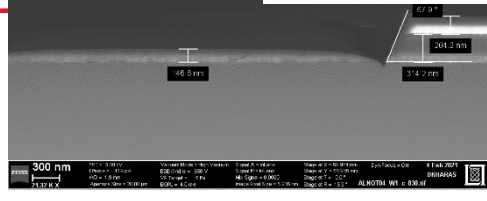
Higher Argon flow	
26	B23
POR	WG01_V7
1000	1000
125	125
6	6
120	120
20	20
40	80
180	220
6	6
50.4	57
50	50
228	245
	4.90

resist only etching, eliminate impact of oxide etch byproducts		
30	31	32
POR	WG01_V10	WG01_V11
1000	1000	1000
125	100	200
6	6	6
120	100	120
20	10	20
40	20	40
180	130	180
6	10	6
58	45	40
45	45	45
145	130	220
3.22	2.89	4.89
		resist only
		7.4
		8.4
		4.8
		1.02

variables	Best Condition
ICP	1000, 1200
BIAS	100, 125
Press mtor	4, 6, 15
CI2	0,40,82,120,
BCI3	0,10,20,58,100
Ar	0,20,40,80
total flow	100,160,170,180,220
angle	65 deg



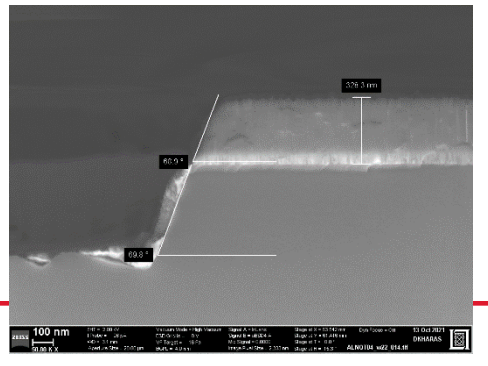
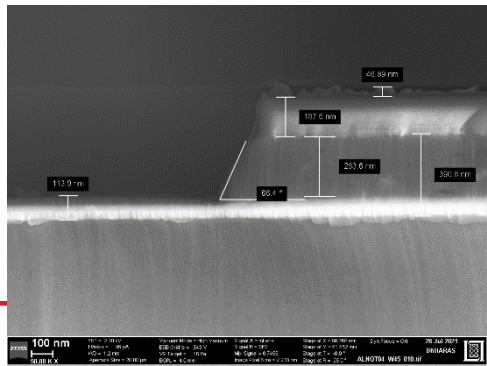
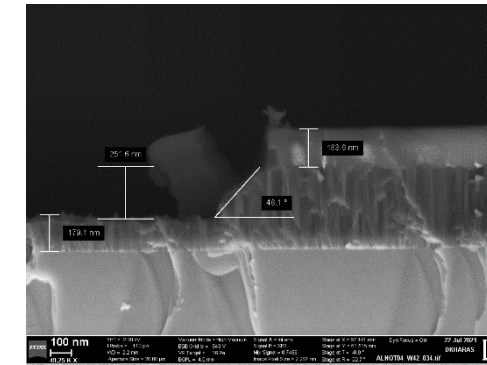
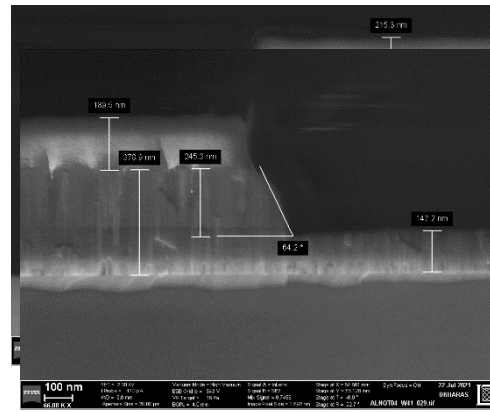
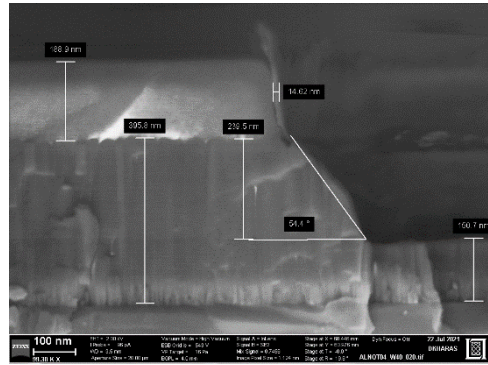
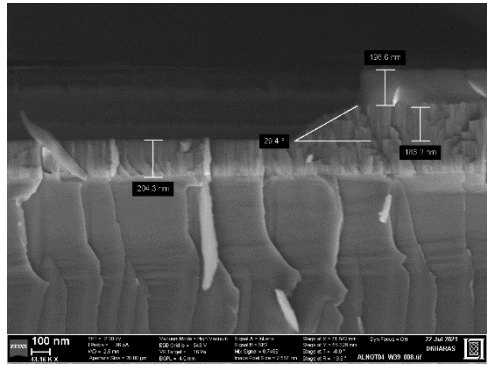
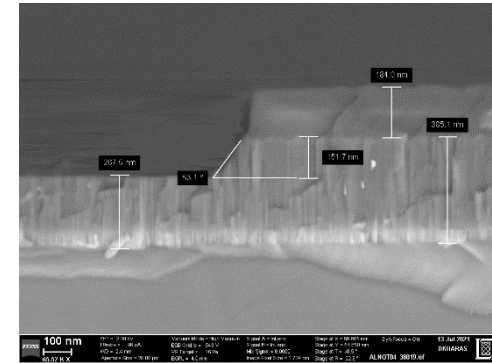
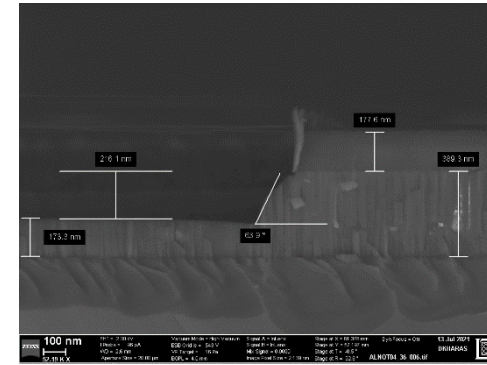
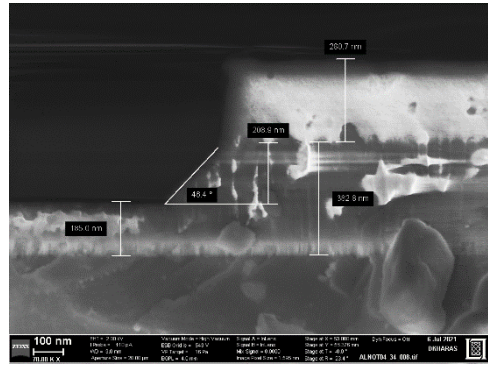
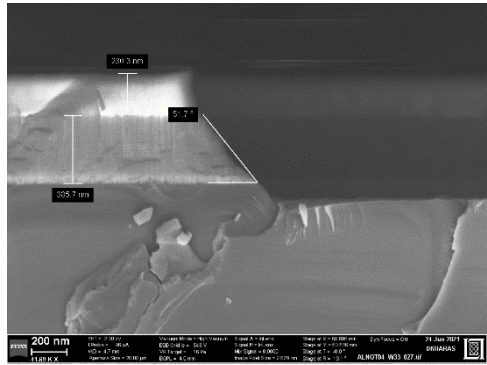
AMAT Etch Variants (refer to wafer id)



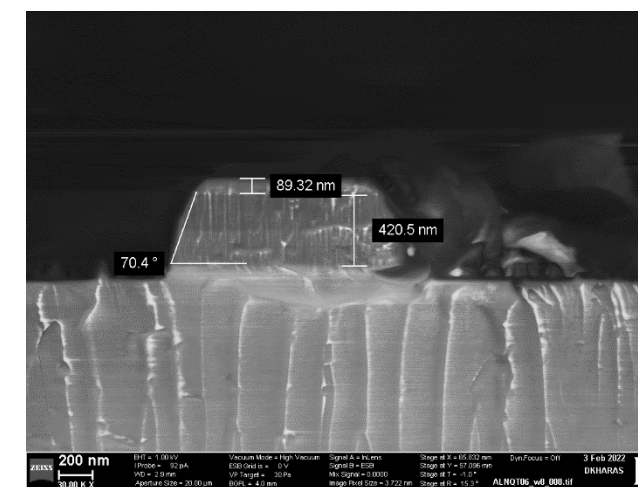
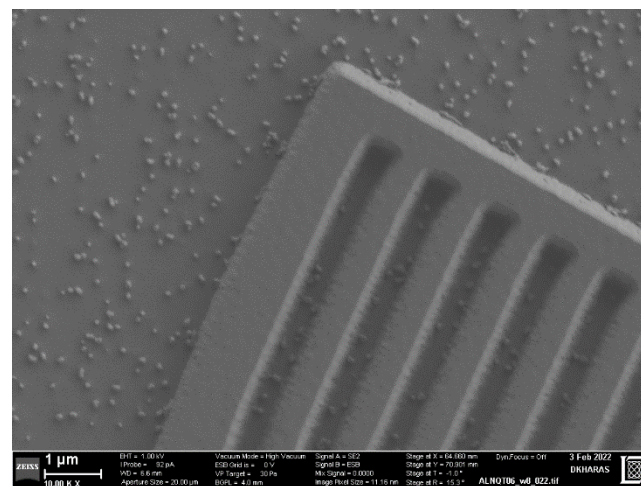
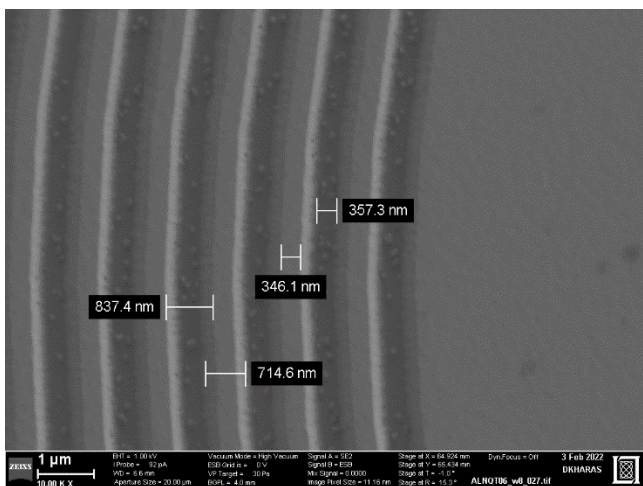
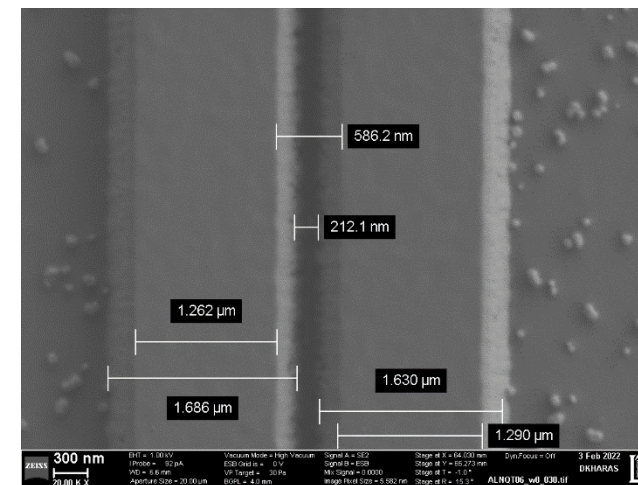
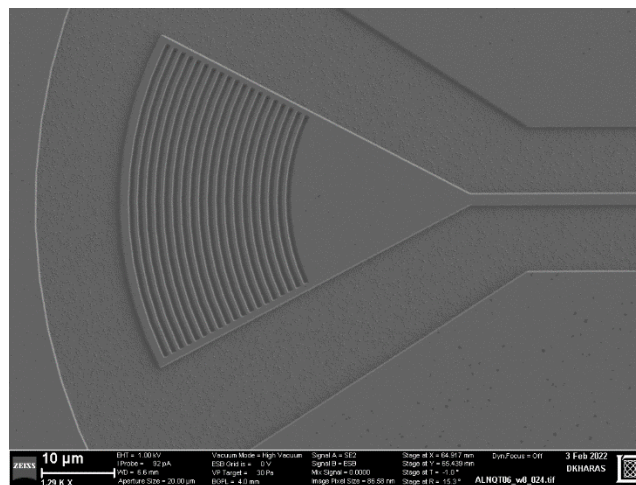
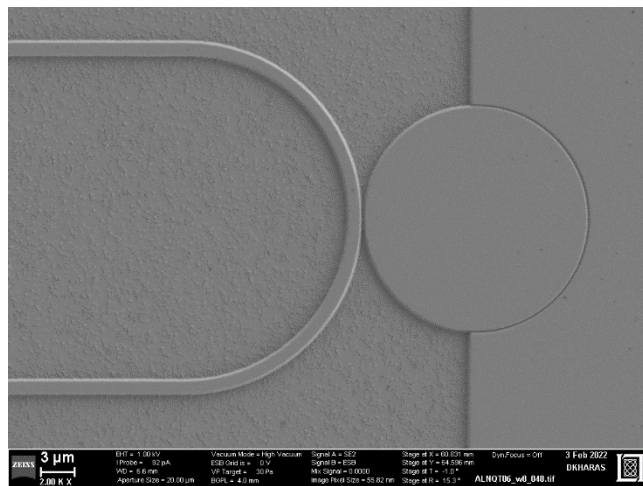
SAMCO Etch Trials grouped by Variable

SAMCO Metal Etcher		higher BCl3 worse angle reduced total flow better angle				lower pressure slightly better reduced Ar dilution reduced BCl3				increased Bcl3 worse		Higher Pressure worse angle	
	1st	35	34	36	38	41	44	45	72	42	41	42	
Wafer ID	33				38	41	44	45	72	42	41	42	
Recipe variant	72 Samco	74 sam	73 sam	73 sam	74 sam	74	77	77	72	76	74	76	
ICP	600	600	600	600	600	600	600	600	600	600	600	600	
BIAS	200	200	200	200	200	200	200	200	200	200	200	200	
Press	0.7 PA	0.7 PA	0.7 PA	0.7 PA	0.4	0.4	0.4	0.4	1.1	1.1	0.4	1.1	
Cl2	90	90	65	30	14	40	20	20	20	40	40	40	
BCl3	15	15	40	5	10	10	0	0	10	0	10	0	
Ar	10	50	10	0	6	0	0	0	0	0	0	0	
total flow	115	155	115	35	30	50	20	20	30	40	50	40	
Cl2/BCl3 ratio	6	6	1.625	6	1.4	4			2		4		
etch angle	58	52	47	64	53	64	53	60	30	48	64	48	
etch time	90	50	50	50	50	50	50	50	50	50	50	50	
depth	385+30	381+162	207	216	152	245	200	200	186	250	245	250	
Etch rate	4.6	10.9	4.1	4.3	3.0	4.9	4.0	4.0	3.7	5.0	4.9	5.0	
Oxide HM BT Recipe	WG0X14 50	WG0X14 51	WG0X14 5	WG0X14 38	WG0X14 38				WG0X14 3	WG0X14 38	WG0X14 38		
Oxide HM thickness	300	301	300	200	200				200	200			
AIN/RES													
	variables	Best Condition											
ICP	600	600											
BIAS	200	200											
Press pa	0.4, 0.7, 1.1	0.4											
Cl2	14,20,30,40,65,90	40		20									
BCl3	0,5,10,15,40	10		0									
Ar	0,6,10,15	0											
total flow	20, 30,35,40,50,115	50		20									
	angle	65 deg											

SAMCO Etch Variants

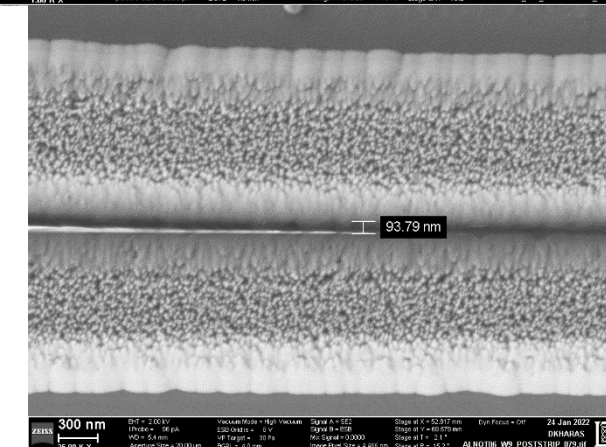
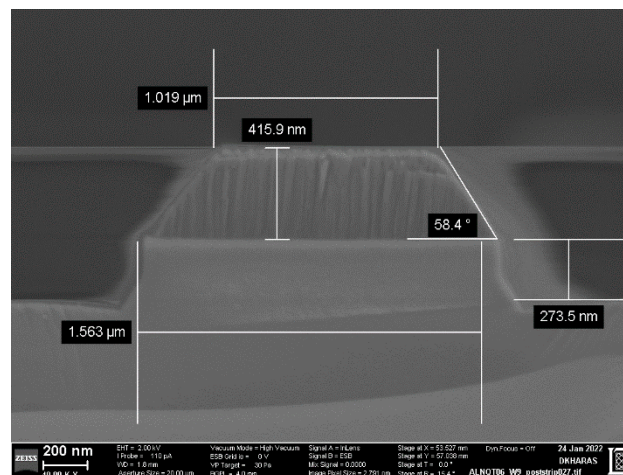
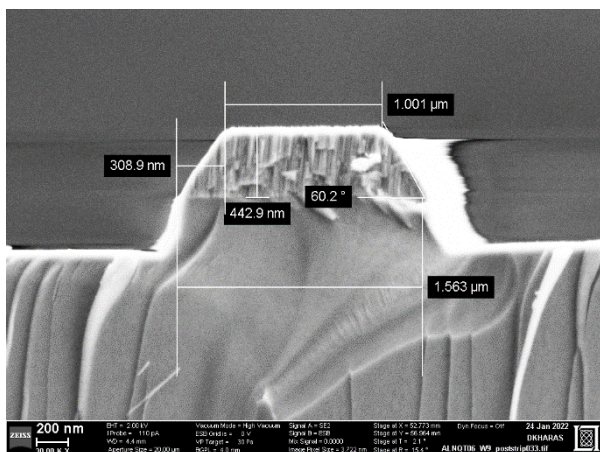
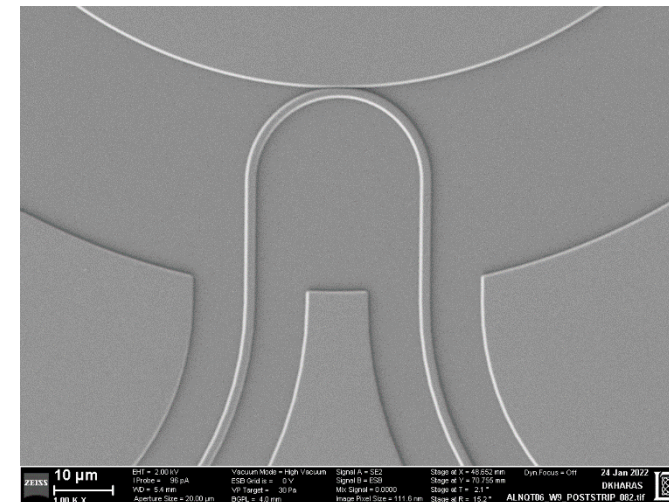
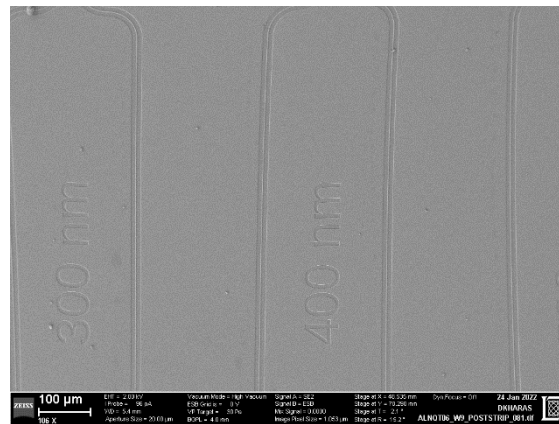
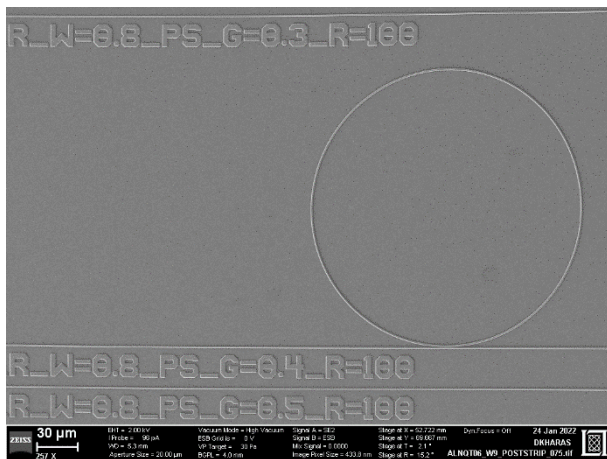


Group 1 ALNQT06 wafer 8 AIN Photonics SEM



\\lf\div8\GROUPS\G89\G89MEMBERSHARE\Programs\Quantum Interface\QT Fab Lots (ML)\ALNQT06\Fab Images _SEM and Optical

Group 1 ALNQT06 wafer 9 AlN Photonics SEM



\\lfs\div8\GROUPS\G89\G89MEMBERSHARE\Programs\Quantum Interface\QT Fab Lots (ML)\ALNQT06\Fab Images _SEM and Optical

Task 1. Aluminum Nitride Photonics ML Fabrication

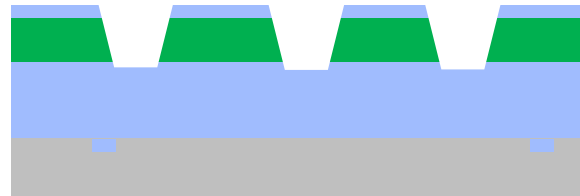
1. Alignment mark pattern and Si etch and deposit bottom oxide



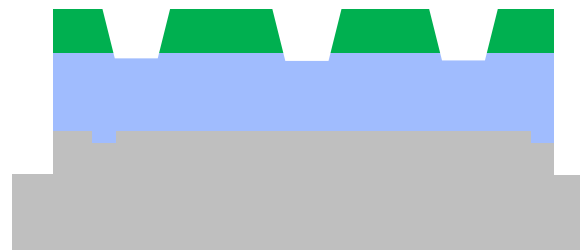
2. Sputter 400 nm Aluminum Nitride (external to ML) and deposit oxide hardmask



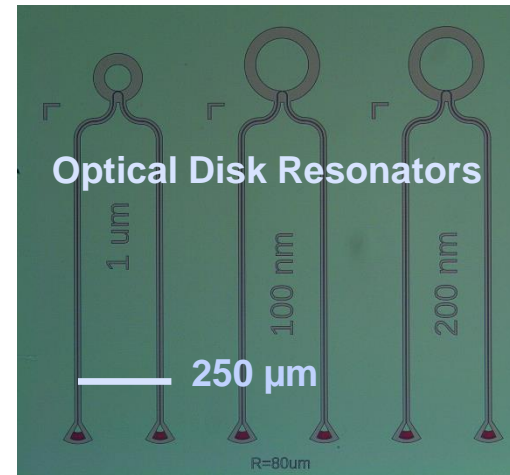
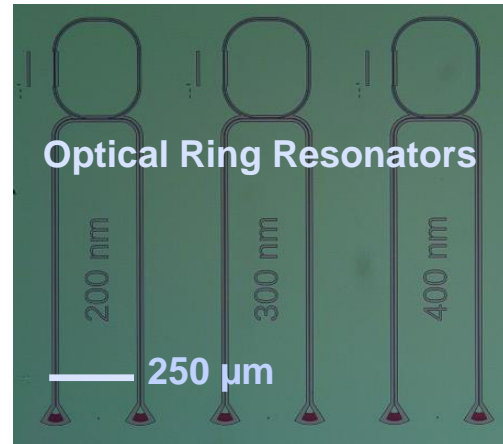
3. Pattern AIN WG layer, etch oxide HM, AIN



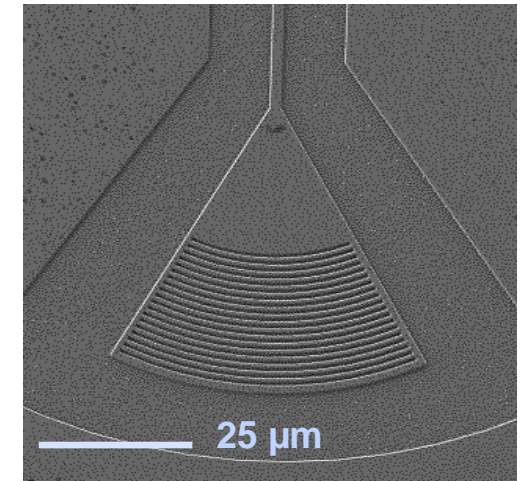
4. Remove excess oxide hardmask, and pattern and etch a deep facet to enable fiber coupling testing



Si substrate
 PECVD SiO₂
 AIN



Vertical grating coupler



Ring and Disk optical resonators have been fabricated

Task 2: AlN Optomechanical Resonators

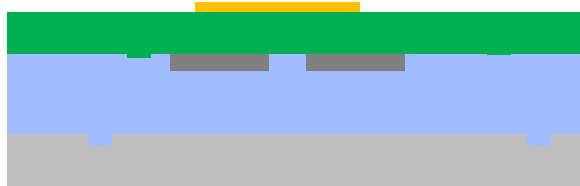
1. Deposit bottom clad oxide, dep polysilicon release layer, pattern



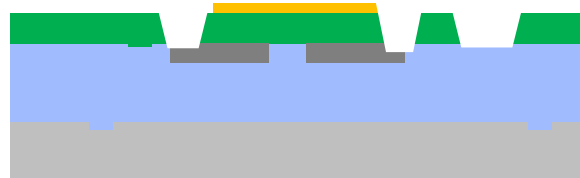
2. Cap release layer with oxide and CMP flat



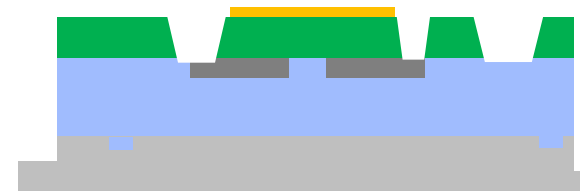
3. Sputter AlN and Al electrode metal, pattern etch metal electrode.



4. Pattern AlN Waveguide



5. Deep Facet Pattern and etch.



Si substrate
 Polysilicon
 PECVD SiO₂
 AlN
 Top metal

